Theses and Dissertations

Spring 2010

Toxic intermediates and protein quality control in the polyglutamine disease, SCA3

Aislinn Joanmarie Williams
University of Iowa

TOXIC INTERMEDIATES AND PROTEIN QUALITY CONTROL

IN THE POLYGLUTAMINE DISEASE, SCA3

by

Aislinn Joanmarie Williams

An Abstract

Of a thesis submitted in partial fulfillment
of the requirements for the Doctor of Philosophy
degree in Neuroscience in
the Graduate College of
The University of Iowa

May 2010

Thesis Supervisors: Adjunct Professor Henry L. Paulson
Professor Beverly Davidson

ABSTRACT

Polyglutamine (polyQ) diseases are progressive fatal neurodegenerative movement disorders. Although many cellular processes are perturbed in polyQ disease, recent studies highlight the importance of protein misfolding as a central event in polyQ toxicity. Spinocerebellar ataxia type 3 (SCA3), also known as Machado-Joseph disease, is a particularly interesting polyQ disease because of the special qualities of the disease protein ataxin-3, which normally participates in cellular protein quality control. Here I use multiple mouse models of disease to explore toxic protein species and the role of protein homeostasis in SCA3 pathogenesis.

In Chapter 1, I review the key features of polyQ disease, and outline the background and rationale behind our strategy for identifying toxic protein species in SCA3.

In Chapter 2, I examine the role of the protein quality control ubiquitin ligase, CHIP (C-terminus of Hsp70 interacting protein), in regulating the toxicity of expanded ataxin-3 *in vivo*. Genetic reduction or removal of CHIP increases formation of detergent-resistant ataxin-3 microaggregates specifically in the brain. Concomitant with this, reduction or removal of CHIP exacerbates the phenotype of SCA3 mice, revealing a correlation between high levels of microaggregates and phenotypic severity. Additional cell-based studies confirm that CHIP may not directly mediate ataxin-3 degradation, suggesting that CHIP reduces expanded ataxin-3 toxicity in the brain primarily by enhancing ataxin-3 solubility.

In Chapter 3, I use various biochemical techniques to reveal the presence of brain-specific ataxin-3 microaggregates in two genetically distinct mouse models of SCA3.

Selective neuropathological evaluation of SCA3 mice reveals that major neuronal loss and reactive glial proliferation are not shared features of phenotypically-manifesting SCA3 mice. Additional studies fail to provide evidence for loss-of-function of endogenous ataxin-3 in SCA3 mice. Our results suggest that neuronal dysfunction in SCA3 is mediated through a toxic gain-of-function mechanism by ataxin-3 microaggregates in the CNS.

In Chapter 4, I discuss important areas for future research in polyQ disease. I describe studies that would help elucidate the structural nature of toxic soluble microaggregates, and their effects on other cellular proteins. I also consider how the results described in this thesis inform potential treatment strategies.

Abstract Approved: _____
                                  Thesis Supervisor

                                  _____
                                  Title and Department

                                  _____
                                  Date

                                  _____
                                  Thesis Supervisor

                                  _____
                                  Title and Department

                                  _____
                                  Date

TOXIC INTERMEDIATES AND PROTEIN QUALITY CONTROL

IN THE POLYGLUTAMINE DISEASE, SCA3

by

Aislinn Joanmarie Williams

A thesis submitted in partial fulfillment
of the requirements for the Doctor of Philosophy
degree in Neuroscience in
the Graduate College of
The University of Iowa

May 2010

Thesis Supervisors: Adjunct Professor Henry L. Paulson
Professor Beverly Davidson

Graduate College
The University of Iowa
Iowa City, Iowa

CERTIFICATE OF APPROVAL

_____

PH.D. THESIS

_____

This is to certify that the Ph. D. thesis of

Aislinn Joanmarie Williams

has been approved by the Examining Committee for the thesis requirement for the Doctor
of Philosophy degree in Neuroscience at the May 2010 graduation.

Thesis Committee: _____
                      Henry L. Paulson, Thesis Supervisor

                      _____
                      Beverly Davidson, Thesis Supervisor

                      _____
                      Steven Moore

                      _____
                      Peter Snyder

                      _____
                      Joshua Weiner

To my family

ACKNOWLEDGEMENTS

TABLE OF CONTENTS

LIST OF TABLES

Table

LIST OF FIGURES

Figure

CHAPTER 1

INTRODUCTION

Abstract

Collectively the polyglutamine (polyQ) expansion diseases are a major cause of neurodegeneration worldwide. Recent studies highlight the importance of protein quality control mechanisms in regulating polyQ-induced toxicity. This introductory chapter outlines a model of disease pathogenesis that integrates current understanding of the role of protein folding in polyQ disease with emerging evidence that alterations in native protein interactions of specific polyQ disease proteins contribute to toxicity. I also discuss evidence supporting the involvement of protein quality control machinery in the neuronal response to polyQ-mediated toxicity. Lastly, I incorporate new findings on other age-related neurodegenerative diseases in an effort to explain how protein aggregation and normal aging processes might be involved in polyQ disease pathogenesis.

Most of this chapter has been published in the following manuscripts:

Williams, A.J. and H.L. Paulson (2008) Polyglutamine neurodegeneration: Protein misfolding revisited. *TINS* 31: 521-528.

Todi, S.V., Williams, A.J. and H.L. Paulson (2007) Polyglutamine diseases, including Huntington's Disease. In *Molecular Neurology* (1st ed) (Waxman, S., ed.) pp. 257-275, Academic Press.

Introduction

The polyglutamine (polyQ) diseases represent an important cause of heritable neurodegeneration, comprising at least nine disorders (reviewed in Zoghbi and Orr, 2000; Fig. 1.1). All nine result from the expansion of a CAG repeat in the respective disease genes, encoding an abnormally long glutamine tract in the disease proteins. With one exception (the X-linked disorder SBMA), CAG/polyQ repeat expansions are transmitted to successive generations in affected families through an autosomal dominant manner. In all nine diseases, including SBMA, CAG/polyQ expansions act in a dominant toxic manner to cause disease. This shared mutation suggests a common pathogenic mechanism among the polyQ diseases, notwithstanding the fact that the pathogenic proteins are evolutionarily and functionally unrelated.

A decade ago, a clue to pathogenesis came from the discovery that expanded polyQ proteins accumulate within intraneuronal inclusions in select brain regions. This observation, coupled with *in vitro* experiments modeling polyQ protein aggregation, quickly led to the hypothesis that polyQ protein aggregation, and perhaps the inclusion itself, mediated neurodegeneration. The appeal of this hypothesis stemmed partly from the mechanistic link it suggested to other, more common age-related neurodegenerative disorders in which aggregates of specific proteins accumulate, including Alzheimer's disease (AD) and Parkinson's disease (PD).

Subsequently inclusions have fallen out of favor as a primary pathogenic entity. Many cell-based, animal model and human autopsy studies suggest that inclusions are simply the byproduct of abnormal protein accumulation or perhaps even a cytoprotective response that sequesters abnormal proteins (Arrasate et al., 2004; Rüb et al., 2006; Slow

et al., 2005; Saudou et al., 1998). This has led to understandable confusion in the field about whether protein misfolding and aggregation are indeed central to disease pathogenesis. Recent studies using divergent approaches, however, now support the importance of protein misfolding in polyQ disease pathogenesis. Here we synthesize these findings into a broader understanding of the role played by protein misfolding and aggregation in these intriguing neurodegenerative disorders, and place them in the larger context of age-related neurodegeneration.

Lots of Trouble From One Amino Acid

PolyQ diseases fall within the larger category of protein conformational brain disorders. As with most age-related neurodegenerative disorders, polyQ diseases are characterized by amyloid-like deposits of the disease protein in the central nervous system (CNS). Expanded polyQ proteins are prone to aggregate and, the longer the expansion, the more robust the aggregation. Disease severity also correlates directly with the length of the expansion, measured both by the age of symptom onset and by the extent of CNS pathology: longer repeats lead to earlier onset and more widespread degeneration. With the most common sized expansions, disease typically does not manifest until well into adulthood despite expression of the mutant protein throughout life.

Despite their presumably shared disease mechanism, polyQ diseases differ clinically and neuropathologically (Fig. 1.1). While many are degenerative spinocerebellar ataxias, one is primarily a motor neuron disorder (SBMA) and another is characterized by striatal and cortical degeneration (Huntington's disease, HD). This

preferential loss of specific neuronal populations occurs despite widespread expression of the disease proteins (Zoghbi and Orr, 2000). A closer look reveals that even the polyQ expansions differ somewhat among the diseases: although the commonly accepted disease threshold for glutamine repeats is ~37-40 residues, a much smaller repeat causes disease in one disorder (SCA6), and the encoded proteins normally contain glutamine repeats up to 42 residues in two others (SCA3, SCA17). Clearly, then, not all expansions are the same. The host protein context influences both the biochemical properties of expanded polyQ and, importantly, the resultant disease phenotype.

Many hypotheses have been put forward to explain polyQ disease pathogenesis. These hypotheses are by no means mutually exclusive. For any given polyQ disease more than one mechanism likely contributes to neuronal dysfunction and eventual cell death. They include: i) misfolding of the disease protein resulting in altered function, ii) deleterious protein interactions engaged in by the mutant protein, iii) formation of toxic oligomeric complexes; iv) transcriptional dysregulation, v) mitochondrial dysfunction resulting in impaired bioenergetics and oxidative stress, vi) impaired axonal transport, vi) aberrant neuronal signaling including excitotoxicity, vii) cellular protein homeostasis impairment, and viii) RNA toxicity (Todi et al., 2007; Gatchel and Zoghbi, 2005; Li et al., 2008; Bennett et al., 2007; Pandey et al., 2007) (Fig. 1.2).

Compelling data support each of these mechanisms in one or more polyQ diseases. But which among these are key, early events in polyQ neurodegeneration and which are secondary? As we discuss below, the most compelling argument can be made for a mechanism that combines the first three listed above: polyQ-induced

conformational changes in the disease protein resulting in altered and abnormal protein-protein interactions as outlined in Figure 1.3.

The identity of the putative toxic species in polyQ disorders has been the subject of much research and debate. The search for toxic species has been complicated by the fact that divergent results can be obtained with expanded polyQ peptides versus polyQ protein fragments versus full-length polyQ disease proteins. One possibility is that the polyQ disease protein (or a proteolytic fragment) itself is directly toxic, either as a misfolded monomer or homo-oligomeric complex. For example, Nagai and colleagues (2007) showed that misfolded beta-sheet-rich polyQ protein monomers and oligomers are toxic to cells, but properly folded alpha-helical polyQ monomers are not. The conformational change from alpha-helix to beta-sheet correlated with cellular toxicity, which agrees with the generally accepted view that expanded polyQ is prone to adopt a beta-sheet-rich conformation and assemble into amyloid-like complexes through a nucleation-seeded polymerization process. Based on calculations from *in vitro* reactions, a single abnormally folded monomer seeds the growth of larger oligomeric complexes and, ultimately, amyloid-like fibrils (Chen et al., 2002a and 2002b). The structure adopted by expanded polyQ, however, is still unknown. One crystallographic study of polyQ protein has been published, describing the structure of polyQ peptide bound to a polyQ-specific monoclonal antibody (Li et al., 2007b). In antibody-polyQ crystals, polyQ peptides have an extended linear shape. Surface plasmon resonance studies showed that isolated polyQ peptides and polyQ-expanded huntingtin possess similar antibody binding properties (Li et al., 2007b). These results suggest that polyQ proteins adopt the same shape regardless of repeat length, which would not support the model of a distinct, toxic

conformer. Structural studies using circular dichroism (Nagai et al., 2007), dynamic light scattering (Bulone et al., 2006), nuclear magnetic resonance (Klein et al., 2007) and simulation methods (Marchut and Hall, 2006) have reported a variety of possible polyQ structures, making it currently difficult to draw conclusions regarding local domain misfolding in polyQ disease proteins.

Many studies support the view that, as in AD, putative toxic oligomeric species exist somewhere upstream of amyloid fibrils along the aggregation pathway. For example, in cells overexpressing polyQ fusion proteins, fluorescence resonance energy transfer experiments demonstrate the formation of soluble oligomeric species whose appearance correlates with toxicity (Takahashi et al., 2008). Furthermore, in some mouse models of disease, polyQ protein microaggregates that are resistant to denaturing detergents accumulate before, or simultaneous with, the first signs of CNS dysfunction, consistent with their being causative pathogenic agents (Li et al., 2007a; Weiss et al., 2008).

Routes to Neuronal Toxicity

Is there, in fact, a single toxic polyQ species? In other words, is there a particular monomeric conformer or oligomer that, relative to other conformations or complexes generated by expanded polyQ proteins, is especially deleterious to neurons? Current evidence suggests that there probably is not a single neurotoxic species; rather, the situation is likely much more biologically complex. We favor the view that the toxicity of expanded polyQ proteins is a more general byproduct of the misfolded protein's propensity to engage in aberrant protein interactions, which can be deleterious whether

mediated by monomeric protein, by homo-oligomeric complexes, or by more subtle disruptions in the balance of heteroprotein complexes through which the native polyQ protein normally functions (Fig. 1.3). In short, there may be multiple, distinct, toxic polyQ species depending on a host of factors. The extent to which any of these occurs in a given disease will vary depending on the structural and functional properties of the protein, the size of the expansion, the protein's subcellular localization, the occurrence of proteolytic events that liberate polyQ fragments from the surrounding polypeptide, and the integrity of protein homeostatic pathways in the cell. In the case of extremely long expansions or those diseases in which proteolysis generates polyQ fragments (e.g. HD), a relatively high concentration of misfolded, unconstrained polyQ may favor the formation of homo-oligomeric complexes. For example, the detergent-resistant microaggregates observed in the R6/2 transgenic mouse, which expresses a very small fragment of mutant huntingtin, likely are homo-oligomers (Weiss et al., 2008). Indeed many studies in the field have relied on the analysis of polyQ protein fragments or isolated polyQ peptides, with which the formation of polyQ oligomers clearly occurs. In Chapters 2 and 3 of this dissertation, I will explore the role of microaggregates containing ataxin-3, the disease protein in spinocerebellar ataxia type 3 (SCA3), in disease pathogenesis.

By contrast, in the more typical disease state in which a modest expansion remains constrained within the full protein, a smaller fraction of the cellular pool of mutant protein will adopt an abnormal polyQ conformation. In this case, specific interactions ordinarily engaged in by the native polyQ protein will be altered more subtly and the mutant protein likely retains many normal functions; a good illustration is the fact that mutant huntingtin can compensate for the embryonic lethality of huntingtin knockout

mice. It is important to emphasize that, rather than being structural proteins or self-sufficient enzymes, most polyQ-containing proteins tend to be regulatory cofactors within macromolecular assemblies, often linked to gene regulation (Butland et al., 2007). Rather subtle changes in such assemblies could have tremendous consequences in neurons. These changes could occur through toxic gain of function in the polyQ disease protein, a loss of function, or both simultaneously.

A recent example of this is provided by the SCA1 disease protein, ataxin-1. Lim and colleagues (2008) showed that ataxin-1 exists in multiple heteroprotein complexes. PolyQ expansion in ataxin-1 promotes the formation of a complex containing RBM17, a putative RNA binding protein, which enhances neurotoxicity through an unknown gain of function. Simultaneously, polyQ expansion reduces the formation of an ataxin-1 complex containing the transcriptional repressor, Capicua, thereby exacerbating pathology through a loss of function (Lam et al., 2006). These results suggest a model of pathogenesis in which conformational changes in mutant ataxin-1 alter the balance of macromolecular assemblies through which this protein acts. The resultant imbalance has deleterious consequences for specific neurons including, in this instance, cerebellar Purkinje cells. Importantly, this model does not require global protein misfolding, widespread perturbations in cellular protein homeostasis, or even the formation of mutant ataxin-1 homo-oligomers.

Another example of polyQ-induced alterations in heteroprotein complexes was recently described for the SCA17 disease protein, TATA-box binding protein (TBP) (Friedman et al., 2007). TBP normally forms transcriptionally incompetent homodimers, preventing unregulated TBP activity. PolyQ expansion inhibits the formation of TBP

homodimers while promoting interaction with the transcription factor, TFIIB. These polyQ-TBP/TFIIB heterocomplexes lack normal DNA-binding capacity, resulting in reduced expression of TFIIB-dependent genes. SCA17 transgenic mice, like most animal models of polyQ disease, develop nuclear inclusions. However, this does not imply that inclusions are pathogenic structures: the presence of both TFIIB and TBP in inclusions may simply be the end-stage product of interactions initiated between the two proteins in the soluble, pre-aggregation state, as has been suggested elsewhere for expanded polyQ proteins that interact with transcription factors (Schaffar et al., 2004).

Additional illustrations of polyQ-induced changes in native protein complexes exist for the SCA7 and DRPLA disease proteins, ataxin-7 and atrophin, respectively (Palhan et al., 2005; Helmlinger et al., 2006; Zhang et al., 2002). While the examples discussed here involve transcriptionally active complexes, other expanded polyQ disease proteins not directly implicated in transcriptional regulation also may display alterations in the balance of native macromolecular complexes.

The above examples lead one to predict that interacting partners of polyQ proteins will often be genetic modifiers of pathogenesis. A recent study makes good on this prediction (Kaltenbach et al., 2007). Using complementary approaches, Hughes and colleagues identified 234 proteins that interact with the amino-terminal domain of huntingtin. When a subset of 60 interactors were tested in a *Drosophila* model of HD, a remarkably high percentage, 45%, proved to be genetic modifiers. Thus, many modifiers of polyQ toxicity will likely prove to be the very proteins with which the disease protein normally interacts. Translating the discovery of genetic modifiers from animal and

cellular models to the human diseases, in which (with few exceptions) genetic modifiers have not yet been identified, is a pressing area of investigation.

Evidence for Perturbations in Protein Homeostasis

The known functions of certain polyQ disease modifiers – which in some cases modulate the toxicity of multiple polyQ disease proteins – argue that polyQ-induced protein misfolding and resultant stress on protein homeostatic pathways play a central role in pathogenesis. Several classes of heat shock proteins (Hsp) have been extensively studied in the context of polyQ disease and are potent modulators of polyQ toxicity in cellular and animal models. They are divided into six classes, denoted by the approximate size of the protein in kilodaltons: HSP100, 90, 70, 60, 40 and smaller HSPs of less than 40 kD (Macario, 1995). Collectively these chaperones act cotranslationally on nascent polypeptide chains or posttranslationally on stress-denatured proteins.

If a protein does not fold properly despite the assistance of chaperones, it is often then degraded by the ubiquitin proteasome system (UPS), the key protein degradation pathway in the cell. Certain bifunctional proteins, like CHIP, link the chaperone system to the UPS. Other chaperones, like valosin-containing protein (VCP), facilitate the delivery of misfolded proteins in the ER to the cytosolic UPS (Jarosch et al., 2002; Rabinovich et al., 2002; Ye et al., 2001). This system, known as endoplasmic reticulum associated degradation (ERAD), has not been invoked as a major degradation route for most polyQ proteins. However, when the ERAD system is overwhelmed, cells turn on the ER stress response (Yoshida, 2007), which is also induced by many polyQ proteins (Reijonen et al., 2008; Kouroku et al., 2007; Thomas et al., 2005; Nishitoh et al., 2002;

Kouroku et al., 2002). The polyQ protein ataxin-3 is part of the machinery by which misfolded ER proteins get delivered to the proteasome (Zhong and Pittman, 2006; Wang et al., 2008). Another major route for abnormal protein elimination is lysosome-mediated autophagy, which engulfs and destroys damaged cellular components ranging from individual proteins to entire organelles. Increasing evidence suggests that autophagy plays a role in the destruction of polyQ proteins in at least some diseases (Ravikumar and Rubinsztein, 2004).

Only recently was the chaperonin, TRiC, identified as a suppressor of polyQ aggregation and toxicity. A hetero-oligomer of 16 subunits, TRiC forms a capsule with a central chamber reminiscent of the prokaryotic GroEL/GroES chaperonin complex. TRiC interacts with the Hsp network both by refolding substrates bound to Hsp70 and by functioning with Hsp70 in the assembly of oligomeric protein complexes (Melville et al., 2003; Fig. 1.4). TRiC was first identified as a modulator of polyQ protein aggregation in a genome-wide RNAi screen in *C. elegans* (Nollen et al., 2004). Three later studies sought to explain the mechanism by which TRiC suppresses polyQ toxicity. Kitamura et al. (2006) and Tam et al. (2006) demonstrated that TRiC prevents the formation of toxic misfolded polyQ intermediates, as assayed by a decrease in biochemically detectable protein aggregates and cellular toxicity (Fig. 1.4). Kitamura et al. (2006) concluded that the TRiC holocomplex was required for suppression, whereas Tam et al. (2006) showed suppression of polyQ toxicity simply by overexpressing the substrate binding domain of the TRiC subunit that bound polyQ substrates best. Behrends et al. (2006) concluded, somewhat differently, that TRiC does not reduce oligomer formation but rather cooperates with Hsp70 and Hsp40 to promote the formation of nontoxic oligomers over

toxic oligomers (Fig. 1.4). Taken together, these TRiC studies support a role for polyQ aggregation in toxicity and underscore the importance of protein quality control machinery in reducing that toxicity.

Recent genetic screens have expanded the range of modifiers to include additional classes of quality control proteins that maintain protein homeostasis, including ubiquitin-proteasome system components (Table 1.1). Some screens have identified still other genes that do not appear to function directly in protein quality control, including signal transduction pathway components, cytoskeletal proteins and transcription factors (Table 1.1). Although these proteins have diverse cellular functions, many have been shown to alter the aggregation state of polyQ protein in animal models, such as alpha- and beta-tubulin, and ribosomal components (Nollen et al., 2004; Bilen and Bonini, 2007).

Gidalevitz et al. (2006) asked a broader question: do expanded polyQ proteins cause unassociated proteins in the cell to misfold? That is, could the constant presence of a protein that is prone to misfold disrupt protein homeostasis throughout the cell? To answer this question, metastable temperature-sensitive proteins were expressed in worms with or without coexpressed polyQ protein. Co-expression of a polyQ protein fragment promoted the misfolding of temperature-sensitive proteins even at normally permissive temperatures. It is currently unknown whether this effect would manifest in cells expressing physiological levels of the implicated proteins, or whether there are similar endogenous, metastable proteins in neurons. Nevertheless, these results suggest a mechanism whereby polyQ proteins could wreak general havoc on cellular protein homeostasis, especially when proteolysis releases a highly aggregation-prone polyQ protein fragment. Importantly, even subtle impairment of cellular homeostasis could

disrupt the intricate balance of macromolecular complexes through which many polyQ proteins act.

Folding and Degradation Enzymes as Quality Control Partners

Quality control (QC) ubiquitin ligases, a special class of ubiquitin ligases that link protein refolding and protein degradation pathways, have recently emerged as modifiers of various age-related, neurodegenerative proteinopathies. This class of enzymes currently includes CHIP, parkin, and E4B, though others will likely be identified. Rather than simply ubiquitinating one or a few substrates, QC ubiquitin ligases act on a broader range of abnormally folded polypeptides. They accomplish this partly by constituting a scaffold that brings together components of protein refolding, most notably molecular chaperones, with ubiquitination machinery.

Among these, the C-terminus of Hsp70-interacting protein, CHIP, is of particular interest in proteinopathies. CHIP interacts with numerous neurodegenerative disease proteins, including polyQ disease proteins, and modulates their solubility and degradation (Miller et al., 2005; Jana et al., 2005; Shin et al., 2005; Dickey et al., 2006; Choi et al., 2007; Al-Ramahi et al., 2006; Kumar et al., 2007; Adachi et al., 2007). CHIP plays an important role in modulating the toxicity of all polyQ proteins with which it is known to interact. So far, these include huntingtin (Miller et al., 2005), ataxin-1 (Choi et al., 2007; Al-Ramahi et al., 2006), ataxin-3 (Jana et al., 2005), and androgen receptor (Adachi et al., 2007). Interestingly, CHIP's action on polyQ proteins is influenced by the substrate's protein context (Branco et al., 2008; Miller et al., 2005; Al-Ramahi et al., 2006), although

the mechanisms underlying this are not understood. In Chapter 2 of this dissertation, I will investigate the role of CHIP in modulating ataxin-3 toxicity and regulating microaggregate formation in the brain.

Currently, other ubiquitin ligases in this group are less well-studied with respect to polyQ diseases, but some connections have been made. In cell models, parkin reduces the aggregation and toxicity of polyQ-containing protein and colocalizes to inclusions in HD mouse and human disease brain (Tsai et al., 2003). E4B appears to be important for the degradation of the SCA3 disease protein, ataxin-3, and suppresses ataxin-3 toxicity in flies (Matsumoto et al., 2004). Finally, some evidence suggests that E6-AP is also a QC ubiquitin ligase, as it regulates the aggregation, degradation and toxicity of expanded huntingtin and ataxin-3 in cell models (Mishra et al., 2008) and the toxicity of expanded ataxin-1 in transgenic mice (Cummings et al., 1999). Much more work is still needed to identify the ligases and other factors mediating turnover of specific polyQ proteins.

Lessons from Other Age-Related Amyloidopathies

Mutant polyQ proteins adopt amyloid-like conformations (Nagai et al., 2007; Ellisdon et al., 2007; Diaz-Hernandez et al., 2005), suggesting that mechanistic insights from other amyloidopathies may shed light on polyQ disorders. In the most common CNS amyloidopathy, AD, the putative culprit is A-beta, a cleavage product of amyloid precursor protein (Walsh and Selkoe, 2007). Although extensive A-beta plaques accumulate in AD brain, soluble A-beta oligomers appear to be the principal neurotoxic species (Walsh and Selkoe, 2007). In the Tg2576 transgenic mouse model of AD, Lesné and colleagues (2006) reported an extracellular A-beta dodecamer, A-beta*56, whose

appearance in brain correlated with the onset of memory problems and which, when injected into rats, elicited similar cognitive deficits. More recently, toxic dimers have been reported in human AD brain samples (Shankar et al., 2008). Additional studies are needed to establish whether specific prefibrillar oligomeric forms of A-beta, including dimers or A-beta *56, are indeed the primary species underlying neurotoxicity in AD.

While these investigations suggest there are one or a few identifiable neurotoxic, oligomeric A-beta species, it is important to note that A-beta is a highly aggregation-prone, wholly amyloidogenic fragment of a protein, and is therefore likely to generate pure homo-oligomers of discrete size. In contrast, polyQ proteins tend to be much larger and, even when cleaved by intracellular proteases, the resultant polyQ fragments often retain substantial flanking sequences. Accordingly, they are less likely to aggregate into homogenous oligomers than A-beta. Nevertheless, polyQ proteins and their resultant aggregates have much in common with A-beta amyloid, and the methods used to identify specific A-beta oligomers, including conformational specific antibodies (Kayed et al., 2003; Kayed et al., 2007), might prove useful in detecting pathological polyQ species as well.

Another recent study linked A-beta aggregation to aging pathways in *C. elegans* (Cohen et al., 2006), a finding that may also shed light on the age-related nature of polyQ diseases (Fig. 1.5). In the major aging pathway in worms, the insulin/IGF-1 receptor *daf-2* inhibits the transcription factor, *daf-16*. *Daf-2* signaling is critical for normal aging: when *daf-2* is inhibited, worms live longer. Another transcription factor, *hsf-1*, is important for aging: inhibition of *hsf-1* blocks the lifespan extension resulting from *daf-2* inhibition. To complete the loop, *hsf-1* effects on aging are dependent on *daf-16*, the very

transcription factor that is inhibited by *daf-2* signaling. Importantly, this pathway regulates both the aging process and protein aggregation (Cohen et al., 2006). In worms treated with RNAi against *daf-2*, lifespan was extended and worms manifested A-beta toxicity at much later ages. Conversely, RNAi against either pro-longevity gene, *daf-16* or *hsf-1*, caused worms to manifest A-beta toxicity more severely and at younger ages. This increased A-beta toxicity directly correlated with increased levels of A-beta trimer, suggesting that trimers or some higher order structure composed of A-beta trimers (perhaps A-beta*56-like) is the toxic species.

Further investigation of the mechanism by which *hsf-1* and *daf-16* regulate A-beta toxicity revealed that *hsf-1* is important for dissociating protein aggregates, whereas *daf-16* enhances the aggregation of small toxic oligomers into larger, nontoxic fibrils (Cohen et al., 2006; Fig. 1.5). Thus, *daf-16* and *hsf-1* regulate distinct and complementary pathways that decrease levels of pathogenic A-beta aggregates and reduce the toxicity of aggregation-prone proteins.

Importantly, *hsf-1* and *daf-16* have also been shown to reduce polyQ aggregation in worms (Hsu et al., 2003). Because *hsf-1* and *daf-16* regulate protein aggregation pathways and aging pathways simultaneously, functional compromise of these systems during aging may explain why diseases of protein misfolding and aggregation manifest in an age-related manner. Lifespan extension in worms delays both polyQ aggregation and toxicity (Morley et al., 2002), suggesting that the studies linking A-beta aggregation and aging will inform our understanding of how these two processes are linked in polyQ disease as well.

Rationale and Aims of the Thesis

Our lab is interested in how protein quality control mechanisms in the cell regulate protein misfolding and aggregation in polyQ disease. We use SCA3 as a model polyQ disease because the disease protein, ataxin-3, has several interesting qualities. It normally functions in several protein quality control pathways (discussed in Chapters 3 and 4) and it also suppresses the toxicity of other polyQ disease proteins (Warrick et al., 2005). Moreover, ataxin-3 is known to self-associate *in vitro* with or without polyQ expansion (Gales et al., 2005; Ellisdon et al., 2006). Given our interest in both ataxin-3 function and SCA3, we wanted to investigate the role of protein quality control mechanisms in SCA3 pathogenesis, and to identify the toxic protein species responsible for neuronal dysfunction in SCA3.

Overall, the studies presented here describe the role of oligomerization and protein aggregation in SCA3 pathogenesis using multiple transgenic mouse models. In Chapter 2 I investigate the role of the protein quality control ubiquitin ligase and co-chaperone CHIP in ataxin-3 aggregation and SCA3 pathogenesis, using SCA3 transgenic mice as a model. In Chapter 3, I identify and analyze putative toxic protein intermediates in SCA3 using two genetically different SCA3 transgenic mouse models. Using brain tissue from phenotypically expressing SCA3 mice, I also investigate in Chapter 3 whether overexpression of polyQ-expanded ataxin-3 alters the localization or protein complexes formed by ataxin-3 or its interacting proteins.

Table 1.1. Genetic modifiers of polyglutamine toxicity in animal models.

Name	Class	Function	Effect on PolyQ Toxicity	Animal Model	Refs
Hsp70	Chaperone	Binds unfolded proteins, ATP hydrolysis	Suppressor	fly, worm	Nollen et al., 2004; Bilen and Bonini, 2007; Branco et al., 2008
Hsp60/ TRiC/ CCT	Chaperone	Binds unfolded proteins, ATP hydrolysis	Suppressor	worm	Nollen et al., 2004
Hsp40	Chaperone	Binds unfolded proteins, co-chaperone for Hsp70	Suppressor	fly, worm	Nollen et al., 2004; Bilen and Bonini, 2007; Branco et al., 2008
alpha-B-crystallin	Chaperone	Small heat-shock protein	Suppressor	fly	Bilen and Bonini, 2007
VCP	Chaperone, ERAD	translocation of substrates from ER to cytosol, ATP hydrolysis	Suppressor	fly	Boeddrich et al., 2006
CHIP	Chaperone UPS	Bind chaperones, ubiquitin ligase	Suppressor	fly, mouse	Branco et al., 2008; Miller et al., 2005; Adachi et al, 2007
E6-AP	Chaperone UPS	Ubiquitin ligase, may functionally interact with Hsp70	Suppressor	mouse	Cummings et al., 1999
E4B	UPS	Ubiquitin ligase	Suppressor	fly	Matsumoto et al., 2004
Ubiquitin	UPS	Targets proteins for degradation, various cellular processes	Suppressor	fly, worm	Nollen et al., 2004; Branco et al., 2008
Uba	UPS	Ubiquitin activating enzyme	Suppressor	worm	Nollen et al., 2004
Ubc-E2H	UPS	Ubiquitin conjugating enzyme	Suppressor	fly	Branco et al., 2008
Usp9X/fat facets	UPS	Deubiquitinating enzyme	Suppressor	fly	Kaltenbach et al., 2007; Bilen and Bonini, 2007

Table 1.1. Continued.

Proteasome core subunits	UPS	Protein degradation	Suppressor	worm	Nollen et al., 2004
Proteasome cap subunits	UPS	Regulation of proteasome activity	Variable (depends on specific cap subunit)	fly, worm	Kaltenbach et al., 2007; Nollen et al., 2004
Atg proteins (atg6, atg7, atg12, atg18)	Autophagy	Components of autophagic cycle	Suppressor	fly, worm	Pandey et al., 2007; Jia et al., 2007
HDAC6	Autophagy	Histone deacetylase	Suppressor	fly	Pandey et al., 2007
14-3-3	Signal transduction	Binds phosphorylated proteins	Enhancer	fly	Kaltenbach et al., 2007; Branco et al., 2008
Akt	Signal transduction	Serine/threonine kinase	Variable (depends on polyQ disease)	fly	Branco et al., 2008
RhoGAP	Signal transduction	Regulates GTPases	Enhancer	fly	Branco et al., 2008
Tubulins	Cytoskeleton	Vesicle trafficking, cell structure	Suppressor	worm	Nollen et al., 2004
Exportin-1	Nuclear export	Binds and transports proteins	Suppressor	fly	Bilen and Bonini, 2007
HSF-1	Transcription factor	Regulates chaperone expression	Suppressor	worm	Nollen et al., 2004
Ribosom-al proteins	Protein synthesis	Protein synthesis, binds mRNA	Suppressor	worm	Nollen et al., 2004

Note: Genetic screening in animal models has identified multiple gene families that modulate polyQ toxicity, including genes encoding chaperones, components of the ubiquitin proteasome system (UPS) and endoplasmic reticulum associated degradation (ERAD), proteins implicated in RNA metabolism, and proteins of diverse signal transduction pathways. A unifying feature of many implicated modifier genes is involvement in the maintenance of cellular proteostasis. This table is a representative listing, restricted to modifier genes that are 1) directly involved in cellular protein quality control, 2) have been identified in multiple animal models, or 3) have been shown to regulate polyQ protein aggregation.

Disease	Protein Name	Protein Size, PolyQ Position and Disease Repeat Range	Protein Function
SBMA	Androgen Receptor	40-62	Testosterone-activated steroid receptor
HD	Huntingtin	36-121	Possible scaffolding protein linked to diverse cellular pathways
DRPLA	Atrophin-1	49-88	Possible transcriptional co-repressor
SCA1	Ataxin-1	39-91	Transcriptional co-repressor involved in transcription regulation, cell specification, synaptic activity
SCA2	Ataxin-2	32- ~200	Component of RNA processing and translational regulation pathways
SCA3	Ataxin-3	52-86	Deubiquitinating enzyme involved in protein quality control
SCA6	P/Q type Calcium Channel Subunit α1A	20-33	Voltage-sensitive calcium channel subunit
SCA7	Ataxin-7	34- ~300	Component of histone acetyl-transferase complex (TFTC/STAGA) and transcriptional regulation pathways
SCA17	TATA-box Binding Protein	47-63	Component of core transcriptional complex TFIID

Figure 1.1. Polyglutamine disease proteins and their functions. The nine known polyQ diseases are listed along with their causative proteins, the protein's relative size compared to other polyQ disease proteins, and their putative functions. Gold bars represent the relative location of the polyQ repeat in each protein, with the gold arrows indicating the range of repeat lengths that have been associated with disease in humans. While polyQ repeat length is stable within an individual (with some modest somatic mosaicism), polyQ repeat length can vary between generations. SBMA, spinobulbar muscular atrophy; HD, Huntington's disease; DRPLA, dentatorubral-pallidoluysian atrophy; SCA, spinocerebellar ataxia. From Williams, A.J. and H.L. Paulson (2008) *TINS* 31: 521-528.
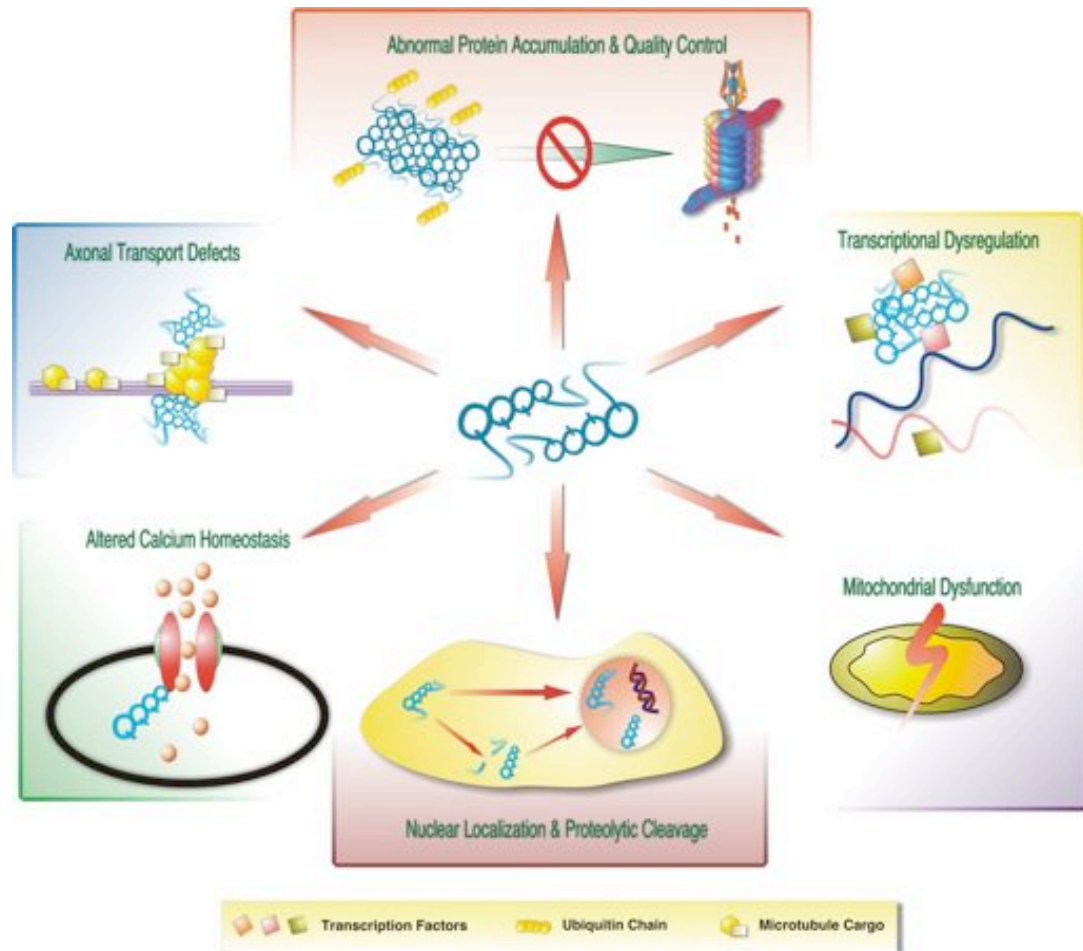
Figure 1.2. Potential mechanisms to explain polyglutamine toxicity. As shown in the center, a toxic conformation of expanded polyQ, either monomeric or oligomeric, is thought to underlie pathogenesis. As shown from the top, all polyQ diseases demonstrate accumulation of toxic protein and some degree of impairment in protein quality control, either in proteasomal degradation (as pictured) or in chaperone-mediated refolding (not shown). Moving clockwise, evidence suggests transcriptional dysregulation in many polyQ diseases, pictured here as polyQ disease proteins abnormally interacting with transcription factors. PolyQ-mediated mitochondrial dysfunction may occur through a variety of pathways, though these are currently less well defined than those for other potential mechanisms listed. Nuclear localization of full-length, mutant protein or cleavage fragments (as in HD) -- a recurrent theme in polyQ diseases – may contribute to transcriptional dysregulation and/or interference with other normal nuclear functions. Altered calcium homeostasis may be an intrinsic feature of SCA6, as the mutation is in a calcium channel, although there is also evidence for its importance in HD. Lastly, axonal transport defects are an important cause of neurodegeneration beyond polyQ disorders; the extent to which they represent a pathogenic feature in polyQ diseases is under investigation. From Todi, S.V., Williams, A.J. and H.L. Paulson (2007) Molecular Neurology (1st ed) (Waxman, S., ed.) pp. 257-275, Academic Press.
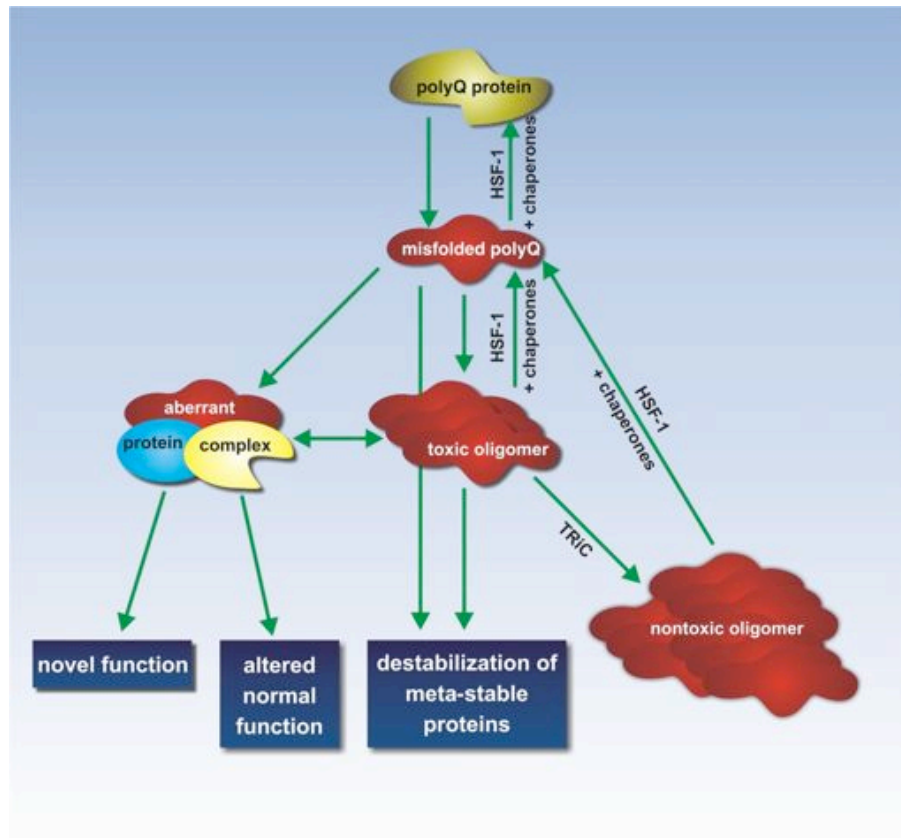
Figure 1.3. Possible cellular sequelae of expanded polyQ protein misfolding. PolyQ proteins, when expanded, are prone to misfold. HSF-1 can trigger the expression of certain chaperones, including Hsp70 and Hsp40, which help refold misfolded polyQ proteins. When misfolded polyQ monomers form oligomers, chaperones can help to dissociate them. Misfolded monomers can also form complexes with other proteins. These heteroprotein complexes may be aberrant in that they involve 1) imbalances in the levels of normally-occurring protein complexes, or 2) the generation of novel protein complexes. These aberrant complexes may also cause the affected proteins to adopt novel functions or alter their normal functions. Oligomers may interact with cellular proteins to cause similar alterations in function, though currently there is no direct experimental evidence. Some protein quality control components, such as the TRiC chaperonin complex, may reduce the toxicity of oligomers by changing their size and conformation. Based on current evidence, we suggest misfolded, polyQ-expanded monomers and resultant oligomers display reactive, accessible polypeptide surfaces that cause neuronal dysfunction and ultimately cell death. From Williams, A.J. and H.L. Paulson (2008) *TINS* 31: 521-528.
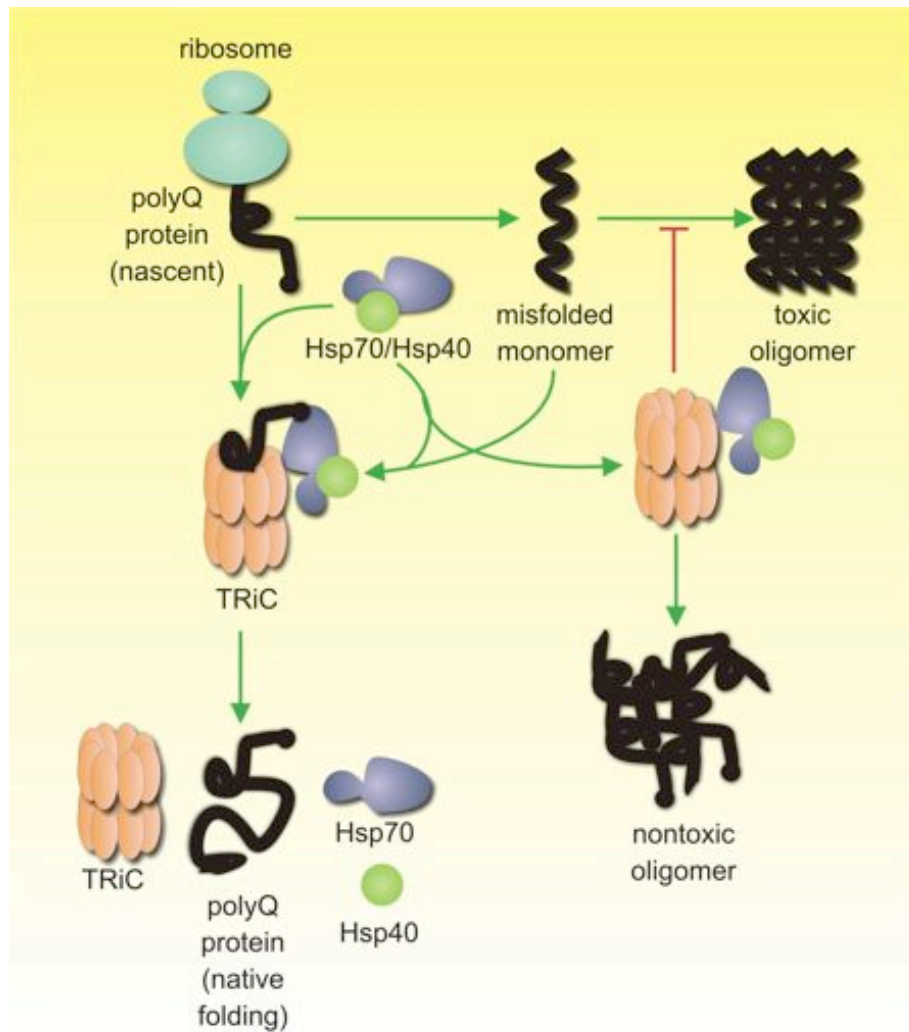
Figure 1.4. The eukaryotic chaperonin, TRiC, works with Hsp70 and Hsp40 to promote nontoxic protein folding. Proteins forming at the ribosome often require chaperones and other protein quality control machinery to fold correctly. Members of the Hsp70 family of chaperones bind unfolded proteins and work with Hsp40 co-chaperones and the eukaryotic chaperonin, TRiC, to fold nascent proteins at the ribosome. This TRiC/Hsp70/Hsp40 protein folding complex interacts with misfolded cytosolic proteins by two mechanisms: 1) bind misfolded proteins and facilitate their refolding; 2) consolidate misfolded monomers into nontoxic larger protein aggregates. Although the ability of TRiC to promote the formation of nontoxic large aggregates has only been studied thus far with polyQ proteins, the effect likely extends to other misfolded proteins as well.
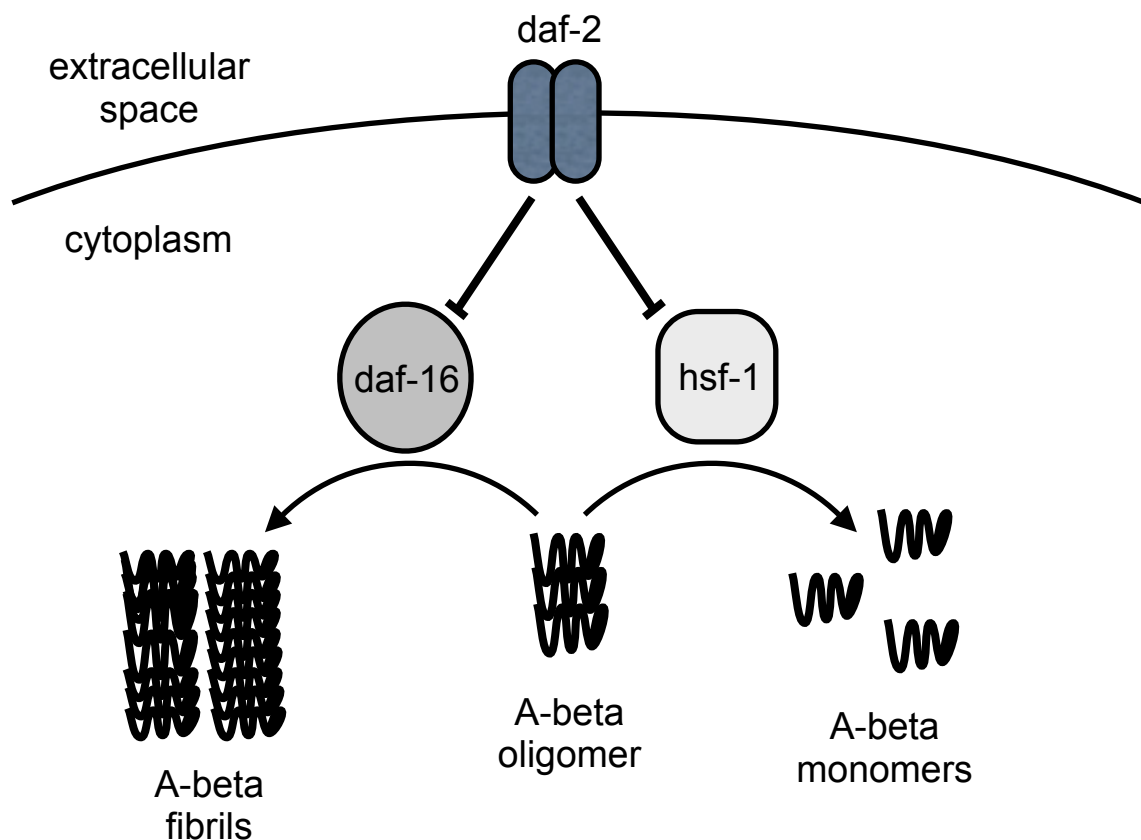
Figure 1.5. The insulin growth factor signaling pathway targets daf-16 and hsf-1 inhibit amyloid oligomer toxicity in two ways. In worms, the insulin growth factor receptor, *daf-2*, inhibits both *daf-16* and *hsf-1* function. When *daf-2* is mutated, not only do worms live longer (not pictured), but *daf-16* and *hsf-1* can then function to prevent toxic A-beta aggregate formation. The action of *hsf-1* causes a decrease in A-beta oligomeric species and an increase in A-beta monomers. On the other hand, *daf-16* causes A-beta oligomers to aggregate further into nontoxic amyloid fibrils, thereby decreasing the amount of toxic oligomers present. Cohen et al. (2006) propose that these two systems work simultaneously to prevent the accumulation of misfolded proteins in the cell, with the *hsf-1* pathway being preferred, and the *daf-16* pathway kicking in when the *hsf-1* pathway gets overwhelmed. Since both *daf-16* and *hsf-1* have been shown to decrease polyQ toxicity in the worm (Hsu et al., 2003), these pathways may also prevent polyQ toxicity by decreasing toxic polyQ oligomer concentrations in the cell.

CHAPTER 2

IN VIVO SUPPRESSION OF POLYGLUTAMINE

NEUROTOXICITY BY C-TERMINUS OF HSP70

INTERACTING PROTEIN (CHIP) SUPPORTS AN

AGGREGATION MODEL OF PATHOGENESIS

Abstract

Perturbations in neuronal protein homeostasis likely contribute to disease
pathogenesis in polyglutamine (polyQ) neurodegenerative disorders. Here we provide
evidence that the co-chaperone and ubiquitin ligase, CHIP (C-terminus of Hsp70-
interacting protein), is a central component to the homeostatic mechanisms countering
toxic polyQ proteins in the brain. Genetic reduction or elimination of CHIP accelerates
disease in transgenic mice expressing polyQ-expanded ataxin-3, the disease protein in
Spinocerebellar Ataxia Type 3 (SCA3). In parallel, CHIP reduction markedly increases
the level of ataxin-3 microaggregates, which partition in the soluble fraction of brain
lysates yet are resistant to dissociation with denaturing detergent, and which precede the
appearance of inclusions. The level of microaggregates in the CNS, but not of ataxin-3
monomer, correlates with disease severity. Additional cell-based studies suggest that
either of two quality control ubiquitin ligases, CHIP or E4B, can reduce steady state
levels of expanded, but not wild-type, ataxin-3. Our results support an aggregation model
of polyQ disease pathogenesis in which ataxin-3 microaggregates are a neurotoxic
species, and suggest that enhancing CHIP activity is a possible route to therapy for SCA3
and other polyQ diseases. These results have been published in the following manuscript:

Williams, A.J., Knutson, T.M., Colomer Gould, V.F. and Paulson, H.L. (2008) In vivo suppression of polyglutamine neurotoxicity by C-terminus of Hsp70 interacting protein (CHIP) supports an aggregation model of pathogenesis. *Neurobiol. Dis.*, in press.

Introduction

The crowded intracellular environment presents obstacles to proper folding of proteins. Accordingly, cells contain a molecular chaperone network that facilitates protein folding and promotes degradation of misfolded proteins. Its importance in the nervous system is highlighted by various neurodegenerative disorders, in which protein conformational defects cause detrimental accumulation of misfolded or aggregated protein. Protein misfolding and aggregation may underlie neurodegeneration in diseases such as Parkinson's disease, Alzheimer's disease and the polyglutamine (polyQ) diseases (Taylor et al., 2002; Selkoe, 2004; Walsh and Selkoe, 2004). Although protein aggregation occurs in all of these diseases, how protein misfolding and aggregation damages neurons is unclear. In the polyQ diseases, moreover, it is unknown which protein species are neurotoxic: monomers, oligomers, or higher order aggregates.

Aggregation is a common byproduct of protein misfolding, suggesting that protein quality control (PQC) systems are important in countering diseases where aggregation occurs. Two PQC pathways implicated in disease are the molecular chaperone system and the ubiquitin-proteasome pathway (Bence et al., 2001; Hay et al., 2004; Marques et al., 2006). The cochaperone and ubiquitin ligase, CHIP, links these two systems. Through its N-terminus, CHIP binds heat shock proteins and modulates protein refolding (Ballinger et al., 1999; Connell et al., 2001). Through its C-terminus, CHIP

ubiquitinates substrates and targets them for degradation (Connell et al., 2001; Meacham et al., 2001).

The dual roles of CHIP in chaperone- and ubiquitin-dependent pathways suggest it might be important in neuronal PQC. Numerous studies support a role for CHIP in countering neurodegenerative diseases. For example, CHIP enhances the activity of parkin, a protein associated with recessive parkinsonism (Imai et al., 2002), and regulates the degradation of phosphorylated tau, a protein implicated in various neurodegenerative diseases (Dickey et al., 2006; Dickey et al., 2007a). Although CHIP modulates the toxicity of several polyQ disease proteins (Jana et al., 2005; Miller et al., 2005; Al-Ramahi et al., 2006; Choi et al., 2007; Branco et al., 2008), the precise role of CHIP in polyQ diseases is difficult to delineate because it may regulate polyQ proteins differently depending on protein context (Al-Ramahi et al., 2006; Bulone et al., 2006; Dickey et al., 2007b; Branco et al., 2008).

Expansion of the polyQ domain in the ataxin-3 protein causes the polyQ disease, SCA3. While normal ataxin-3 can self-associate (Gales et al., 2005), polyQ expansion enhances its aggregation and promotes amyloid-like aggregate formation (Chow et al., 2004; Ellisdon et al., 2006). Here, we used transgenic mice expressing full-length expanded ataxin-3 (Goti et al., 2004) as a disease model of polyQ protein misfolding to: 1) define the role of CHIP in disease and 2) identify putative toxic protein species in SCA3. We find that CHIP regulates the level of expanded (pathogenic) ataxin-3 in neuronal cells, and the solubility of expanded ataxin-3 in the brain. Additionally, reduction in CHIP expression enhances expanded ataxin-3 toxicity *in vivo*. Since CHIP

reduction exacerbates the disease phenotype and increases microaggregate levels in the brain, our results support an aggregation-based model of polyQ disease pathogenesis.

Methods

Mouse strains. Q71-B hemizygous mice, a mouse model of SCA3/MJD (Goti et al., 2004) were bred to *CHIP* haploinsufficient mice (Dai et al., 2003) to obtain Q71-B hemizygous transgenic/*CHIP* haploinsufficient mice ($Q^{+/-}C^{+/-}$). These F1 progeny were bred to *CHIP* haploinsufficient mice to obtain F2 generation Q71-B mice with zero, one or two *CHIP* alleles. Mice were genotyped by standard two-way PCR as previously described (Goti et al., 2004; Dai et al., 2003). Q71-B/*CHIP* mice were maintained on a mixed genetic background (C3H/HeJ/C57BL6 x 129SvEv/C57BL6). Survival analysis was performed by determining how many animals of each genotype died by 12 months of age, excluding animals that were euthanized for tissue collection at predetermined time points. This was plotted as the percentage of animals of that genotype still alive at a specific month of age.

Rotarod analysis. Mice were trained on an accelerating rotarod apparatus (Ugo Basile, Comerio, Italy) for 2 days prior to testing. Training consisted of acclimating animals to the rotarod for 2 trials per day with 10 minutes rest between trials. For testing, the apparatus was set to accelerate from 3 to 30 rpm over the course of 5 minutes. Animals performed 3 trials with at least 10 minutes rest between trials. Trials ended when animals fell off the rod, began to rotate passively (i.e. clinging to the rod as it rotated) or completed the trial.

Open field analysis. Animals were tested for spontaneous activity using the Open Field

16x16 Photobeam Activation System and Flex-Field software (San Diego Instruments,

San Diego, CA). Naïve animals were placed into a 41cm x 41cm clear plastic box inside

a 16x16 array of infrared beams, and movement was calculated as the number and

sequence of beam breaks over the course of 30 minutes. Animals were tested under dark

conditions during their dark cycle (between 18:30-22:30 hrs).

Statistical Analysis. Statistical analyses were performed using Microsoft Excel with the

Data Analysis ToolPak. Behavioral data were grouped by age and genotype, then tested

for significance with a two-way ANOVA for independent samples. When main effects

were significant at $p < 0.05$, they were also tested by one-way ANOVA for independent

samples, then significant differences were further tested post-hoc using Tukey's Honestly

Significant Difference (HSD, calculated online at

http://web.mst.edu/~psyworld/virtualstat/tukeys/tukeycalc.html).

Echocardiography. Echocardiography was performed in sedated mice as previously

described (Weiss et al., 2006). Mice were sedated with midazolam, and a 15 MHz linear

array probe was applied horizontally to the chest. The imaging probe was coupled to a

Sonos 5500 imager (Philips Medical Systems, Bothell, WA), generating ~180-200 two-

dimensional frames per second in both short- and long-axis LV planes. Images were

acquired and analyzed in blinded fashion with custom-designed software (Freeland

Medical Systems, Louisville, CO). Endocardial and epicardial borders were traced in the

short-axis plane at end-diastole and end-systole. The lengths from left ventricular outflow tract to endocardial apex and epicardial apex, respectively, were measured at end-diastole and end-systole. The bi-plane area-length method (Hill et al., 2000) was used to calculate end-diastolic and end-systolic left ventricular volumes and ejection fraction.

Immunohistochemistry and immunofluorescence. Mice were perfused transcardially with cold sterile PBS followed by 4% paraformaldehyde in PBS. Brains were fixed overnight in 4% paraformaldehyde, rinsed in PBS overnight, then cryoprotected in 30% sucrose for at least 18 hrs at $4^{o}C$. Brains were cut serially into $30\mu m$ floating sections on a sledge microtome (Leitz) and stored at $-20^{o}C$ in cryoprotectant (5mM sodium phosphate pH 7.4, 75mM sodium chloride, 30% w/v sucrose, 30% v/v ethylene glycol) until use. For DAB immunohistochemistry with polyclonal antibodies, sections were blocked in H_2O_2 to quench endogenous peroxidase activity, then blocked in 5% normal goat serum and incubated in primary antibody (rabbit anti-MJD 1:1000 (Paulson et al., 1997a) or rabbit anti-ubiquitin 1:500 (Dako USA, Carpinteria, CA)). Sections were rinsed and incubated in biotinylated goat-anti-rabbit 1:500 (Vector Laboratories, Burlingame, CA), then developed in 0.5mg/ml DAB (Sigma, St. Louis, MO) with 9% H_2O_2, rinsed and mounted on gelatin-coated slides. For DAB immunohistochemistry with monoclonal GFAP-Cy3 antibody (Sigma), we used the Mouse-on-Mouse Peroxidase Kit (Vector Laboratories) according to manufacturer's instructions. To quantify ubiquitin-positive inclusions, every 24th section of the brain was stained for ubiquitin and the total number of inclusions in sections of pontine nuclei were counted. For immunofluorescence, samples were fixed in 4% paraformaldehyde, rinsed in PBS, then incubated overnight with primary antibodies

in 5% normal goat serum: anti-FLAG antibody for cell culture experiments (mouse anti-

FLAG M5, Sigma, 1:500) or, for brain immunofluorescence, a combination of rabbit

anti-ubiquitin (Dako, 1:500) and mouse anti-ataxin-3 (1H9, provided by Y. Trottier,

1:500). The next day, samples were rinsed and incubated in fluorescent secondary

antibodies (goat anti-mouse Alexa 488 with or without goat anti-rabbit Alexa 568,

Molecular Probes, Carlsbad, CA, 1:500) and nuclei were counterstained with DAPI

(Sigma). Cells were coverslipped and sealed with Vectashield Hard-Set fluorescence

mounting medium (Vector Laboratories).

Tissue collection and lysates. Mice were perfused transcardially with 20ml cold sterile

PBS plus protease inhibitor cocktail (PI) (Complete Mini tablets, Roche, Indianapolis,

IN). Whole tissues were dissected, minced in RIPA (50mM Tris-HCl pH 7.4, 150mM

sodium chloride, 0.1% SDS, 0.5% sodium deoxycholate, 1% NP-40) with PI, then

homogenized in a Dounce homogenizer in RIPA plus PI lysis buffer. Lysates were

diluted to 100mg/ml (based on wet weight) in RIPA plus PI lysis buffer and centrifuged

at 4000 rpm for 15 minutes at 4°. The pellet was rehomogenized in the same volume of

RIPA plus PI. Lysates were stored at -80° until use.

Western blot analyses. Soluble fractions were sonicated twice for 10 seconds each, then

spun at 15,000xg for 10 minutes at 4^oC to remove particulate debris (these pellets were

not saved). Pellets from first 4000 rpm spin were vortexed and sonicated vigorously.

Samples were diluted 1:1 in 2X Laemmli buffer plus DTT, then separated on

discontinuous 10% or 12% acrylamide gels, or pre-cast 4-20% SDS Tris-HCl gradient

gels (BioRad), and transferred to PVDF membranes. For SDS-agarose gels, gels

contained 1.5% w/v high-melting-point agarose (ISC Bioexpress, Kaysville, UT) in TAE

buffer (40mM Tris-acetate, 1mM EDTA) with 0.1% SDS. SDS-agarose gels were run in

protein running buffer (5mM Tris base, 38mM glycine, 0.02% SDS) and transferred to

PVDF membranes using a BioRad TransBlot SD semi-dry apparatus in a discontinuous

buffer system (cathode buffer: 12mM Tris base, 8mM CAPS, 0.1% SDS; anode buffer:

12mM Tris base, 8mM CAPS, 15% methanol) (Bagriantsev et al., 2006). Membranes

were briefly rinsed in Tween-TBS, blocked in 5% milk in Tween-TBS, and probed with

the following primary antibodies: rabbit anti-human MJD 1:20,000 (Paulson et al.,

1997a), mouse anti-polyglutamine 1:2000 (1C2, Chemicon, Temecula, CA), mouse anti-

GAPDH 1:500 (Chemicon), rabbit anti-CHIP 1:1000 (Calbiochem, San Diego, CA),

rabbit anti-CHIP 1:1000 (abcam, Cambridge, MA), mouse anti-Hsp90 1:1000 (SPA-830,

Stressgen, Ann Arbor, MI), mouse anti-Hsp70 1:1000 (SPA-810, Stressgen), rabbit anti-

Hsp40 1:10,000 (Stressgen), rabbit anti-Bag-1 1:1000 (Santa Cruz Biotechnology, Santa

Cruz, CA), mouse anti-Hop 1:1000 (SRA-1500, Stressgen), mouse anti-E4B 1:500 (BD

Biosciences, San Jose, CA), or mouse anti-alpha-tubulin 1:20,000 (Sigma). Membranes

were rinsed in milk and incubated in peroxidase-conjugated goat anti-rabbit or goat anti-

mouse secondary antibodies 1:15,000 (Jackson Immunoresearch, West Grove, PA) and

imaged by enhanced chemiluminescence (Western Lightning, Perkin Elmer, Waltham,

MA). Quantification of immunoblots was performed with NIH ImageJ software (NIH,

Bethesda, MD).

Size exclusion chromatography. Soluble fractions of brain lysates were sonicated and centrifuged at 15,000x*g* for 10 min. 200μl of this lysate was loaded onto a Waters BioSuite 450 column (Milford, MA), and run in mobile phase buffer (150mM sodium chloride, 50mM sodium phosphate, pH 7.4) at 0.5ml/min. Fractions were collected every 2 minutes, and precipitated with 14% trichloroacetic acid for 30 min on ice. Fractions were centrifuged at 15,000x*g* for 30 min at 4°C, pellets were washed twice with ice-cold acetone, and then were resuspended in 2X Laemmli buffer plus DTT. Fractions were analyzed by SDS-PAGE on 10% polyacrylamide gels, and processed by Western blot for ataxin-3. Column was calibrated with NativeMark protein standards (Invitrogen, Carlsbad, CA).

Denature/renature immunoprecipitation. 200μl brain lysate was sonicated and centrifuged as described above and diluted with 800μl RIPA buffer. Samples were denatured with SDS (1% final concentration) for 30 minutes at room temperature, then renatured with Triton X-100 (4.5% final concentration) for 30 minutes at room temperature. Ataxin-3 was immunoprecipitated from each lysate with 4μl MJD antibody and 25μl EZview Red Protein A Affinity Gel beads (Sigma) for 4 hours at 4°C. Beads were washed 4 times with cold RIPA buffer, then protein was eluted with 60μl 2X Laemmli buffer plus DTT by boiling for 2 minutes.

Cell culture and transfection. FLP-In HEK-293 cells (Invitrogen) were engineered to stably express FLAG-tagged ataxin-3 with either 22 or 80 glutamine repeats, as described (Todi et al., 2007). FLP-In HEK-293 cells were maintained in complete FRT medium

(DMEM, 10% fetal bovine serum, 1% penicillin/streptomycin, 0.2% hygromycin B).
M17 human neuroblastoma cells were maintained in DMEM supplemented with 10%
fetal bovine serum and 1% penicillin/streptomycin. Cells were transfected with
Lipofectamine PLUS (Invitrogen) according to the manufacturer's recommendations.
The following constructs were used, alone or in combination: empty pcDNA3.1 vector,
FLAG-ataxin-3-Q25, FLAG-ataxin-3-Q80, pcDNA3.1-CHIP (provided by C. Patterson,
Chapel Hill, NC), and pCMV-HA-E4B (provided by K. Nakayama, Fukuoka, Japan). For
steady-state ataxin-3 level experiments in M17 cells, constructs were expressed for 48 hr
prior to cell harvest.

Pulse-chase analysis. FLP-In HEK-293 cells stably expressing FLAG-ataxin-3-Q22 or
FLAG-ataxin-3-Q80 were transiently transfected with empty pcDNA3.1 vector,
pcDNA3.1-CHIP or pCMV-HA-E4B. Forty-eight hr after transfection, cells were starved
for 30 minutes in DMEM without methionine and cysteine (Gibco, Carlsbad, CA)
supplemented with 2mM glutamine (Gibco). Cells were pulsed for 40 minutes in
starvation medium plus ^{35}S-labeled methionine and cysteine mix ($0.22\mu Ci/\mu l$ in a 60cm
dish, EasyTag EXPRESS Protein Labeling Mix, Perkin Elmer), then chased for 0, 8 or 24
hr in complete FRT medium supplemented with 2mM unlabeled methionine and cysteine.
Cells were harvested from plates in PBS plus PI, lysed in RIPA plus PI, then subjected to
immunoprecipitation using EZview Red ANTI-FLAG M2 Affinity agarose gel (Sigma)
and subsequent elution with 3X FLAG peptide (Sigma). Immunopurified samples were
run on 12% SDS-PAGE gels for autoradiography, and autoradiograms were analyzed
with NIH ImageJ software.

Results

Reduction or absence of CHIP worsens polyQ disease in Q71-B transgenic mice.

Because CHIP has been shown to regulate polyglutamine toxicity (Miller et al., 2005;

Jana et al., 2005; Al-Ramahi et al., 2006; Choi et al., 2007), we hypothesized that

reducing CHIP would exacerbate the phenotype of Q71-B mice, a cDNA transgenic

model of SCA3/MJD (Goti et al., 2004). These mice overexpress human expanded, full

length ataxin-3 with 71 glutamine repeats, which is within the pathologic range of

glutamine expansion for SCA3 in humans. Hemizygous Q71-B mice ($Q^{+/-}$) were crossed

with *CHIP*-deficient mice to generate Q71-B mice with zero ($C^{-/-}$), one ($C^{+/-}$) or two

alleles ($C^{+/+}$) of *CHIP*. Q71-B hemizygous mice with a full complement of CHIP ($Q^{+/-}$

$C^{+/+}$) are phenotypically indistinguishable from wild-type mice ($Q^{-/-}C^{+/+}$) (Fig. 2.1),

consistent with the initial report of hemizygous Q71-B mice indicating no behavioral

phenotype and a normal life span (Goti et al., 2004). In contrast, hemizygous Q71-B mice

lacking CHIP ($Q^{+/-}C^{-/-}$) develop severe, progressive neurologic deficits including

kyphosis, pelvic depression, hindlimb splaying and whole body tremor, dying at 3-6

months (Fig. 2.1). Q71-B mice with a single *CHIP* allele ($Q^{+/-}C^{+/-}$) display an

intermediate phenotype: while they do not die prematurely, they start to develop mild,

progressive motor incoordination around 6 months of age and an action-dependent, body

tremor by 9 months of age (Fig. 2.1A). *CHIP*-null mice that do not express expanded

ataxin-3 ($Q^{-/-}C^{-/-}$) occasionally develop kyphosis but without premature death, tremor, or

other neurological signs (Fig. 2.1B-C).

In CHIP-haploinsufficent Q71-B mice ($Q^{+/-}C^{+/-}$), we searched for milder,

quantifiable motor deficits. Mice were screened for motor incoordination and impaired

general activity with the rotarod and open field tests, respectively (outlined in Fig. 2.2A).

Rotarod testing revealed age-dependent motor incoordination in $Q^{+/-}C^{+/-}$ mice that

became statistically significant by 9-11 months (Fig. 2.2B). Likewise, in open field

testing, $Q^{+/-}C^{+/-}$ mice displayed significantly decreased spontaneous activity by 9 months

(Fig. 2.2C). In contrast, Q71-B mice with normal CHIP levels ($Q^{+/-}C^{+/+}$) did not develop

age-related motor abnormalities in either assay (Fig. 2.2B-C), whereas $Q^{+/-}C^{-/-}$ mice

showed statistically significant motor incoordination by rotarod analysis prior to their

accelerated, early death (Fig. 2.3). Thus, the Q71-B behavioral phenotype increases in

severity as *CHIP* is reduced from two to one to zero alleles, indicating that CHIP

suppresses polyQ disease in a dose-dependent manner.

The progressive neurobehavioral phenotype caused by expanded ataxin-3 in

CHIP-null mice suggests that the observed early death directly reflects CNS dysfunction.

But since *CHIP*-null mice are sensitive to cardiac stress (Zhang et al., 2005), we sought

to exclude cardiac dysfunction as the cause of death. Transthoracic echocardiography was

performed on mice from the Q71-B/*CHIP* cross. $Q^{+/-}C^{-/-}$ mice displaying behavioral

symptoms exhibited normal cardiac function (Table 2.1) without evidence of cardiac

hypertrophy, infarction, or valvular defects (data not shown). Therefore, we conclude that

the early demise of $Q^{+/-}C^{-/-}$ mice reflects CNS rather than cardiac dysfunction.

CHIP reduction exacerbates neuropathological markers in Q71-B mice. In parallel with

the worsened behavioral phenotype, we tested whether CHIP reduction also caused

earlier or more severe polyQ-associated neuropathology in Q71-B mice. To do this, we

examined brain sections from $Q^{+/-}C^{+/-}$ mice for the presence of intranuclear inclusions

and for altered subcellular localization of ataxin-3. By six months of age, ubiquitin-positive inclusions were detected in pontine neurons of $Q^{+/-}C^{+/-}$ mice (average number of inclusions per section = 6.33, s.d. = 5.9, n = 3 animals) but not in age-matched $Q^{+/-}C^{+/+}$ animals (average number of inclusions per section = 0.00, s.d. = 0.0, n = 2 animals) (Fig. 2.4A). Importantly, no ubiquitin-positive inclusions were detected at 3 months of age in either genotype, although 3-month-old $Q^{+/-}C^{+/-}$ mice did display increased ubiquitin immunostaining in some pontine neurons (Fig. 2.4A, arrows and inset). No inclusions were detected in the hippocampus, a brain region spared in SCA3, at 3 or 6 months in either genotype (Fig. 2.4B). Ubiquitin-positive inclusions were not detected in other brain regions, including cerebellar cortex, deep cerebellar nuclei, striatum, thalamus, and brainstem nuclei at 3 or 6 months of age (data not shown). Because expanded ataxin-3 is expressed throughout the CNS of both $Q^{+/-}C^{+/+}$ and $Q^{+/-}C^{+/-}$ animals (Figs. 2.4C, 2.5A, and data not shown), the region-specific, age-dependent inclusion formation we observe is not attributable to regional differences in transgene expression. These ubiquitinated inclusions contain ataxin-3, as shown by double immunofluorescence (Fig. 2.4D). Although such inclusions are not likely to be pathogenic (Branco et al., 2008), they do demonstrate that the neuropathology seen in Q71-B mice is similar to that observed in SCA3 patients. Expanded ataxin-3 localized primarily to neuronal cell nuclei by 3 months of age in all examined brain regions of Q71-B mice, regardless of CHIP status (Figs. 2.4C, 2.5A, and data not shown); however, ataxin-3 nuclear staining was more intense in $Q^{+/-}C^{+/-}$ mice than in $Q^{+/-}C^{+/+}$ mice at all time points. Endogenous murine ataxin-3 in nontransgenic mice, which immunostains much less robustly than expanded human ataxin-3, appears diffuse throughout the neuronal cytoplasm (Fig. 2.5A). Both

ubiquitin and ataxin-3 immunostaining are similar in $Q^{+/-}C^{-/-}$ mice and $Q^{+/-}C^{+/-}$ mice,

albeit with more complete nuclear localization and more intense staining of ataxin-3 in

$Q^{+/-}C^{-/-}$ mice (Fig. 2.5B). In agreement with previously published results from

hemizygous Q71-B mice (Goti et al., 2004), we observed no increase in the astrocytic

marker, glial fibrillary acidic protein (GFAP), in affected and unaffected brain regions in

Q71-B/*CHIP* mice (Fig. 2.6), suggesting that there is not significant astrogliosis.

CHIP reduction leads to increased ataxin-3 microaggregates in Q71-B mouse brain. The

dose-dependent phenotype caused by CHIP reduction in Q71-B mice allowed us to

determine whether CHIP reduction enhances ataxin-3 aggregation and to correlate

biochemically detectable changes in aggregation to behavioral phenotype. CHIP has been

shown to promote the degradation of polyQ proteins and/or modulate their aggregation

(Choi et al., 2007; Al-Ramahi et al., 2006; Miller et al., 2005; He et al., 2004). Consistent

with this, reducing or eliminating CHIP in Q71-B mice resulted in a marked, stepwise

increase in expanded ataxin-3 species that electrophorese on SDS-PAGE as high

molecular weight complexes after sonication and centrifugation to remove particulate

matter (Fig. 2.7A, bracket). Because these ataxin-3 complexes are detectable at 3 months,

when few if any inclusions are present, and are resistant to denaturing detergent yet

partition into the soluble fraction of brain lysates, we conclude that they represent

detergent-resistant microaggregates. Very few microaggregates partition in the brain

pellet (Fig. 2.8). While these microaggregates may be pure ataxin-3 oligomers, we cannot

currently rule out the presence of other proteins. In contrast, CHIP reduction or

elimination did not alter the levels of endogenous ataxin-3 or of monomeric, expanded

(i.e. human mutant) ataxin-3 (Figs. 2.7A, 2.7B, and 2.9), nor did reducing CHIP levels induce formation of microaggregates from endogenous ataxin-3.

To confirm that the high-molecular-weight ataxin-3 complexes in the soluble brain fraction correspond to microaggregates rather than inclusions, we electrophoresed brain lysates on 1.5% SDS-agarose gels which, due to their large pore size, can resolve larger protein complexes than a standard polyacrylamide gel (Bagriantsev et al., 2006). The calculated pore size we used (~130nm, according to the method of Xiong et al., 2005) is too small to permit entry of inclusions into the gel. As shown in Figure 2.7C, CHIP reduction or elimination leads to a stepwise increase in soluble ataxin-3 microaggregates in the brain. We also tested whether the microaggregates were 1C2-positive, since this polyQ-specific monoclonal antibody is thought to detect specific, nontoxic types of polyQ oligomers (Behrends et al., 2006). As shown in Figure 2.7A, 1C2 detects expanded ataxin-3 monomer, but not endogenous ataxin-3 monomer or ataxin-3 microaggregates (Figs. 2.7A and 2.7C); this result is similar to 1C2 labeling of expanded huntingtin monomer versus putative toxic huntingtin oligomers (Behrends et al., 2006). Since we cannot reliably size microaggregates on SDS-agarose gels (Fig. 2.10), we performed size exclusion chromatography on clarified brain lysates to assess microaggregate size. Microaggregates from $Q^{+/-}C^{+/+}$ mouse brain fractionated between ~700-7000kD in size, confirming that they are soluble high-molecular-weight complexes (Fig. 2.11). Reduction or loss of CHIP corresponded with progressively greater levels of microaggregates compared to monomeric ataxin-3 species, but did not change the fractions in which microaggregates or monomeric ataxin-3 eluted (Fig. 2.11). Stringent immunoprecipitations employing a denature-renature step further demonstrated that

ataxin-3 microaggregates are not highly ubiquitinated (Fig. 2.12), arguing that the large electrophoretic shift in these HMW ataxin-3 species is not due to conjugation to poly-ubiquitin chains. Although the Q71-B transgene is expressed in many tissues, ataxin-3 microaggregates were only present in the brain, not other tissues (Fig. 2.13). Taken together, these results indicate that 1) ataxin-3 microaggregate burden correlates with disease severity, and 2) CHIP regulates microaggregate levels in the brain *in vivo.*

Analysis of the effects of CHIP reduction on specific heat shock protein levels in brain. CHIP activates HSF1 and triggers expression of heat shock proteins (Dai et al., 2003), and loss of CHIP has been reported to correlate with a decrease in Hsp90 and Hsp40 levels in mouse brain (Dickey et al., 2007a). CHIP also induces Hsp70 expression during conditions of increased proteotoxic stress, and triggers Hsp70 degradation once cells return to basal conditions (Qian et al., 2006). Some studies have shown that when mutant polyQ protein is present, levels of stress-associated proteins, including some heat shock proteins, are dysregulated (Tagawa et al., 2007; Hay et al., 2004). Perhaps the simplest explanation for the worsened disease phenotype when CHIP is reduced or eliminated would be a deleterious imbalance in molecular chaperones. Therefore, we asked whether Q71-B mice with reduced or absent CHIP have lower levels of key heat shock proteins compared to Q71-B mice with normal CHIP levels.

Expression of expanded ataxin-3 on all CHIP backgrounds does not increase Hsp90 or Hsp40 above wild-type levels (Fig. 2.14), suggesting no major imbalance in these key chaperones. Hsp70 levels trended higher in CHIP-null animals with or without expanded ataxin-3 (Fig. 2.14B), consistent with results reported in Qian et al. (2006), but

did not reach statistical significance (Table 2.2). Removal of one $Q^{-/-}C^{-/-}$ animal from the analysis, thereby reducing the variability of the results, revealed that CHIP-null animals express significantly higher levels of Hsp70 than wild-type animals (Fig. 2.15), but this effect is independent of expanded ataxin-3 expression (Table 2.3). Neither levels of Bag1 nor of Hop (co-chaperones for CHIP and Hsp90, respectively) varied with CHIP levels (Fig. 2.14A). Additionally, the levels of E4B, another protein quality control ubiquitin ligase implicated in ataxin-3 regulation, did not change with expression of expanded ataxin-3 or reduction in CHIP (Fig. 2.14A). Therefore, in this model system, CHIP reduction does not impair expression of key heat shock proteins when polyQ disease protein is present. We conclude that CHIP reduction does not enhance polyQ toxicity primarily by altering levels of these key molecular chaperones.

Two protein quality control ubiquitin ligases can regulate levels of expanded ataxin-3 in cell culture. Whether CHIP is the primary mediator of ubiquitin-dependent degradation of ataxin-3 is controversial: Jana et al. (2005) reported that CHIP ubiquitinates ataxin-3 and directs it to the proteasome for degradation, whereas Matsumoto et al. (2004) reported that another ubiquitin ligase, E4B, mediates ataxin-3 degradation while CHIP has no effect. CHIP and E4B share properties indicating that both may represent protein quality control ubiquitin ligases that preferentially act on nonnative polypeptides and facilitate other PQC components (Qian et al., 2006; Richly et al., 2005). Our results above show that modulating the levels of quality control ubiquitin ligases like CHIP does influence ataxin-3 levels, but whether this is a direct or indirect effect cannot easily be assessed *in vivo*. To clarify the role of CHIP and E4B in ataxin-3 degradation, we

assessed their effect on steady-state ataxin-3 levels in transiently transfected neural cells.

When CHIP is overexpressed in M17 cells, steady-state levels of coexpressed

nonpathogenic ataxin-3 levels remain unchanged, but pathogenic (expanded) ataxin-3

levels decrease (Fig. 2.16A). Similarly, overexpression of E4B selectively decreases

expanded ataxin-3 levels without affecting levels of wild-type, nonpathogenic ataxin-3

(Fig. 2.16A). Thus, both ligases may selectively enhance the clearance of expanded

ataxin-3.

In an effort to confirm these results, we performed pulse-chase assays of ataxin-3

degradation. FLP-In HEK-293 cells that stably express FLAG-ataxin-3-Q22 or FLAG-

ataxin-3-Q80 were transfected with constructs expressing CHIP, E4B or an empty vector.

Cells were pulse-labeled with ^{35}S-methionine/cysteine, then chased for 0, 8 or 24 hrs.

FLAG-ataxin-3 was immunoprecipitated from cell lysates, then analyzed by SDS-PAGE

and autoradiography. In this experimental system, CHIP did not significantly accelerate

degradation of either wild-type or expanded ataxin-3 compared to empty vector (Figs.

2.16B, 2.17; Table 2.4). E4B may have slightly enhanced the degradation of expanded

ataxin-3 but this did not reach statistical significance; E4B overexpression had no effect

on wild-type ataxin-3 (Figs. 2.16B, 2.17; Table 2.4). It is important to note that we did

not detect ataxin-3 aggregation in either of these experiments, either by

immunofluorescence or western blot (Fig. 2.18), so these systems do not replicate all of

the disease protein features observed *in vivo*.

Discussion

Our results establish CHIP as a central component of homeostasis mechanisms countering polyQ toxicity in the brain. Complete loss of CHIP converts an asymptomatic mouse model of SCA3, the hemizygous Q71-B mouse, into one with an early onset, rapidly progressive behavioral phenotype with massive accumulation of soluble ataxin-3 microaggregates (Figs. 2.1, 2.3, 2.7, 2.8, 2.11). CHIP haploinsufficiency in the same model causes a less severe phenotype with moderate levels of ataxin-3 microaggregates (Figs. 2.1, 2.2, 2.7, 2.11). The fact that we observe robust phenotypic exacerbation with loss of a single *CHIP* allele highlights the importance of CHIP in decreasing expanded ataxin-3 toxicity. Previously we showed that CHIP haploinsufficiency exacerbates neurotoxicity in another polyQ disease, Huntington's disease (HD, Miller et al., 2005), but did not measure changes in aggregation. The dose-dependent effect of CHIP on both the progressive behavioral phenotype and microaggregate accumulation in Q71-B mice supports a causal link between microaggregates and polyQ neurotoxicity.

Although monomeric ataxin-3 levels in the brain remain unchanged when CHIP is reduced or absent (Figs. 2.7B and 2.9), ataxin-3 microaggregates accumulate. We term these complexes "microaggregates" because they partition in the soluble fraction of brain lysates and can be sized by size exclusion chromatography (Fig. 2.11), yet are resistant to denaturing detergents. Moreover, they accumulate before intranuclear inclusions are observed, and are distinguishable from inclusions by size. Ataxin-3 microaggregates are similar to soluble huntingtin aggregates recently identified in mouse models of HD (Weiss et al., 2008), and may represent ataxin-3 homo-oligomers or heteromeric complexes. Microaggregate levels directly correlate with neuropathological severity and

behavioral disturbance in Q71-B mice, increasing stepwise as CHIP levels are reduced, while monomeric ataxin-3 levels do not. Therefore, we suggest that ataxin-3 microaggregates constitute a neurotoxic species in SCA3. We cannot, however, prove that intracellular ataxin-3 microaggregates are directly toxic in vivo because, unlike the case with transmissible prions, it is not possible to introduce polyQ microaggregates isolated from one animal into the neurons of another animal to establish causality.

In other neurodegenerative diseases CHIP has been shown to regulate disease proteins including alpha-synuclein, parkin and tau (Shin et al., 2005; Imai et al., 2002; Dickey et al., 2006 and 2007a; Tetzlaff et al., 2008). When mutated these proteins tend to misfold, promoting abnormal oligomerization. Oligomers of alpha-synuclein and A-beta have been implicated as neurotoxic species (Danzer et al., 2007; Lesne et al., 2006). Our results likewise support a toxic oligomer model of polyQ disease pathogenesis, with CHIP functioning to reduce levels of these complexes. In this model (Fig. 2.19), expanded polyQ proteins have an increased probability of misfolding (Chen et al., 2002; Bhattacharyya et al., 2005; Colby et al., 2006). Misfolded monomers may be targeted for degradation by quality control ubiquitin ligases such as CHIP and E4B, or undergo chaperone-mediated refolding in a CHIP-facilitated manner. Misfolded polyQ monomers are prone to aggregate, forming homo-oligomers or heteroprotein complexes that may be inefficient proteasomal substrates (Bence et al., 2001; Bennett et al., 2005; Verhoef et al., 2002). Through its actions on misfolded proteins and chaperone regulation, CHIP would be expected to inhibit aggregate formation and facilitate the dissociation of aggregates.

Several recent studies have explored the identity of neurotoxic protein species in polyQ disease. For example, Behrends et al. (2006) found that expanded huntingtin

formed soluble oligomers that inhibited cell growth and were amyloid-antibody positive. Nagai et al. (2007) showed that both monomeric and oligomeric polyQ proteins are toxic when microinjected into cells. Takahashi et al. (2008) used a FRET-based assay to show that soluble polyQ oligomer formation correlated with death in neuronal cells. Our data with a full length disease protein provide animal model support for the hypothesis that soluble oligomers are the neurotoxic species in polyQ diseases. Determining whether ataxin-3 microaggregates are pure homo-oligomers or heteroprotein complexes would require that microaggregates be purified and analyzed by mass spectrometry. Their stability on agarose gels suggests this may be possible.

CHIP has been called a central regulator of HSP expression because it activates HSF-1 (Dai et al., 2003) and helps terminate the stress response by targeting Hsp70 for degradation (Qian et al., 2006). Since HSF-1 is the principal stress-induced transcription factor (Morimoto, 1998), CHIP reduction would be expected to lead to reduced levels of HSF-regulated genes (e.g. heat shock proteins). While previous studies have shown decreases in Hsp40, Hsp90 and Hop in *CHIP*-null mouse brain (Dickey et al., 2007a), we did not observe this (Fig. 2.14). This discrepancy could be explained by two factors: 1) our Q71-B/*CHIP* mouse line is maintained on a different background than the original *CHIP*-null line (C3H/HeJ/C57BL6 x 129SvEv/C57BL6 versus 129SvEv/C57BL6, respectively); and 2) previous studies in *CHIP*-null mice focused on a subset of "symptomatic" mice that die by 25-35 days postpartum (Dickey et al., 2006; Dickey et al., 2007a). "Symptomatic" *CHIP*-null mice constitute ~20% of the *CHIP*-null animals in a colony, while the remaining 80% of *CHIP*-null mice have a normal lifespan and remain phenotypically normal if unstressed (Dai et al., 2003). Our studies were performed in

CHIP-null mice that survive well past 30 days. Although a recent paper shows a 50% mortality rate in *CHIP*-null mice by 12 months (Min et al., 2008), we did not observe increased mortality in our experiments unless the Q71-B transgene was also present (Fig. 2.1C). When CHIP is absent in our experiments, the normal expression level of the tested chaperones suggests that other neuronal pathways may activate HSF-1 or otherwise trigger chaperone gene expression. Indeed recent data show that polyQ protein expression induces Hsp70 in certain neurons in an HSF-1-independent manner (Tagawa et al., 2007). At least in the case of Hsp70, HSF-1 apparently is not the only regulator.

It should be emphasized that we only assessed certain key chaperones implicated in neurodegeneration: Hsp40, 70 and 90. We did not find significant changes in either Hsp40 or Hsp90, implying that the mechanism by which CHIP reduction worsens disease is not primarily a perturbation in the balance of these key chaperones. We found that loss of CHIP correlates with increased Hsp70 levels in most CHIP-null mice, independent of expanded ataxin-3 overexpression (Figs. 2.14B, 2.15; Tables 2.2, 2.3), confirming that a) CHIP plays an important role in Hsp70 regulation, and b) changes in Hsp70 levels caused by loss of CHIP are unrelated to behavioral phenotype. Our results do not rule out CHIP-mediated effects on other undefined chaperones or accessory factors in the CNS. The CNS "chaperome" is likely vast and remains mostly uncharted. It would be useful to transcriptionally profile the functional chaperome of the mouse brain and determine which chaperone components are regulated by CHIP, both under basal and disease conditions.

CHIP acts in several ways on substrate proteins: it can refold proteins in concert with interacting chaperones (Kampinga et al., 2003; Rosser et al., 2007), ubiquitinate

proteins (Marques et al., 2006), or facilitate other ubiquitin ligases (Imai et al., 2002). With respect to specific polyQ proteins, CHIP can regulate degradation of ataxin-1 and androgen receptor (Al-Ramahi et al., 2006; He et al., 2004). CHIP was also shown to regulate degradation of huntingtin (Jana et al., 2005), while another study showed that CHIP promoted polyQ-expanded huntingtin solubility rather than degradation (Miller et al., 2005). The results for ataxin-3 have been equivocal, as two groups reported opposing effects of CHIP on ataxin-3 degradation (Matsumoto et al., 2004; Jana et al., 2005). The massive accumulation of ataxin-3 microaggregates in $Q^{+/-}C^{-/-}$ mice, despite stable levels of monomeric ataxin-3, could be explained either by a failure to promote degradation when CHIP is missing, or a failure to keep ataxin-3 in a soluble, degradable state. CHIP may be important for both expanded ataxin-3 solubility and degradation. While CHIP reduction also increases inclusion formation at later times, these may be byproducts of abnormal protein accumulation rather than directly pathogenic structures. Recent work shows that CHIP-mediated changes in inclusion formation can be dissociated from its ability to suppress polyQ toxicity (Branco et al., 2008).

The regulation of ataxin-3 may be complex and involve multiple degradation pathways (Matsumoto et al., 2004; Jana et al., 2005; Todi et al., 2007). Our steady-state results show that both CHIP and E4B overexpression reduce expanded ataxin-3 levels, though neither reduces wild-type ataxin-3 levels in neuronal cells (Fig. 2.16A). CHIP and E4B have been shown to work together to ubiquitinate and regulate the levels of the *C. elegans* protein, UNC-45 (Hoppe et al., 2004); a similar phenomenon could underlie ataxin-3 regulation in the mammalian brain. It would be interesting to assess the effect of E4B on polyQ disease phenotype and ataxin-3 stability using the E4B-null mouse

(Kaneko-Oshikawa et al., 2005). We suggest that loss of E4B, like loss of CHIP, would cause a buildup of expanded ataxin-3.

It is still unclear which processes favor aggregation of expanded ataxin-3 selectively in the brain and not elsewhere (Fig. 2.13). Comparative transcriptional profiling of the basal and stress-induced components of PQC in the CNS versus non-neuronal tissues might shed light on the selective vulnerability of the brain and suggest therapeutic targets. Certain classes of drugs, such as the Hsp90 inhibitors, show therapeutic promise by enhancing neuronal chaperone activity, through either increased refolding activity or targeting of chaperone client proteins for degradation (Waza et al., 2005; Thomas et al., 2006; Dickey et al., 2007a). Since CHIP is an important regulator of cellular responses to misfolded protein, enhancers of CHIP's ligase and/or co-chaperone functions might augment pathways necessary to counter polyQ disease.

Table 2.1. Q71-B mice lacking CHIP have normal cardiac function.

Q71-B	CHIP	Sex	Age (wks)	EF
-/-	+/+	M	11	78.82
+/-	+/-	M	11	83.80
+/-	-/-	M	11	74.68
-/-	+/+	F	16	74.91
-/-	-/-	F	16	83.06
+/-	+/-	F	16	70.99
+/-	-/-	F	16	81.09

Note: Male and female $Q^{+/-}C^{-/-}$ mice were assessed by transthoracic echocardiography. Each row in the table represents one mouse. Although there is no standard in the literature for the normal EF in this mixed background mouse line, previous studies report an EF of 80% +/- 5% in adult C57BL/6 mice (Weiss et al, 2006).

Table 2.2. One-way ANOVA of Hsp70 levels in Q71-B/*CHIP* mouse brain.

SUMMARY						
Groups	Count	Sum	Average	Variance		
Q-/- C+/+	3	0.630135	0.21004494	0.000703737		
Q-/- C-/-	4	2.636409	0.659102357	0.12871174		
Q+/-C-/-	2	1.780072	0.890035912	0.195000999		
Source of Variation	SS	df	MS	F	P-value	F crit
Between Groups	0.6245	2	0.312266641	3.216239177	0.112403702	5.14325285
Within Groups	0.5825	6	0.097090615			
Total	1.2071	8				

Note: One-way ANOVA of Hsp70 levels (expressed graphically in Fig. 2.14B) shows that there is a trend toward higher Hsp70 expression in $Q^{-/-}C^{-/-}$ and $Q^{+/-}C^{-/-}$ mouse brain compared to $Q^{-/-}C^{+/+}$, but the difference is not statistically significant (p=0.11).

Table 2.3. One-way ANOVA of Hsp70 levels in Q71-B/*CHIP* mouse brain after Q$^{-/-}$C$^{-/-}$ outlier removed.

SUMMARY						
Groups	Count	Sum	Average	Variance		
Q-/- C+/+	3	0.630135	0.210045	0.000703737		
Q-/- C-/-	3	2.501727	0.833909	0.009723177		
Q+/-C-/-	2	1.780072	0.890036	0.195000999		
Source of Variation	SS	df	MS	F	P-value	F crit
Between Groups	0.787	2	0.393505	9.115047383	0.021493026	5.786135043
Within Groups	0.2159	5	0.043171			
Total	1.0029	7				
Tukey's HSD	hsd	! =0.05?	! =0.01?			
wt v ko	5.2052	yes	no			
wt v hem-ko	5.1789	yes	no			
ko v hem-ko	0.4273	no	no			

Note: After removal of one Q$^{-/-}$C$^{-/-}$ animal from the analysis, one-way ANOVA followed by post-hoc testing (Tukey's HSD) shows that Hsp70 levels (expressed graphically in Fig. 2.9A) are significantly higher in Q$^{-/-}$C$^{-/-}$ and Q$^{+/-}$C$^{-/-}$ mouse brain than in Q$^{-/-}$C$^{+/+}$ (p=0.02). There is no difference in Hsp70 levels between Q$^{-/-}$C$^{-/-}$ and Q$^{+/-}$C$^{-/-}$ mice.

Table 2.4. One-way ANOVA of FLAG-ataxin-3-Q80 levels from 24-hour pulse-chase timepoint.

FLAG-ataxin-3-Q80	vector	CHIP	E4B			
	0.92333783	0.5908648	0.5731582			
	0.65022889	0.7790296	0.6955958			
	1.15969328	1.2861352	0.699286			
SUMMARY						
Groups	Count	Sum	Average	Variance		
vector	3	2.73326	0.91108667	0.06500106		
CHIP	3	2.6560295	0.8853432	0.12932716		
E4B	3	1.96804	0.6560133	0.00515213		
Source of Variation	SS	df	MS	F	P-value	F crit
Between Groups	0.11831731	2	0.0591587	0.88969146	0.45879461	5.1432529
Within Groups	0.3989607	6	0.0664935			
Total	0.51727801	8				

Note: Raw data quantification of FLAG-ataxin-3-Q80 levels in pulse-chase experiments at 24 hours with vector, CHIP or E4B overexpression (expressed in graphical form in Figs. 2.16B and 2.17). ANOVA shows no significant difference in FLAG-ataxin-3-Q80 levels at 24 hours (p=0.45).
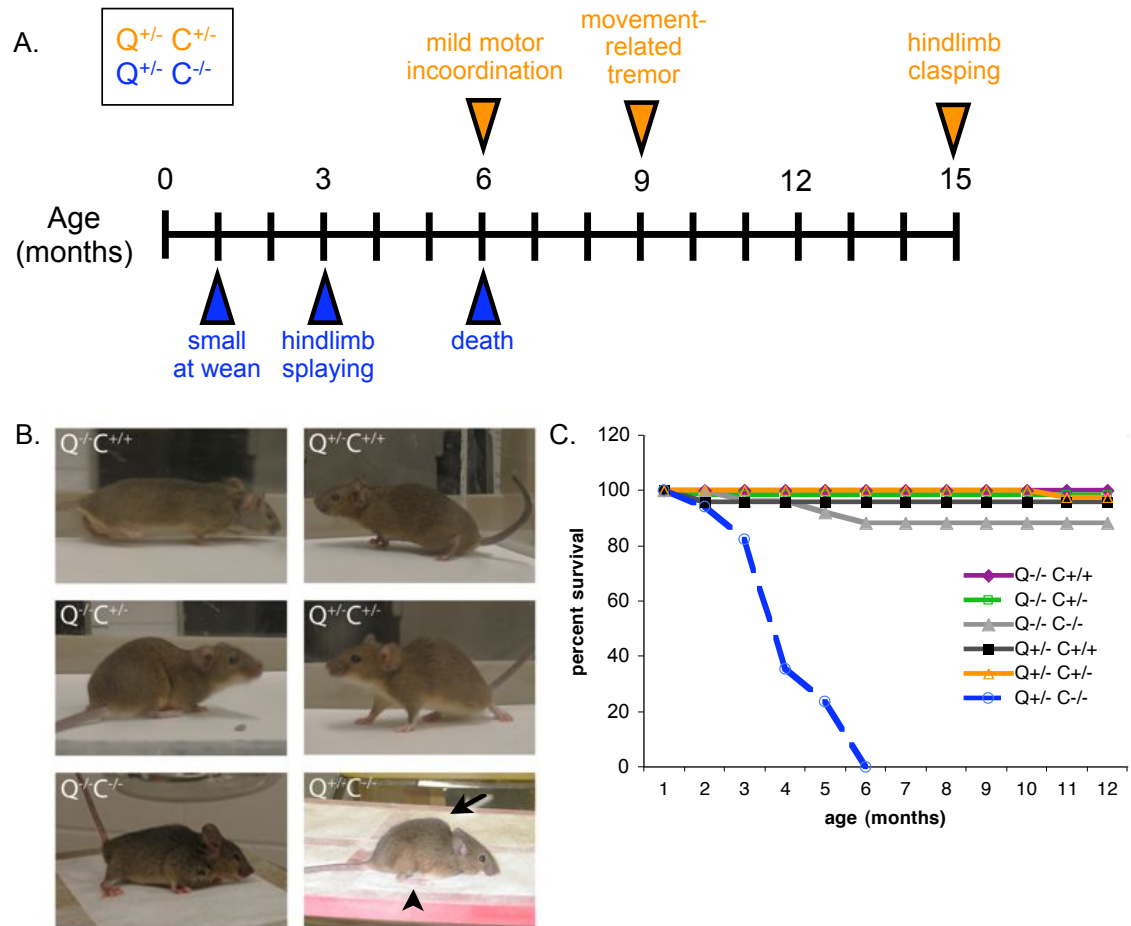
Figure 2.1. Loss of CHIP exacerbates expanded ataxin-3 toxicity *in vivo*. *A.* Timeline of symptom onset for Q71-B hemizygous mice on a *CHIP* haploinsufficient (Q$^{+/-}$C$^{+/-}$) or null (Q$^{+/-}$C$^{-/-}$) background. No behavioral abnormalities developed in Q71-B mice on a *CHIP* wild-type background over the 15-month study period (Q$^{+/-}$C$^{+/+}$, not shown). *B*. Representative photographs of 4-month-old mice from Q71-B/*CHIP* crosses. Q71-B mice lacking CHIP (Q$^{+/-}$C$^{-/-}$) develop kyphosis (arrow) and splaying of hindlimbs (arrowhead). In contrast, Q71-B mice haploinsufficient for *CHIP* (Q$^{+/-}$C$^{+/-}$) or wild-type for *CHIP* (Q$^{+/-}$C$^{+/+}$) appear healthy, as do nontransgenic mice with reduced CHIP (Q$^{-/-}$C$^{+/-}$). Nontransgenic *CHIP* knockout mice (Q$^{-/-}$C$^{-/-}$) occasionally develop kyphosis, as shown here, but retain normal motor behavior and lifespan. *C*. Survival curves for Q71-B/*CHIP* crosses. Q71-B mice lacking CHIP (Q$^{+/-}$C$^{-/-}$, open circles, blue line) die by 6 months of age while all other genotypes show normal survival rates. The number of animals followed for each genotype was: Q$^{-/-}$C$^{+/+}$ *n*=34, Q$^{-/-}$C$^{+/-}$ *n*=65, Q$^{-/-}$C$^{-/-}$ *n*=26, Q$^{+/-}$C$^{+/+}$ *n*=25, Q$^{+/-}$C$^{+/-}$ *n*=44, Q$^{+/-}$C$^{-/-}$ *n*=17.
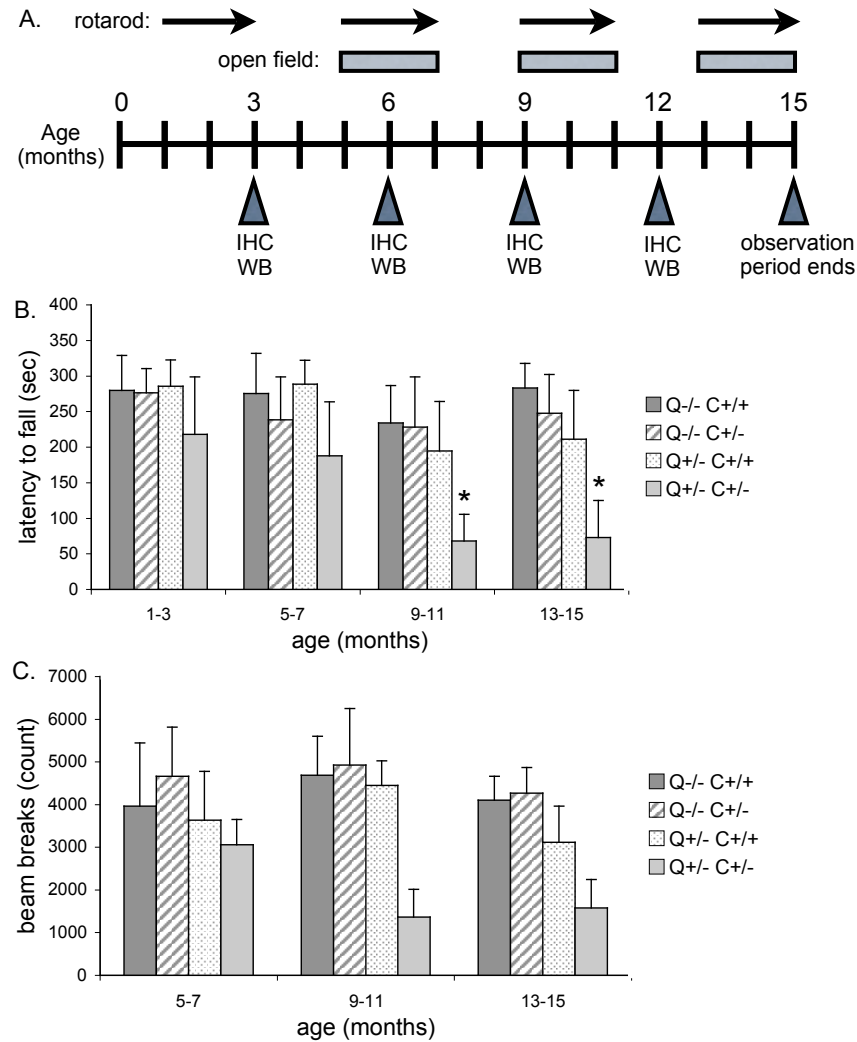
Figure 2.2. Reduction of CHIP causes progressive motor deficits in Q71-B mice.
A. Timeline for behavioral testing and tissue collection from Q71-B/*CHIP* cross.
Animals were tested for motor function by rotarod (arrows) and open field analyses
(gray bars) at the indicated ages (top). Brains were harvested for
immunohistochemistry (IHC) and western blot (WB) at the ages noted (bottom). *B.*
Motor coordination was assessed by rotarod for the indicated age groups and
genotypes. By 9 months of age, $Q^{+/-}C^{+/-}$ mice (light gray) develop statistically
significant motor impairment on the rotarod, measured by decreased average latency to
fall from the rod compared to all younger genotypes and ages (*p<0.01, one-way
ANOVA with Tukey's HSD post-hoc test; number of animals per genotype varied from
5-9 per bin.) *C.* Spontaneous motor activity was assessed by open field activity.
Spontaneous movement is measured as the total number of beam breaks in 30 minutes.
By 9 months, $Q^{+/-}C^{+/-}$ mice exhibit significantly decreased spontaneous motor activity
compared to all younger genotypes and ages (p<0.05, one-way ANOVA with
Tukey's HSD post-hoc test; number of mice per genotype and age varied from 2-8 per
bin). Data in *B* and *C* are displayed as the group mean plus standard deviation.
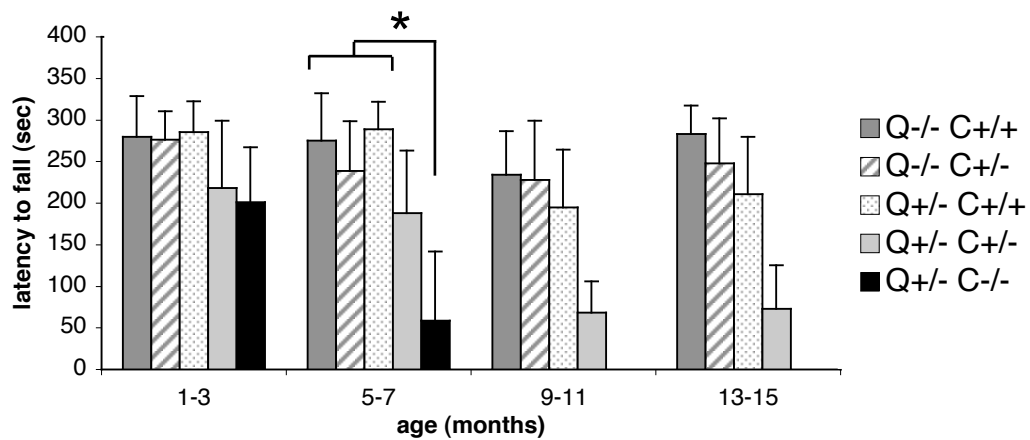
Figure 2.3. Loss of CHIP causes progressive rotarod performance deficit in Q71-B mice. Rotarod results from Fig. 2.2B are repeated here with data from $Q^{+/-}C^{-/-}$ mice added for comparison. $Q^{+/-}C^{-/-}$ mice can perform the task at 1-3 months of age, but are impaired on the task by 5-7 months of age compared to $Q^{-/-}C^{+/+}$, $Q^{-/-}C^{+/-}$, and $Q^{+/-}C^{+/+}$ animals. For $Q^{+/-}C^{-/-}$ mice, n=2 per age group. Data are displayed as the group mean plus standard deviation; *p<0.01, one-way ANOVA with Tukey's HSD post-hoc test.
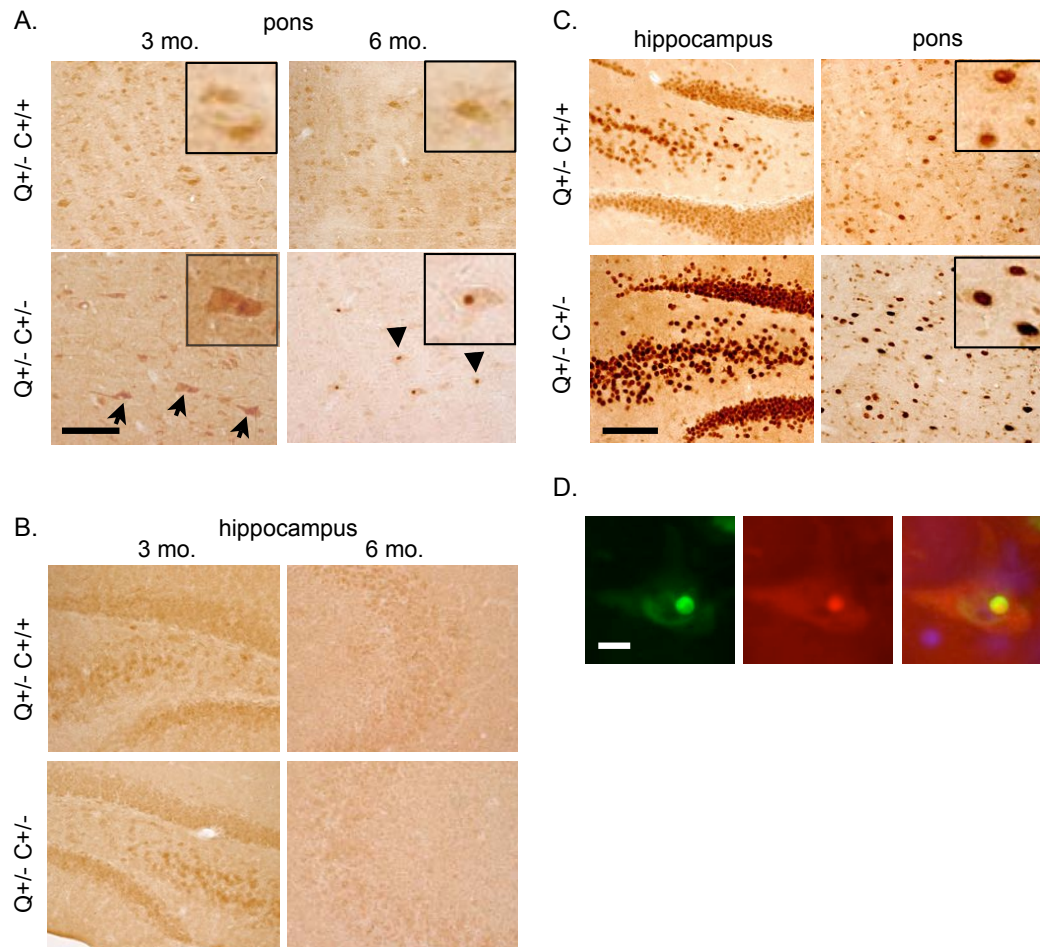
Figure 2.4. Reduction of CHIP increases age-dependent inclusion formation in the brainstem of Q71-B mice. *A*. Brain sections from 3- and 6-month-old mice labeled with anti-ubiquitin antibody reveal the presence of ubiquitin-positive inclusions in pontine neurons only in 6-month-old $Q^{+/-}C^{+/-}$ mice (arrowheads and inset). By 3 months of age, some pontine neurons in $Q^{+/-}C^{+/-}$ mice show increased ubiquitin immunostaining (arrows and inset), but no inclusions. *B*. Brain sections from 3- and 6-month-old mice stained as in *A* show that no inclusions form in the hippocampus, a brain region spared in SCA3. *C.* Immunolabeling with an ataxin-3 antibody reveals that the ataxin-3 transgene in Q71-B mice is expressed widely in the CNS, including in the hippocampus and pons. By 6 months of age, expanded ataxin-3 largely localizes diffusely to neuronal cell nuclei in $Q^{+/-}C^{+/+}$ and $Q^{+/-}C^{+/-}$ mice, both in typically affected regions (e.g. pons) and unaffected brain regions (e.g. hippocampus). Substantial enrichment of ataxin-3 throughout the nucleus may obscure detection of ataxin-3-positive nuclear inclusions by this method. *D*. Double immunofluoresence labeling in $Q^{+/-}C^{+/-}$ pontine neurons shows that ubiquitin-positive (red) nuclear inclusions contain ataxin-3 (green), as shown by the yellow fluorescence in the merged image (far right). Scale bars for A, B and C = 100 micrometers, scalebar for D = 10 micrometers.
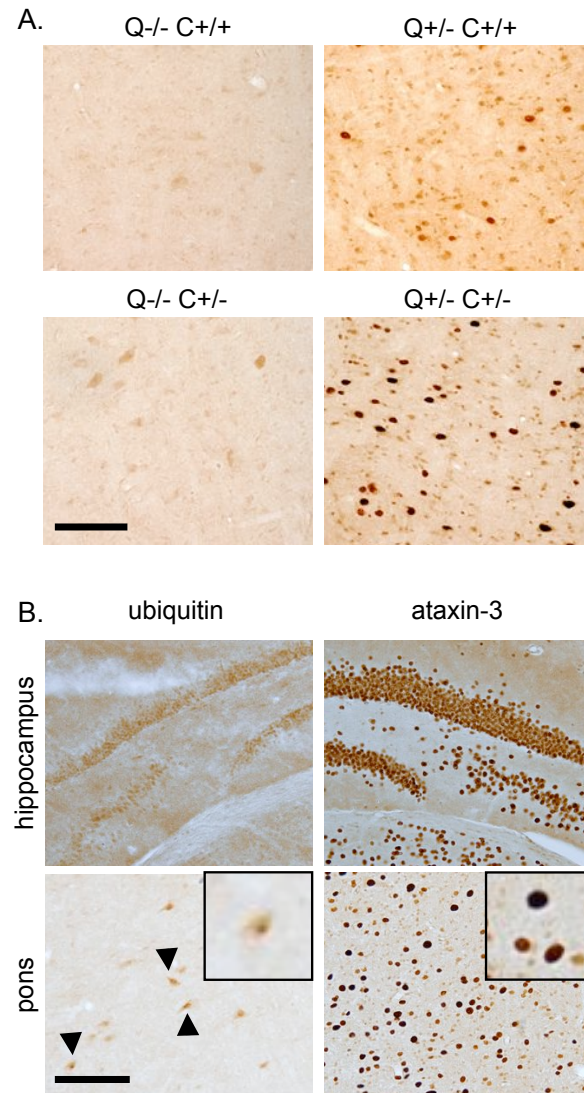
Figure 2.5. Expanded ataxin-3 localizes to the nucleus in Q71-B mice on all CHIP backgrounds. *A.* Wild-type ($Q^{-/-}C^{+/+}$) and CHIP-haploinsufficient ($Q^{-/-}C^{+/-}$) nontransgenic mice show similar subcellular localization of endogenous murine ataxin-3 at 6 months of age. Ataxin-3 immunostaining is much more robust in Q71-B mice transgenic mice. Ataxin-3 predominantly localizes diffusely to the nucleus both in $Q^{+/-}C^{+/+}$ and $Q^{+/-}C^{+/-}$ mice. *B.* Q71-B mice lacking CHIP ($Q^{+/-}C^{-/-}$) show similar subcellular localization of ataxin-3 and ubiquitin as $Q^{+/-}C^{+/-}$ mice at 6 months of age in both the hippocampus and pons. Scale bar in both *A* and *B* = 100 micrometers.
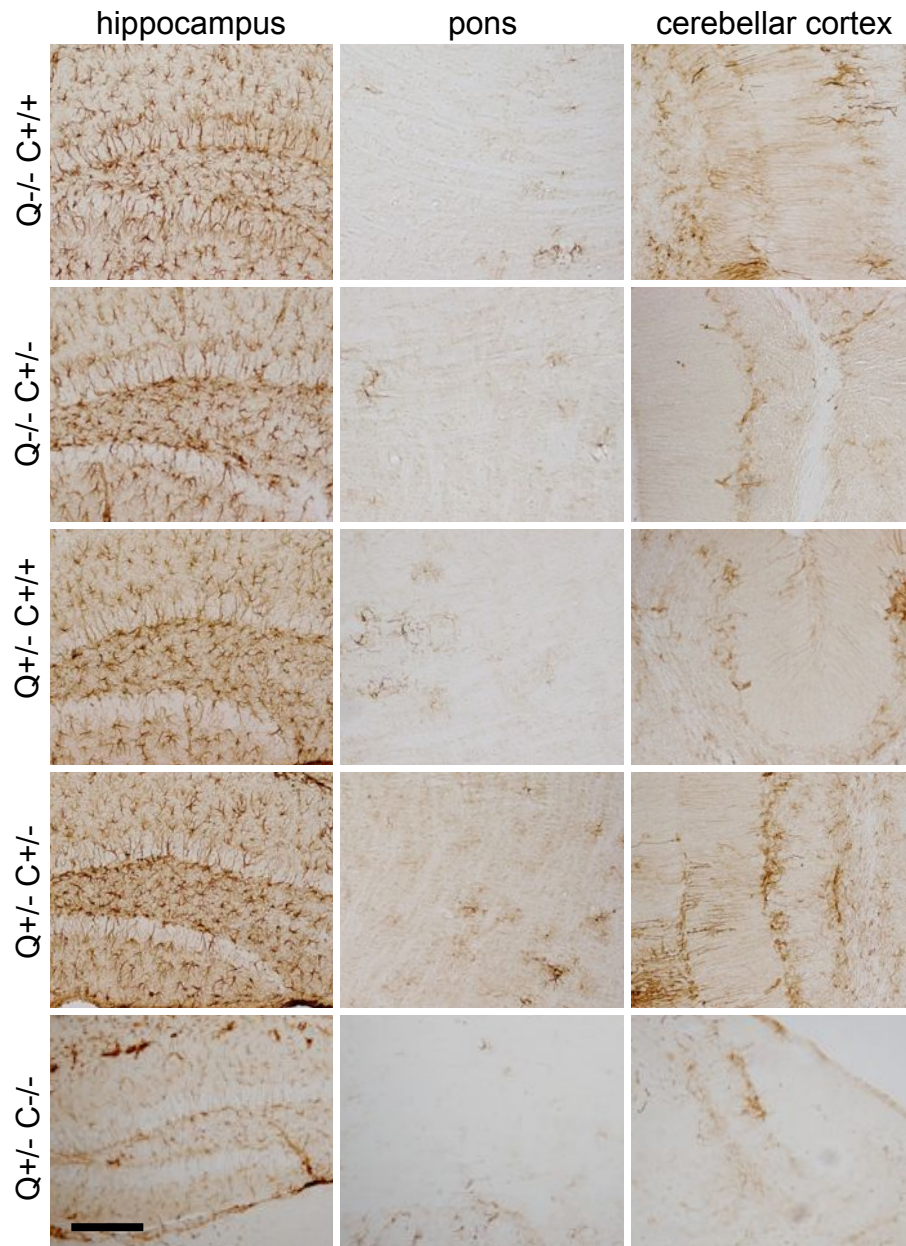
Figure 2.6. Reduction or loss of CHIP does not cause increased GFAP staining in Q71-B mouse brain. Brain sections from 6-month-old mice of the indicated genotypes were stained with monoclonal GFAP antibody. There is no increase in GFAP-positive cells in either typically affected brain regions (pons and cerebellar cortex) or unaffected regions (hippocampus) regardless of CHIP levels. Scale bar = 100 micrometers.
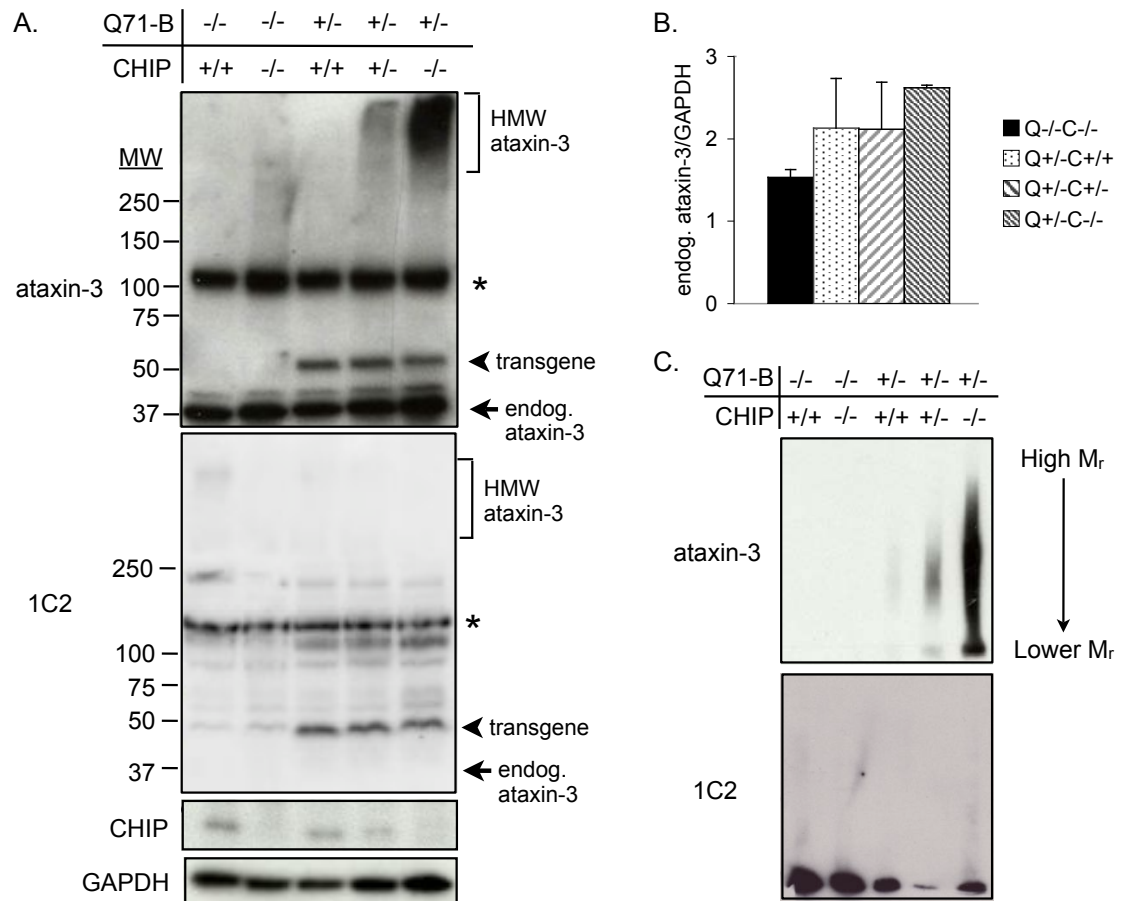
Figure 2.7. Reduction of CHIP increases ataxin-3 microaggregates in brain. *A.* Soluble fractions of brain lysates from 4.5-month-old mice were resolved on a 4-20% Tris-HCl gradient gel, then probed with the indicated antibodies. *CHIP* haploinsufficient Q71-B mice ($Q^{+/-}C^{+/-}$) develop high-molecular-weight (HMW) SDS-resistant ataxin-3 aggregates (bracket) that increase further when CHIP is absent ($Q^{+/-}C^{-/-}$ mice). Levels of soluble ataxin-3 monomer do not change significantly (arrow: endogenous murine ataxin-3; arrowhead: transgenic expanded ataxin-3). The band at ~150kD (asterisk) is nonspecific. The 1C2 anti-polyglutamine monoclonal antibody detects expanded ataxin-3 monomer, but not endogenous ataxin-3 monomer or HMW ataxin-3. GAPDH is shown as loading control. *B.* Quantification of endogenous monomeric ataxin-3 in mouse brain lysates. There is no significant difference in endogenous monomeric ataxin-3 levels between genotypes (one-way ANOVA, alpha=0.05). Blot signals (shown in Fig. 2.9B) were quantified with ImageJ, then the mean optical density for each genotype was normalized to GAPDH and plotted. Number of brains varied from 2-5 per genotype. Error bars = 1 S.D. *C.* Brain lysates prepared as in *A*, but separated instead on 1.5% SDS-agarose gels, reveal ataxin-3 microaggregates that increase stepwise as CHIP is reduced or eliminated (low levels in $Q^{+/-}C^{+/+}$ mice, intermediate in $Q^{+/-}C^{+/-}$ mice, and abundant in $Q^{+/-}C^{-/-}$ mice). Ataxin-3 microaggregates are not recognized by 1C2 monoclonal antibody.
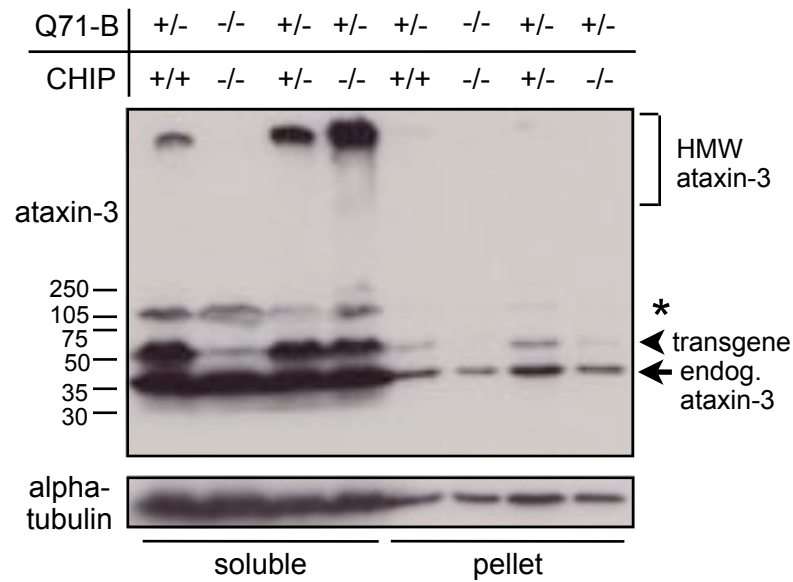
Figure 2.8. Most ataxin-3 detectable by Western blot in Q71-B/*CHIP* mouse brain is soluble. Brain lysates were separated into soluble and pellet fractions and resolved on a standard SDS-PAGE gel, then probed with the indicated antibodies. Regardless of CHIP levels, most endogenous and transgenic ataxin-3 remains soluble. Alpha-tubulin shown as loading control.
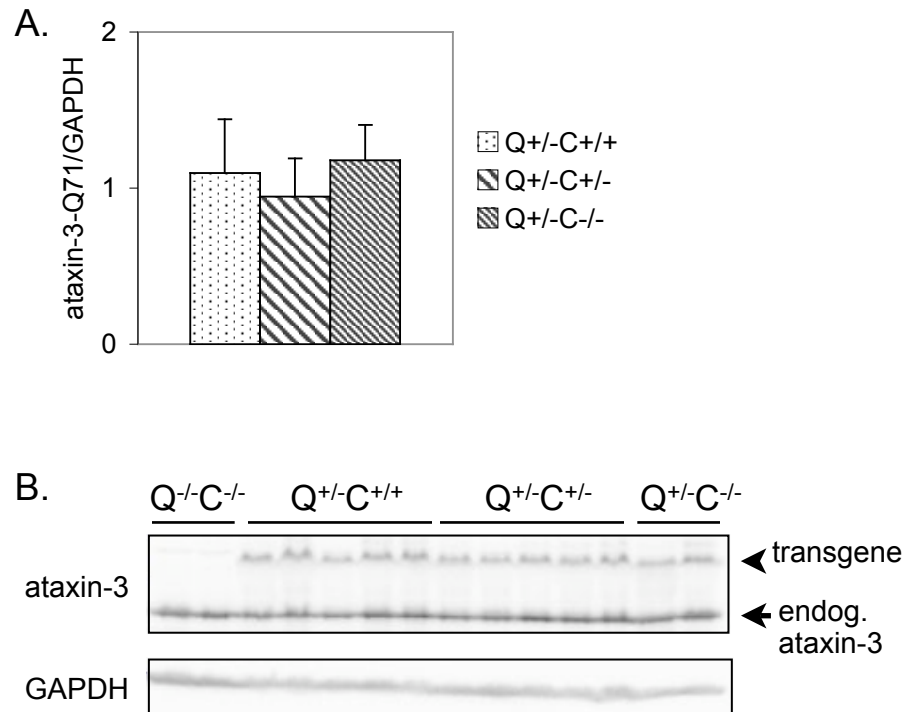
Figure 2.9. Reduction or loss of CHIP does not alter levels of soluble transgenic ataxin-3 monomer. *A*. Quantification of transgenic monomeric ataxin-3 in mouse brain lysates. There is no significant difference in transgenic monomeric ataxin-3 levels between genotypes (one-way ANOVA, alpha=0.05). Blot signals shown in *B* were quantified with ImageJ, then the mean optical density for each genotype was normalized to GAPDH and plotted. Number of brains varied from 2-5 per genotype. Error bars = 1 S.D. *B*. Blots from which Figs. 2.7B and 2.9A were generated.
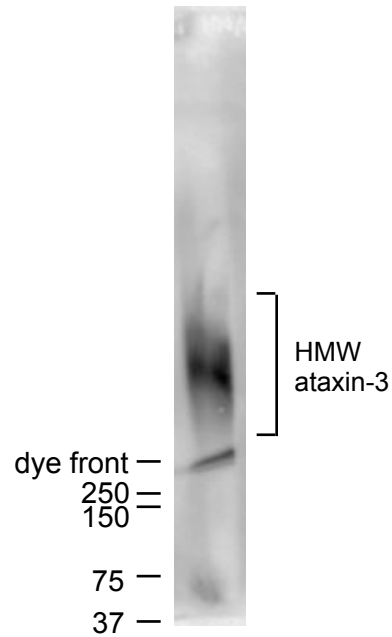
Figure 2.10. Molecular weight markers separate poorly on SDS-agarose gels. BioRad Kaleidoscope Precision Plus Standards were separated on a 1.5% SDS-agarose gel alongside brain lysate from a $Q^{+/-}C^{+/-}$ mouse. The gel was stopped with the dye front 2cm prior to completion in order to retain some of the markers. If an SDS-agarose gel is run to completion, all markers run off the end of the gel and cannot be used for molecular weight estimation.
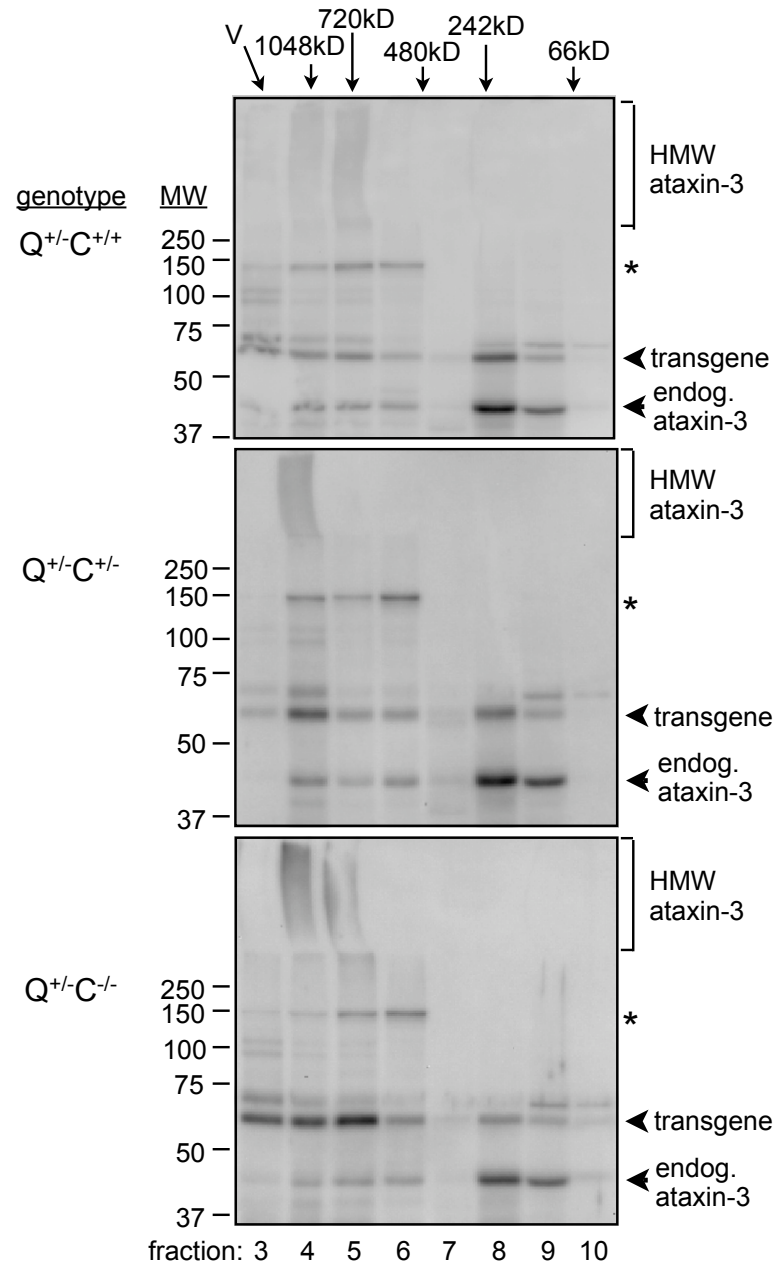
Figure 2.11. Size exclusion chromatography reveals that ataxin-3 microaggregates are soluble HMW complexes. Brain lysates from 4.5-month-old $Q^{+/-}C^{+/+}$, $Q^{+/-}C^{+/-}$ and $Q^{+/-}C^{-/-}$ mice were subjected to size exclusion chromatography, and fractions were analyzed by SDS-PAGE and Western blot for ataxin-3. Soluble ataxin-3 microaggregates elute after the void in fractions 4 and 5, which contain complexes ranging from ~ 700-7000kD in size. When CHIP is reduced or absent, ataxin-3 microaggregate levels increase, especially in fraction 4. The sizing range of the column is 20-7000kD. Bracket: HMW ataxin-3 microaggregates; arrowhead: transgenic expanded ataxin-3; arrow: endogenous murine ataxin-3. The band at ~150kD (asterisk) is nonspecific.
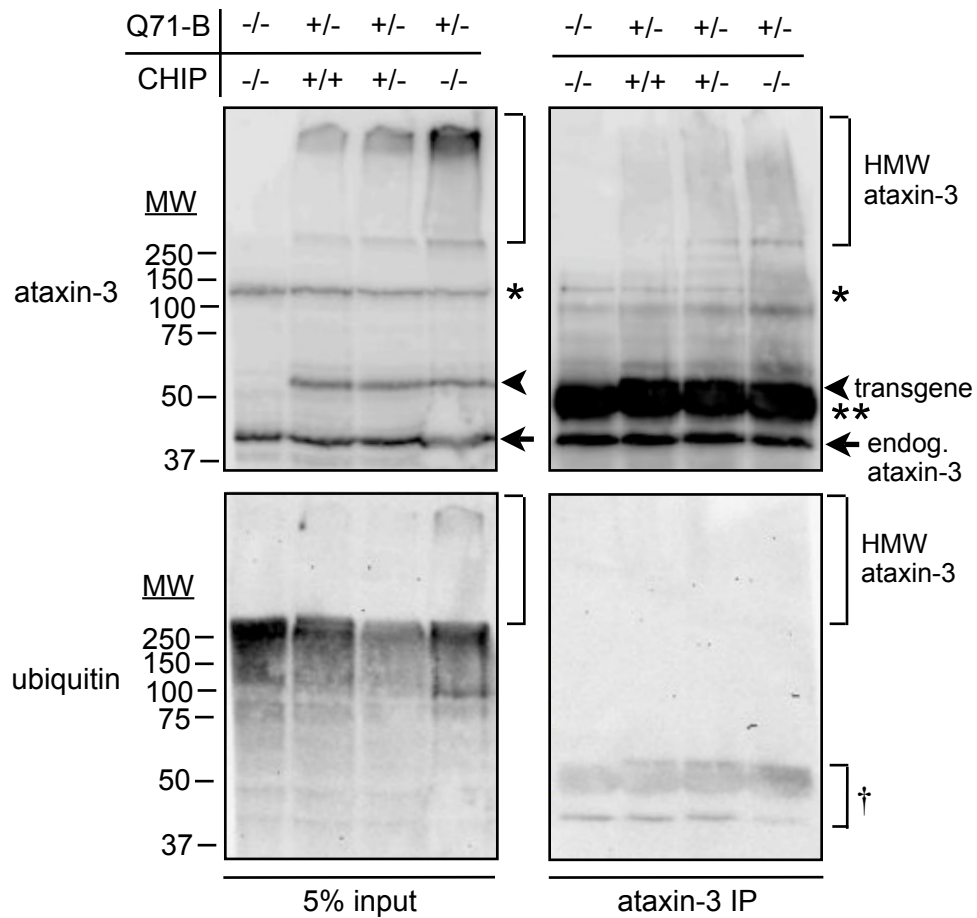
Figure 2.12. SDS-resistant ataxin-3 microaggregates are not heavily ubiquitinated. Brain lysates were subjected to denaturation/renaturation followed by immunoprecipitation with ataxin-3 antibody. Ataxin-3 microaggregates immunoprecipitated in this stringent manner are not detectable with ubiquitin antibody. The monomeric ataxin-3 transgene band electrophoreses just above, and is partly obscured by, the IgG heavy chain band (**). Inputs represent 5% of total volume after denaturation and renaturation. * = nonspecific band from ataxin-3 antibody, † = residual labeling after stripping ataxin-3 polyclonal antibody from blot.
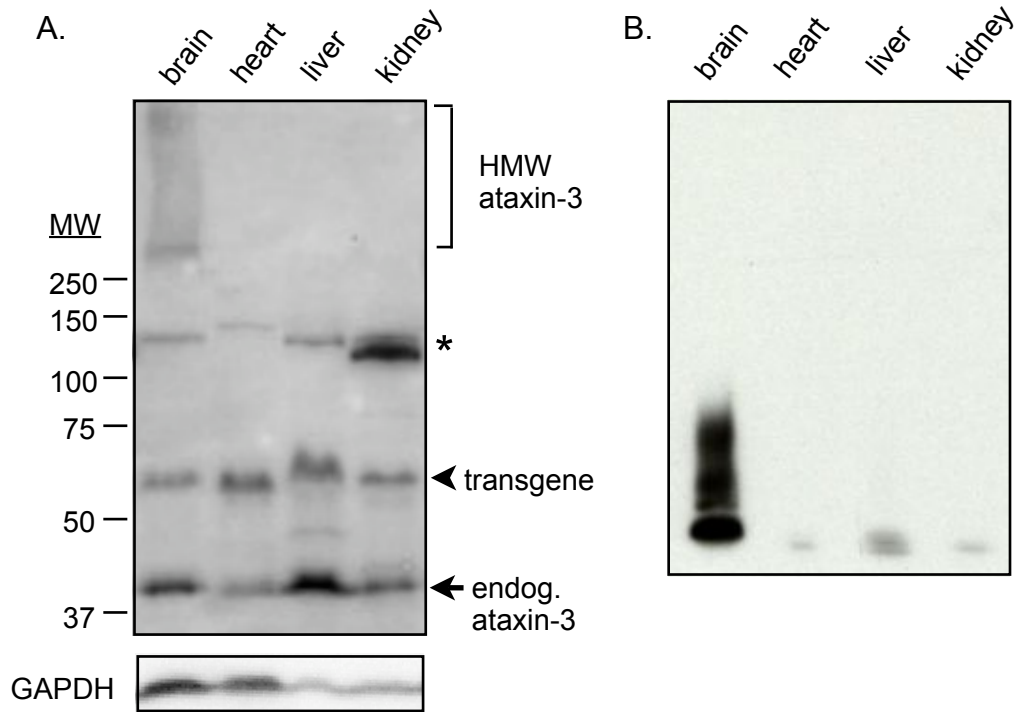
Figure 2.13. Ataxin-3 forms microaggregates in the brain, but not in non-neuronal tissues. Brain, heart, liver, and kidney from a 6-month-old Q+/-C+/- mouse were separated by 10% SDS-PAGE (*A*) or 1.5% SDS-agarose (*B*). Although the Q71-B transgene is present in all tissues (arrowhead), microaggregates are only detected in the brain lysate. GAPDH is shown as a loading control for *A*. The bands of ~150kD (asterisk) are non-specific.
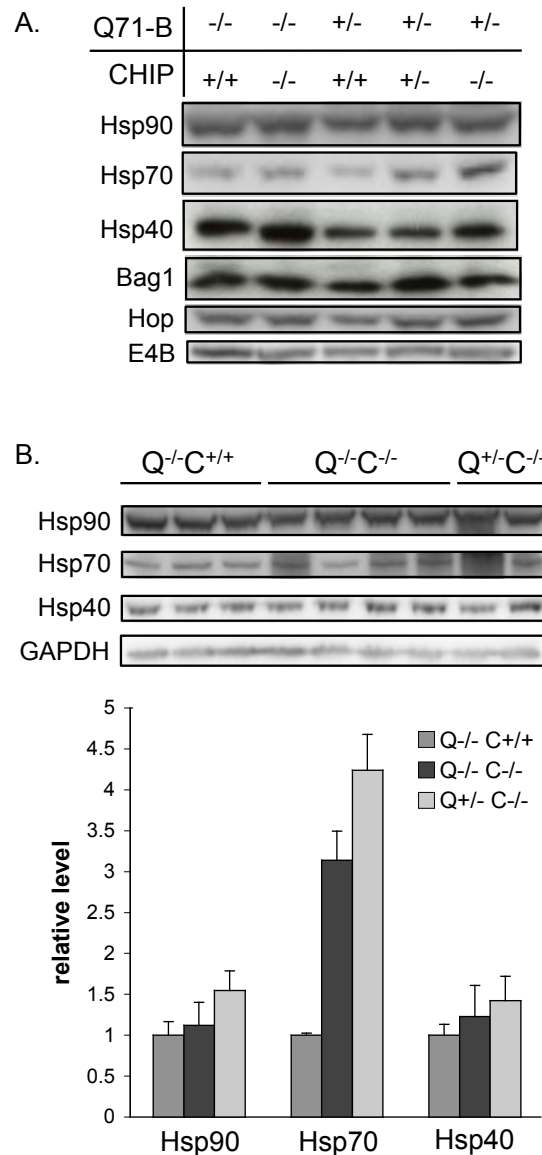
Figure 2.14. CHIP loss does not significantly alter specific stress-response protein levels. *A.* In Q71-B mice, Hsp90 and Hsp40 levels are not greatly increased upon CHIP reduction or removal (compare lane 3, 4, 5). Bag1, Hop, and E4B levels are not altered in any genotype. *B.* Further quantification of heat shock protein levels in mouse brain lysates. Levels of Hsp90 and Hsp40 do not significantly differ between wild-type (Q$^{-/-}$C$^{+/+}$), *CHIP* knockout (Q$^{-/-}$C$^{-/-}$), and Q$^{+/-}$C$^{-/-}$ mice (one-way ANOVA, alpha=0.05). While Hsp70 levels trend higher in Q$^{-/-}$C$^{-/-}$ and Q$^{+/-}$C$^{-/-}$ animals compared to wild-type animals, consistent with the fact that CHIP regulates Hsp70 levels (Qian et al, 2006), this does not reach statistical significance (one-way ANOVA, alpha=0.05, shown in Table 2.2). Blot signals (top) were quantified with ImageJ, then the mean optical density for each genotype was normalized to GAPDH and plotted as a fraction of the wild-type (Q$^{-/-}$C$^{+/+}$) signal (bottom). Error bars = 1 S.D.
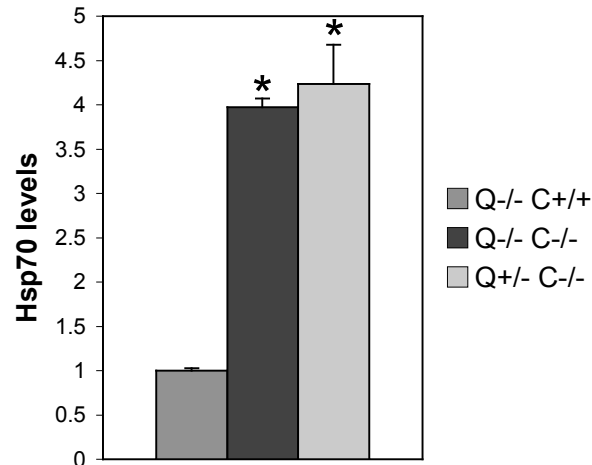
Figure 2.15. Hsp70 levels are dependent on CHIP and independent of expanded ataxin-3 overexpression. Western blot analysis of stress response protein levels in Q71-B/*CHIP* brains revealed variability in Hsp70 expression in Q$^{-/-}$C$^{-/-}$ mice (Fig. 2.14B). After excluding one Q$^{-/-}$C$^{-/-}$ mouse with low Hsp70 levels from the analysis, ANOVA confirmed that Q$^{-/-}$C$^{-/-}$ and Q$^{+/-}$C$^{-/-}$ animals express higher Hsp70 levels than wild-type animals (* alpha = 0.05 by Tukey's HSD post hoc test, shown in Table 2.3), consistent with the fact that CHIP regulates Hsp70 levels (Qian et al, 2006). Hsp70 levels were not different between Q$^{-/-}$C$^{-/-}$ and Q$^{+/-}$C$^{-/-}$ animals (Table 2.3). Blot signals (shown in Fig. 2.14B) were quantified with ImageJ, then the mean optical density for each genotype was normalized to GAPDH and plotted as a fraction of the wild-type (Q$^{-/-}$C$^{+/+}$) signal. Error bars = 1 S.D.
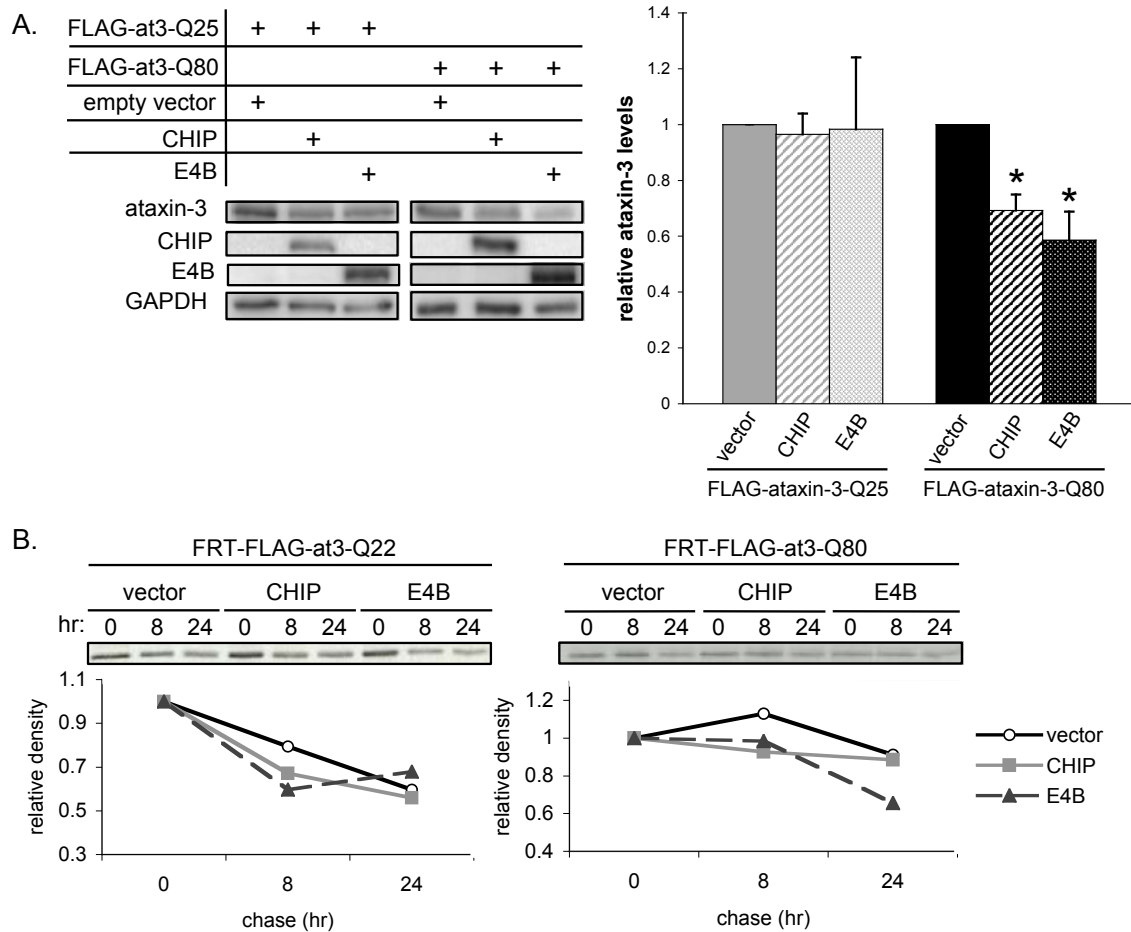
Figure 2.16. Analysis of the role of CHIP and E4B in regulating levels of expanded ataxin-3. *A*. Both CHIP and E4B reduce steady state levels of expanded, but not wild-type, ataxin-3. M17 neuroblastoma cells were transiently cotransfected with the indicated plasmids, and lysates were then examined by western blot. Representative blots are shown, with the proteins detected by specific antibodies shown at left. Ataxin-3 signal was quantified using NIH ImageJ, normalized to GAPDH loading control, then plotted at right as a fraction of the signal from the empty vector control condition. Shown are means (3 independent trials) plus S.D. CHIP or E4B expression significantly reduced expanded ataxin-3 levels (* p<0.01 by Student's *t*-test, comparison to results with empty vector control). *B*. Effect of CHIP and E4B on degradation of normal or expanded ataxin-3. 48 hrs after transfection with the indicated plasmids, FLP-In HEK293 cells stably expressing FLAG-ataxin-3-Q22 or FLAG-ataxin-3-Q80 were pulse labeled with ^{35}S-labeled methionine/cysteine and chased for the indicated times. Plotted are the ataxin-3 signals detected by autoradiography and normalized to ataxin-3 signal immediately after pulse labeling (means of 3 independent experiments). Neither CHIP (gray line) nor E4B (dotted line) significantly enhanced clearance of normal or expanded ataxin-3, though E4B displays a trend toward enhancing expanded ataxin-3 degradation (one-way ANOVA, alpha=0.05). Representative autoradiograms of each experiment are shown above the graphs.
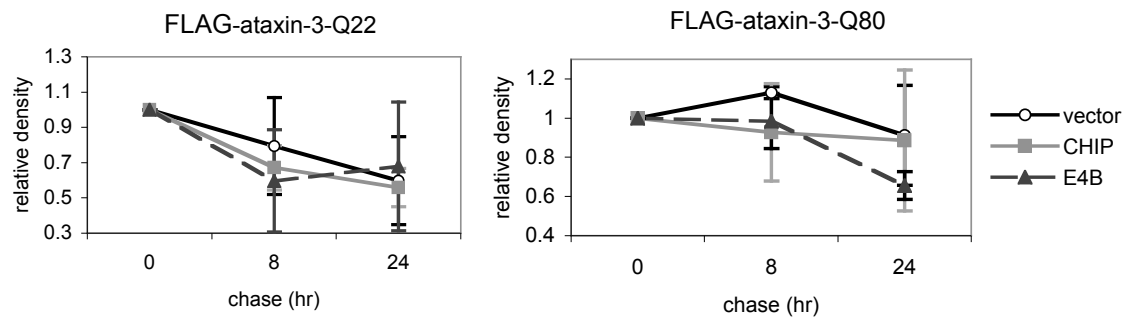
**Figure 2.17. Neither CHIP nor E4B affect the rate of FLAG-ataxin-3-Q80
degradation over a 24-hour period.** Pulse-chase results from Fig. 2.16B are repeated
here with error bars included. At 24 hours, the rate of degradation of polyQ-expanded
FLAG-ataxin-3 is unaffected by CHIP or E4B overexpression (one-way ANOVA,
alpha=0.05; Table 2.4). Error bars = 1 S.D.
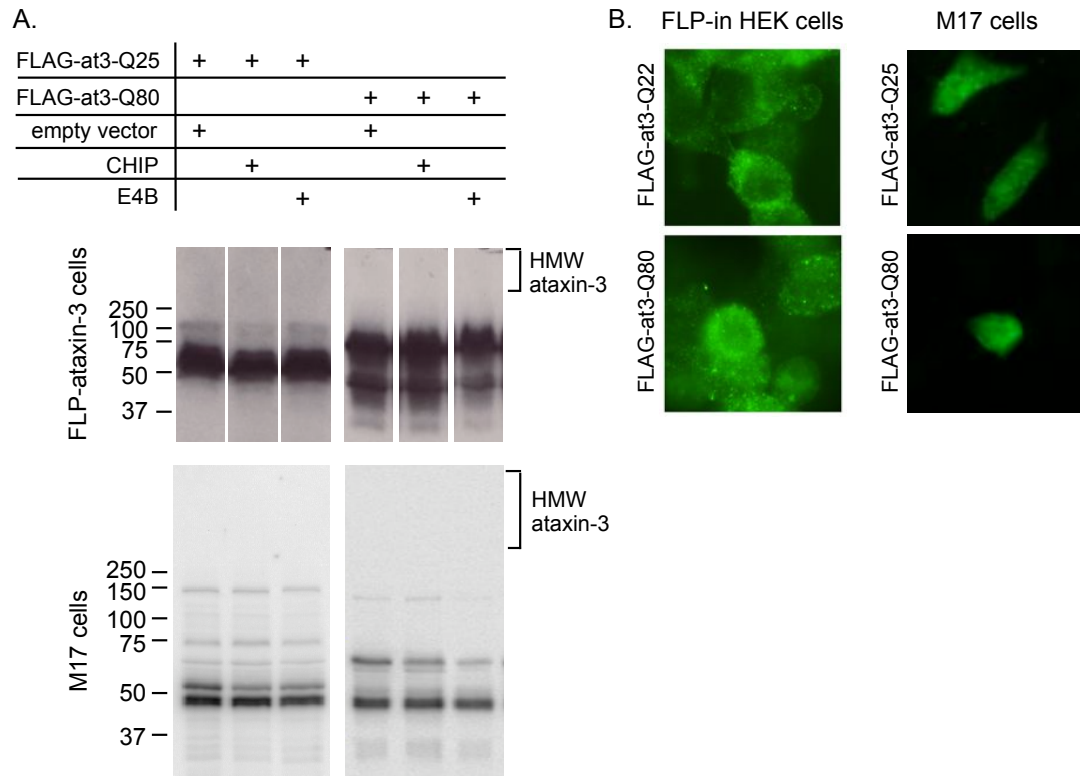
Figure 2.18. Cells transfected with expanded ataxin-3 do not form microaggregates. *A*. FLP-In HEK293 cells stably expressing FLAG-tagged ataxin-3 (top) or M17 neuroblastoma cells transiently transfected with FLAG-tagged ataxin-3 (bottom) were transfected with the indicated plasmids, and lysates were examined by western blot. Representative blots are shown, with the proteins detected by specific antibodies shown at left. No ataxin-3 is detectable in the stacking gel, in contrast to what is observed in brain lysates from Q71-B/*CHIP* mice. *B*. FLP-In HEK293 cells stably expressing FLAG-tagged ataxin-3 (left) or M17 neuroblastoma cells transiently transfected with ataxin-3 constructs (right) were immunolabeled with FLAG antibody. Ataxin-3 does not form visible inclusions or aggregates in these cells.
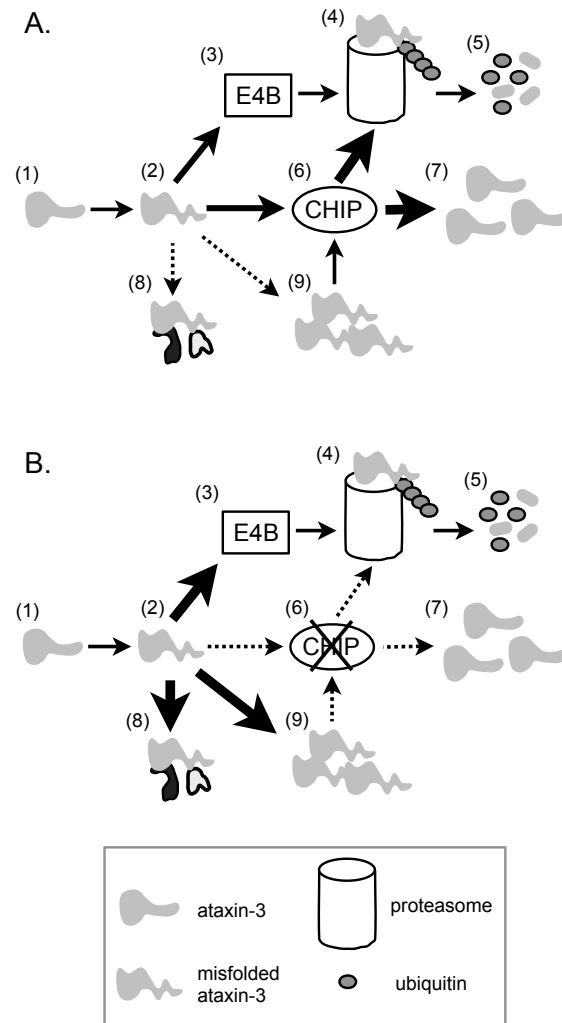
Figure 2.19. Model of CHIP action on mutant ataxin-3 in brain. This model depicting cellular pathways in the presence (*A*) and absence (*B*) of CHIP is based both on results reported here and from previously published studies (Matsumoto et al, 2004; Jana et al, 2005; Miller et al, 2005). Thick arrows indicate predominant pathways, thin arrows less predominant pathways, and dotted arrows unfavored pathways in the given scenario. *A.* Expanded ataxin-3 monomer (A3) (1) has an increased probability of misfolding (2) and forming aberrant heteroprotein and homo-oligomeric complexes (8 and 9, respectively). Misfolded ataxin-3 monomer can be ubiquitinated by E4B (3) or CHIP (6) and targeted for proteasomal degradation (steps 4-5). Misfolded ataxin-3 monomers or oligomers may also bind to CHIP and undergo chaperone-mediated refolding (7). Adequate levels of CHIP favor dissociation and clearance of misfolded aggregated ataxin-3. *B.* When CHIP is reduced or absent, handling of expanded ataxin-3 is impaired. Consequently ataxin-3 microaggregates, comprising hetero-protein complexes (8) and/or homo-oligomers (9), accumulate with deleterious consequences for the neuron. Such microaggregates may represent relatively poor substrates for the proteasome and other ataxin-3 clearance pathways.

CHAPTER 3

FORMATION OF SDS-RESISTANT

MICROAGGREGATES CORRELATES WITH

NEUROTOXICITY IN SCA3 TRANSGENIC MICE

Abstract

There are many hypotheses regarding the identity of the toxic protein species in polyQ expansion disorders. While insoluble, macroscopic polyQ protein inclusions are generally thought to be neutral or adaptive structures, increasing evidence indicates that soluble misfolded monomers or oligomers correlate with toxicity and cell death in cell culture models of polyQ disease. Supporting data from animal models of polyQ disease, however, are lacking. In an effort to identify the toxic protein species in SCA3, we compared two genetically distinct transgenic mouse models of SCA3 to determine whether misfolded, oligomeric complexes of mutant ataxin-3 are a shared pathological feature. Both mouse lines expressing expanded (mutant) ataxin-3 develop soluble, detergent-resistant ataxin-3 microaggregates, while mice expressing nonpathogenic ataxin-3 do not. Mirroring the selective neurotoxicity seen in SCA3 and other polyQ diseases, microaggregates are observed only in brain, not other tissues. Overexpression of expanded ataxin-3 did not alter the size of protein complexes containing endogenous ataxin-3 in brain, and the presence of microaggregates did not deplete the pool of soluble, monomeric endogenous ataxin-3. This last result suggests that dominant loss-of-function is not a major mechanism by which expanded ataxin-3 is toxic. Finally, neuropathological analysis revealed no shared phenotype of reactive astrogliosis, microgliosis, or neuronal loss across the two mouse models. These data support the

hypothesis that brain-specific, soluble ataxin-3 microaggregates exert dominant gain-of-function toxicity in the CNS.

Introduction

The most common dominantly inherited ataxia, SCA3 is a progressive, ultimately fatal neurodegenerative disease (Zoghbi and Orr, 2000). Neuropathological findings in SCA3 include widespread degeneration of cerebellar pathways, pontine and dentate nuclei, substantia nigra, globus pallidus interna, cranial motor nerve nuclei and anterior horn cells (Rüb et al., 2008). The genetic cause of SCA3 is a CAG expansion in the *ATXN3* gene, which is translated into the disease protein, ataxin-3. Ataxin-3 is a ubiquitin-binding protein and deubiquitinating enzyme that functions in multiple protein clearance pathways (Burnett et al., 2003; Zhong and Pittman, 2006; Wang et al., 2008). It is unique among polyQ disease proteins in that it can suppress toxicity from other polyQ proteins via its enzymatic activity (Warrick et al., 2005) and localizes to inclusions that form in other neurodegenerative diseases (Uchihara et al., 2001; Fujigasaki et al., 2001; Seilhean et al. 2004; Takahashi et al., 2001). These characteristics suggest that ataxin-3 normally participates in protein quality control in neurons. Ataxin-3 exists in multiple protein complexes (Burnett et al., 2003; Burnett et al., 2005; Doss-Pepe et al., 2003; Evert et al., 2006; Ferro et al., 2007; Li et al., 2002; Lim et al., 2006; Shen et al., 2005; Wang et al., 2000; Wang et al., 2007; Wang et al., 2008; Zhong and Pittman, 2006), and can interact with other ataxin-3 polypeptides (Ellisdon et al., 2006; Gales et al., 2005; Jia et al., 2008; Mauri et al., 2006). Although the functions of ataxin-3 are beginning to be understood, the exact protein complexes or species through which ataxin-3 causes

neuronal dysfunction in SCA3 have yet to be identified. The following subsections outline the potential toxic protein species investigated in our studies.

Toxic Species in PolyQ Neurodegeneration

PolyQ protein aggregation. Expanded polyQ tracts tend to perturb the native folding of the host protein (Ignatova and Gierasch, 2006) increasing the probability that the disease protein will misfold, oligomerize and aggregate. The tendency for polyQ proteins to misfold correlates with the length of the repeat: longer repeats are more likely to misfold and form aggregates. Posttranslational modifications can also influence the propensity of the protein to aggregate (Humbert et al., 2002; Steffan et al., 2004). Inclusion bodies formed by microtubule-based cellular processes from aggregated polyQ proteins can reside in the nucleus (SCA1, SCA7, SCA17), cytoplasm (SCA2 and SCA6) or both (HD, SCA3, DRPLA, SBMA). These inclusions are a pathological hallmark of polyQ disease; other neurodegenerative diseases feature similar protein accumulations (Takahashi et al., 2001; Gatchel and Zoghbi, 2005; Selkoe, 2004; Seilhean et al., 2004).

As discussed in Chapter 1, the causal link between inclusions and neurodegeneration has been challenged by several reports (Arrasate et al., 2004; Bowman et al., 2005; Saudou et al., 1998; Nagaoka et al., 2003; Rub et al., 2006). A currently prevailing view is that soluble oligomeric or protofibrillar intermediates are likely the cytotoxic polyQ protein species (Muchowski and Wacker, 2005; Poirier et al., 2002; Sanchez et al., 2003; Bucciantini et al., 2002; Takahashi et al., 2008). It is important to recognize that the biochemical process of "aggregation" is not necessarily identical to "inclusion formation". The literature has not always been clear on this point. In the

studies described here, we define "aggregates" as soluble biochemically detectable detergent-resistant protein complexes that range in size from small oligomers to large fibrillar polymers. "Inclusions" are defined as visible, insoluble protein structures generated by cellular processes that sequester proteins away from other cellular components.

Mature polyQ aggregates have a fibrillar, beta-sheet rich amyloid-like structure that can bind lipophilic dyes such as Congo Red and thioflavin. PolyQ-expanded ataxin-3 forms soluble SDS-resistant congophilic fibrillar aggregates *in vitro* (Bevivino and Loll, 2001; Chow et al., 2004; Ellisdon et al., 2006; Ellisdon et al., 2007). The aggregation pathway for expanded polyQ proteins is likely to be complex, with oligomeric, globular and fibrillar intermediates appearing before mature amyloid fibers are present (Ross and Poirier, 2004).

Nuclear localization of disease protein. Attempts to identify toxic species in polyQ diseases have determined that nuclear localization of mutant polyQ protein is necessary for neurodegeneration in several polyQ diseases (Saudou et al., 1998; Klement et al., 1998; Kordasiewicz, et al., 2006; Bichelmeier et al., 2007). For example, when the nuclear localization signal in ataxin-1 is mutated, expanded ataxin-1 no longer causes Purkinje cell degeneration and ataxia in mice (Klement et al., 1998, Cummings et al., 1998). Nuclear localization may also be necessary for apoptotic cell death in HD and SCA6 cell models (Saudou et al., 1998; Kordasiewicz, et al., 2006). Most recently, transgenic mice expressing expanded ataxin-3 with either nuclear localizing or nuclear exporting signals showed that forced nuclear localization of expanded ataxin-3 caused

more severe disease than forced cytoplasmic localization of expanded ataxin-3

(Bichelmeier et al., 2007). Thus, nuclear localization of mutant polyQ species may

promote pathogenesis, and in some cases be required for pathogenesis, in many polyQ

diseases.

Cleavage fragments. Another important issue in polyQ disorders is whether full-length

proteins or proteolytic polyQ-containing fragments are the primary toxic species. The

answer may vary depending on the disease protein. Several proteases can cleave

expanded polyQ proteins (Wellington and Hayden, 2000; Wellington et al., 2000;

Goldberg et al., 1996), and some evidence even suggests that proteolytic cleavage is

required for ataxin-3 aggregation (Haacke et al., 2006). Cleavage of polyQ proteins is

important for pathogenesis in mouse models of several polyQ diseases, including HD,

SBMA, and SCA6 (Ona et al., 1999; Graham et al., 2006; Cowan et al., 2003; Li et al.,

1998; Merry et al., 1998; Kordasiewicz, et al., 2006). Caspase activation has been also

observed in HD patient brains (Ona et al., 1999; Sanchez et al., 1999). Although ataxin-3

can be cleaved *in vitro* and in cells (Wellington et al., 1998; Berke et al., 2004; Pozzi et

al., 2008) and may catalyze its own cleavage (Mauri et al., 2006), conflicting reports exist

about whether ataxin-3 is cleaved in animal models and human SCA3 brains (Goti et al.,

2004; Berke et al., 2004, Cemal et al., 2002). These studies suggest that cleavage

products may contribute to pathogenesis in only a subset of polyQ disorders.

Posttranslational modifications and protein context. Although pure, expanded polyQ

domains without flanking amino acids are toxic, protein context also greatly influences

pathogenesis. The fact that each disease manifests distinct clinical and neuropathological features despite having the "same" mutation, means that disease protein context must contribute to the range and degree of neurodegeneration. The toxicity of several polyQ disease proteins is regulated by phosphorylation at sites distant from the polyQ domain. For example, huntingtin phosphorylated at serine 421 by Akt (a Ser/Thr kinase) has less pro-apoptotic activity *in vivo* and *in vitro* (Humbert et al., 2002). Akt-dependent phosphorylation of ataxin-1 also modulates neurodegeneration in SCA1 models (Chen et al., 2003, Emamian et al., 2003). Ataxin-3 can be phosphorylated by both casein kinase 2 (Tao et al., 2008) and GSK-3beta (Fei et al., 2007), and its phosphorylation status may be related to its aggregation (Fei et al., 2007).

Posttranslational modifications with ubiquitin or SUMO can also modulate toxicity in a protein-context dependent manner. For example, in cell and fruit fly models of HD, SUMOylation of a toxic cleavage product of huntingtin stabilizes the fragment, increases its solubility, and enhances its neurotoxicity (Steffan et al., 2004). In contrast, ubiquitination of this huntingtin fragment at the same lysine residues suppresses degeneration (Steffan et al., 2004). Ataxin-3 is also known to be oligo-ubiquitinated in cells (Berke et al., 2005), which may modulate its activity (Todi, S.V., unpublished data). The effect of ataxin-3 ubiquitination on SCA3 pathogenesis is currently unknown.

There is also evidence that non-polyQ regions of polyQ disease proteins are important to pathogenesis independent of posttranslational modifications. For example, the AXH domain of ataxin-1 reduces the expression of proteins important for cellular survival when overexpressed. PolyQ expansion of ataxin-1 enhances the effect of the AXH domain by rendering ataxin-1 less degradable (Tsuda et al., 2005). In SBMA, the

AR ligand testosterone is necessary for pathogenesis since full blown disease does not occur in women who carry the SBMA disease allele (Schmidt et al., 2002) or in castrated male transgenic mice (Katsuno et al., 2002; Katsuno et al., 2006). With regards to ataxin-3, the N-terminus of ataxin-3 is important for its localization, stability, and oligomerization (Todi et al., 2007; Ellisdon et al., 2006). Therefore, regions outside of the polyQ domain may contribute to polyQ disease pathogenesis.

Rationale and Aims of This Study

We wanted to determine which potential pathogenic protein species could be responsible for the phenotype of SCA3 mice. We reasoned that pathological processes relevant to SCA3 pathogenesis should occur in mouse models expressing the full length disease protein. When we began these studies, only two transgenic mouse models of SCA3 were available: the Q71-B mouse generated in the lab of Veronica Colomer Gould (Johns Hopkins University), and YAC mice overexpressing human ataxin-3 with various length glutamine repeats, generated in the lab of Susan Chamberlain (Imperial College London). The published phenotypes of both models are briefly summarized below.

The Q71-B mouse expresses a cDNA encoding the mjd1a isoform of human ataxin-3 with 71 glutamine repeats at levels 2-3 fold higher than endogenous ataxin-3 (Goti et al., 2004). The mjd1a isoform of ataxin-3 has deubiquitinating enzymatic activity and 2 of the 3 ubiquitin interacting motifs (UIMs) encoded in the MJD1 gene. Although Q71-B$^{+/-}$ (hemizygous) mice are phenotypically normal, Q71-B$^{+/+}$ (homozygous) mice develop an ataxic phenotype at ~2 months of age and die between 4-8 months of age. Intranuclear inclusions are described as "scarce" in both Q71-B$^{+/-}$ and Q71-B$^{+/+}$ mice

(Goti et al., 2004), although they are detected with higher frequency in Q71-B$^{+/+}$ mice in the deep cerebellar nuclei and pons, and increase as the Q71-B$^{+/+}$ animals age (Goti et al., 2004). Neuronal loss occurs in the substantia nigra pars compacta in Q71-B$^{+/+}$ mice, but not in Q71-B$^{+/-}$ mice. Distinct from human SCA3, neuronal loss was not observed in the dentate nucleus of the cerebellum.

MJD15.4 mice express full length human ataxin-3 with 15 glutamines from a yeast artificial chromosome containing the entire *ATXN3* gene; MJD15.4 mice express 4-fold higher levels of human ataxin-3 than endogenous murine ataxin-3 (Cemal et al., 2002). MJD84.2 mice express full length human ataxin-3 with 84 glutamines at levels ~2-fold above endogenous protein. Both animals express multiple splice isoforms of ataxin-3, as they contain the full gene with introns (Cemal et al., 2002; G. M. Harris and K. Dodelzon, unpublished data). The most common isoform expressed by both MJD transgenic mouse lines (and in humans) is mjd2; this isoform is fully active as a DUB and possesses all 3 UIMs encoded in the ATXN3 gene (G. M. Harris and K. Dodelzon, unpublished data). MJD15.4 mice develop no neuropathological or behavioral phenotype. MJD84.2 mice have a mild, progressive ataxic phenotype. The original description of MJD84.2 mice reported loss of Purkinje cells and deep cerebellar nuclei neurons, although stereological analysis was not performed (Cemal et al., 2002).

We reasoned that a pathogenic protein species in SCA3 should meet the following criteria: 1) occur in both mouse models expressing full length mutant ataxin-3; 2) occur to a greater degree in symptomatic animals; 3) occur primarily if not exclusively in the affected tissue (CNS); and 4) its presence should correlate with the onset of disease. We show here that SDS-resistant ataxin-3 microaggregates fit these criteria. Our data support

a model of SCA3 pathogenesis where soluble microaggregates exert dominant gain-of-function toxicity in the brain.

Methods

Mouse strains. Q71-B mice (Goti et al., 2004) were obtained from Veronica Colomer Gould (Johns Hopkins University) and maintained on their published C3H/HeJ x C57BL/6J background. MJD15.4 and MJD84.2 mice were obtained from Mark Pook (Brunel University, Egham, UK) and Ilya Bezprozvanny (Univ Texas Southwestern), respectively. MJD15.4 and MJD84.2 mice were maintained on a C57BL/6J background. Mice were genotyped by standard two-way PCR as previously described (Goti et al., 2004; Cemal et al., 2002). Mice from the two MJD lines were maintained in the hemizygous state; homozygous animals were not bred for the studies described in this chapter.

Open field analysis. Animals were tested for spontaneous activity using the Open Field 16x16 Photobeam Activation System and Flex-Field software (San Diego Instruments, San Diego, CA). Naïve animals were placed into a 41cm x 41cm clear plastic box inside a 16x16 array of infrared beams, and movement was calculated as the number and sequence of beam breaks over the course of 30 minutes. Animals were tested under dark conditions during their dark cycle (between 18:30-22:30 hrs).

Statistical Analysis. Statistical analyses were performed using Microsoft Excel with the Data Analysis ToolPak. Open field data were grouped by age and genotype, then tested

for significance with one-tailed Student's *t*-test for independent samples assuming equal variances. For comparisons between 3 genotypes, data were grouped by genotype, then tested for significance using one-way ANOVA for independent samples. Significant differences were further tested post-hoc using Tukey's Honestly Significant Difference (HSD, calculated online at http://web.mst.edu/~psyworld/virtualstat/tukeys/tukeycalc.html). For comparisons of transgene elution patterns in MJD15.4 and MJD84.2 mice, two-tailed Student's *t*-test for independent samples assuming equal variances was used.

Immunohistochemistry. For 3,3'-diaminobenzidine (DAB) stained sections: Mice were perfused transcardially with cold sterile PBS followed by 4% paraformaldehyde in PBS. Brains were fixed overnight in 4% paraformaldehyde, rinsed in PBS overnight, then cryoprotected in 30% sucrose for at least 18 hrs at 4°C. Brains were cut serially into 30μm floating sections on a sledge microtome (Leitz) and stored at -20°C in cryoprotectant (5mM sodium phosphate pH 7.4, 75mM sodium chloride, 30% w/v sucrose, 30% v/v ethylene glycol) until use. For polyclonal antibody use, sections were blocked in H_2O_2 to quench endogenous peroxidase activity, then blocked in 5% normal goat serum and incubated in primary antibody as indicated (protein A-purified rabbit anti-MJD 1:1000 or unpurified anti-MJD antiserum 1:1000 and 1:10,000 (Paulson et al., 1997), rabbit anti-ubiquitin 1:500 (Dako USA, Carpinteria, CA), goat anti-CHIP 1:200 (Millipore/Chemicon), rabbit anti-E4B 1:200 (Bethyl), mouse anti-ataxin-3 1:500 (1H9, kind gift from Y. Trottier). Sections were rinsed and incubated in biotinylated goat-anti-rabbit 1:500 (Vector Laboratories, Burlingame, CA), treated with avidin-biotin complex

(Standard Elite ABC kit, Vector Laboratories), then developed in 0.5mg/ml DAB (Sigma, St. Louis, MO) with 9% H_2O_2, rinsed and mounted on gelatin-coated slides, and coverslipped after a dehydration and delipidation series with Permount (Fisher Scientific, Pittsburgh, PA). For immunohistochemistry with monoclonal GFAP-Cy3 (1:500, Sigma) or VCP antibody (1:1000, Affinity Bioreagents), we used the Mouse-on-Mouse Peroxidase Kit (Vector Laboratories) according to manufacturer's instructions.

For nickel sulfate-stained sections: Mice were perfused transcardially with a sodium cacodylate wash buffer (0.8% NaCl, 0.8% sucrose, 0.4% dextrose, 0.034% sodium cacodylate, 0.023% $CaCl_2$) followed by sodium cacodylate fixation buffer (4% paraformaldehyde, 4% sucrose, 1.4% sodium cacodylate, pH 7.4), as recommended by NeuroScience Associates (NSA, Knoxville, TN) (instructions at http://www.neuroscienceassociates.com/perf-solution3.htm). Whole heads were fixed overnight in sodium cacodylate fixation buffer and sent to NSA for dissection, blocking and sectioning. Brains were blocked in NSA's proprietary cross-linked gelatin-based matrix, then cut serially into 30-micrometer floating sections on freezing slide microtome and stored at 4^oC in PBS plus 0.01% sodium azide. Staining for ubiquitin and ataxin-3 on NSA-processed tissue was performed by the laboratory of Alexander Osmand (University of Tennessee, Knoxville) according to the method described in Nguyen et al. (2006). Briefly, sections were treated with H_2O_2 and normal goat serum to block, then incubated in primary and secondary as above. Then the tissue was treated with a single round of biotin tyramide amplification prior to detection via avidin-biotin complex and nickel sulfate/DAB/H_2O_2 solution.

Polyglutamine aggregation foci assay. Brains were prepared and sectioned as for nickel-sulfate staining as above, then processed for polyglutamine aggregation foci as described in Osmand et al. (2006). Sections were blocked in 1% sodium borohydride to quench endogenous peroxidase activity, then rinsed in PBS and equilibrated in Tris-imidazole buffer. Sections were labeled with biotinylated PEG-Q30 peptide 1:25,000 in Tris-imidazole buffer overnight at room temperature. The following day, sections were rinsed and incubated in biotinylated tyramine to amplify the signal. Sections were subsequently treated with avidin-biotin complex (Standard Elite ABC kit, Vector Laboratories), then developed in 0.5mg/ml DAB (Sigma, St. Louis, MO) with 9% H_2O_2 and nickel sulfate, rinsed and mounted on gelatin-coated slides, and coverslipped after a dehydration and delipidation series with Permount (Fisher Scientific, Pittsburgh, PA).

Tissue collection and lysates. Mice were perfused transcardially with 20ml cold sterile PBS plus protease inhibitor cocktail (PI) (Complete Mini tablets, Roche, Indianapolis, IN). Whole tissues were dissected, minced in RIPA (50mM Tris-HCl pH 7.4, 150mM sodium chloride, 0.1% SDS, 0.5% sodium deoxycholate, 1% NP-40) with PI, then homogenized in a Dounce homogenizer in RIPA plus PI lysis buffer. Lysates were diluted to 100mg/ml (based on wet weight) in RIPA plus PI lysis buffer and centrifuged at 4000 rpm for 15 minutes at 4°. The pellet was rehomogenized in the same volume of RIPA plus PI. Lysates were stored at -80° until use.

Western blot analyses. Soluble fractions were sonicated twice for 10 seconds each, then spun at 15,000xg for 10 minutes at 4^oC to remove particulate debris (these pellets were

not saved). Pellets from this first 4000 rpm spin were vortexed and sonicated vigorously.

Samples were diluted 1:1 in 2X Laemmli buffer plus DTT, then separated on

discontinuous 10% or 12% acrylamide gels, or pre-cast 4-20% SDS Tris-HCl gradient

gels (BioRad), and transferred to PVDF membranes. For SDS-agarose gels, gels

contained 1.5% w/v high-melting-point agarose (ISC Bioexpress, Kaysville, UT) in TAE

buffer (40mM Tris-acetate, 1mM EDTA) with 0.1% SDS. SDS-agarose gels were run in

protein running buffer (5mM Tris base, 38mM glycine, 0.02% SDS) and transferred to

PVDF membranes using a BioRad TransBlot SD semi-dry apparatus in a discontinuous

buffer system (cathode buffer: 12mM Tris base, 8mM CAPS, 0.1% SDS; anode buffer:

12mM Tris base, 8mM CAPS, 15% methanol) (Bagriantsev et al., 2006). Membranes

were briefly rinsed in Tween-TBS, blocked in 5% milk in Tween-TBS, and probed with

the following primary antibodies: rabbit anti-human MJD 1:5000 (SEC fractions) or

1:20,000 (all other westerns) (Paulson et al., 1997), mouse anti-polyglutamine 1:2000

(1C2, Chemicon, Temecula, CA), mouse anti-GAPDH 1:500 (Chemicon). Membranes

were rinsed in milk and incubated in peroxidase-conjugated goat anti-rabbit or goat anti-

mouse secondary antibodies 1:7500 (SEC fractions) or 1:15,000 (all other westerns)

(Jackson Immunoresearch, West Grove, PA) and imaged by enhanced

chemiluminescence (Western Lightning, Perkin Elmer, Waltham, MA). Quantification of

immunoblots was performed with NIH ImageJ software (NIH, Bethesda, MD).

Size exclusion chromatography. Soluble fractions of brain lysates were sonicated and

centrifuged at 15,000xg for 10 min. 200µl of clarified lysate was loaded onto a Waters

BioSuite 450 column (Milford, MA) or Superdex 200 column (GE Healthcare,

Piscataway, NJ), and run in mobile phase buffer (150mM sodium chloride, 50mM

sodium phosphate, pH 7.4) at 0.5ml/min. Fractions were either analyzed directly on large

gels by diluting with 6X SDS + DTT, or were precipitated for analysis on mini gels as

follows: 14%v/v trichloroacetic acid was added for 30 min on ice, then fractions were

centrifuged at 15,000xg for 30 min at 4°C, pellets were washed twice with ice-cold

acetone, and resuspended in 2X Laemmli buffer plus DTT. Fractions were analyzed by

SDS-PAGE on 10% polyacrylamide gels, and processed by Western blot for the

antibodies indicated. Blots were imaged either with standard enhanced

chemiluminescence (Western Lightning, Perkin Elmer) or chemiluminescent reagents

designed for low-abundance targets (SuperSignal West Femto, Thermo Scientific,

Rockford, IL). Columns were calibrated with either NativeMark protein standards

(Invitrogen, Carlsbad, CA) or BioRad Gel Filtration standards (BioRad, Hercules, CA).

Results

SDS-resistant ataxin-3 microaggregates accumulate in two genetically distinct SCA3

mouse models. We hypothesized that if aggregated forms of ataxin-3 are important for

SCA3 pathogenesis, microaggregates should accumulate in brains from both SCA3

mouse models. As expected, soluble brain lysates from Q71-B$^{+/-}$ and Q71-B$^{+/+}$ mice show

a dose-dependent increase in ataxin-3 microaggregates, noted here at 6 months of age by

standard Western blot (Fig. 3.1A). Analyzed by the same method, MJD84.2 brain lysates

also contain soluble ataxin-3 microaggregates, while MJD15.4 brain lysates do not (Fig.

3.1B). Since polyacrylamide gels cannot resolve protein complexes above ~400kD, we

used SDS-agarose gels to separate microaggregates more effectively. SDS-agarose

electrophoresis confirmed that Q71-B and MJD84.2 mice develop high-molecular-weight

ataxin-3 microaggregates in the brain (Fig. 3.2). Q71-B brains contain greater

microaggregate levels than MJD84.2 brains (Figs. 3.1-3.2), perhaps because the ataxin-3

splice variant expressed in Q71-B mice, which lacks the final exon and third UIM

domain, is more aggregation-prone than the prominent ataxin-3 splice variant expressed

in MJD84.2 mice, which does include the final exon and UIM (G.M. Harris, unpublished

observations). Since MJD15.4 animals express much more human ataxin-3 than the

MJD84.2 or Q71-B lines yet do not develop microaggregates, the formation of

microaggregates cannot be an artifact of ataxin-3 overexpression but correlates with the

presence of a polyQ expansion. Because the MJD and Q71-B lines are maintained on

different genetic backgrounds (detailed in the methods section), microaggregate

formation is also not a byproduct of different genetic backgrounds. Analysis of non-

neuronal tissues from Q71-B mice showed that microaggregates are brain-specific despite

widespread expression of mutant ataxin-3 in the examined tissues (Fig. 3.3). Our attempts

to use the A11 (anti-oligomer) antibody to confirm the identity of microaggregates as

"toxic oligomers" (Behrends et al., 2006; Kostka et al., 2008) were unsuccessful because

in our hands A11 did not even detect A-beta oligomers as a positive control (data not

shown). These results establish that SDS-resistant ataxin-3 microaggregates meet three of

our four criteria for being toxic species. First, they occur in genetically distinct mouse

models. Second, they correlate with phenotypic severity, meaning that the Q71-B$^{+/+}$

mouse has higher levels than the asymptomatic Q71-B$^{+/-}$ mouse, and the milder MJD84.2

mouse has lower microaggregate levels than the more severely affected Q71-B$^{+/+}$ mouse.

Third, they occur only in the affected tissue type.

SDS-resistant ataxin-3 microaggregates are large but soluble. Because we could not

determine the size of microaggregates on SDS-agarose gels due to the lack of suitable

size markers (Fig. 2.10), we turned to size exclusion chromatography (SEC) because it

can provide size estimates for very large soluble protein complexes. Using a Waters

BioSuite 450 column with a high-molecular-weight cutoff of 7 megadaltons, we

separated soluble brain lysates by SEC and analyzed fractions by Western blot on SDS-

PAGE. Attempts to concentrate fractions by precipitating protein with trichloroacetic

acid resulted in artifactual aggregation of the nonpathogenic ataxin-3 protein from

MJD15.4 brain lysate (data not shown), so we opted to analyze fractions from the column

without precipitation. This required that we run larger volumes of fractions on large scale

gels. This method results in fainter signal but without spurious aggregation (compare Fig.

2.11 to Fig. 3.4A). Using this approach, we established that Q71-B$^{+/+}$ mice develop

soluble ataxin-3 microaggregates that elute in fractions of >~720kD (Fig. 3.4A).

Similarly, MJD84.2 mouse brain lysates contained microaggregates of the same size (Fig.

3.4B). Although MJD15.4 mice express 4-fold more MJD15.4 transprotein than

endogenous ataxin-3 we detected no microaggregates in MJD15.4 brains by SEC (Fig.

3.4C). To further assess microaggregate size, we collected double-volume fractions to

increase the detected signal. By this method, the majority of microaggregates in MJD84.2

brain eluted in fraction 4, which contains the 1048kD marker (Fig. 3.4D).

In Q71-B mice, phenotypic severity correlates with polyQ aggregation foci. The

aggregation foci (AF) assay was developed by Wetzel, Osmand and colleagues to detect

subcellular areas in which expanded polyQ proteins actively can recruit polyQ peptides

through an aggregation process (Osmand et al., 2006). Briefly, biotin-tagged polyQ

peptides are incubated with tissue sections, and the biotin tag is then detected by avidin-

biotin-DAB chemistry after one round of amplification with biotinylated tyramine

(Osmand et al., 2006). As shown in Fig. 3.5, Q71-B$^{+/+}$ mice show more AF than Q71-B$^{+/-}$

mice in various brain regions. Sections from nontransgenic mice (ntg) do not display AF.

Since AF do not colocalize with inclusions (Osmand et al., 2006; Nguyen et al., 2006;

data not shown), they are posited to represent soluble areas of polyQ recruitment and

aggregation in neurons (Osmand et al., 2006). As such, they may correspond with soluble

microaggregates. The dose-dependent increase of AF in Q71-B+/+ versus Q71-B$^{+/-}$ mice

mirrors the parallel, dose-dependent increase in microaggregate formation in these mice,

as detected by our biochemical assays.

Expanded ataxin-3 localizes predominantly to the nucleus in both SCA3 mouse models.

Ataxin-3 is known to shuttle between the cytoplasm and nucleus, but the specific cellular

functions this shuttling activity serves are unknown. In normal human brain ataxin-3 is

mostly a cytoplasmic protein. In SCA3 disease brain, however, ataxin-3 localizes

predominantly to the nucleus in affected regions (Paulson et al., 1997b). In both mouse

models expressing expanded ataxin-3, immunostaining for the disease protein is much

stronger in the nucleus than cytoplasm in most brain regions (Fig. 3.6). This preferential

nuclear localization does not change over time from 3 to 12 months of age in the

MJD84.2 line (Fig. 3.7). Although nuclear inclusions occur in MJD84.2 brain, they are

rare (Fig. 3.6 shows an inclusion in the deep cerebellar nuclei). In the Q71-B line,

hemizygous mice also have very rare inclusions, but homozygous mice develop

inclusions in many brain regions including (but not limited to) the basal ganglia, midbrain and brainstem (Table 3.1). By contrast, in MJD15.4 mice the ataxin-3 immunostaining occurs in both the cytoplasm and nucleus (Fig. 3.7). In nontransgenic mice, endogenous ataxin-3 staining is very faint using two different antibodies; it is possible that this represents non-specific labeling (Fig. 3.6), since ataxin-3 antibody staining in ataxin-3 knockout mice is comparable to that in nontransgenic mice (Fig. 3.8). These results suggest that the ataxin-3 antibodies used in our experiments preferentially detect the human protein and may not detect endogenous mouse ataxin-3 in brain sections, despite the fact that they detect both human and mouse ataxin-3 on western blot (Fig. 3.9).

Neuropathological evaluation of two mouse models of SCA3 reveals that glial proliferation and neuronal loss are not correlated with behavioral phenotype. Since MJD84.2 mice develop a behavioral phenotype (Cemal et al., 2002; Chen et al., 2008) we sought to determine whether MJD84.2 brains also showed signs of neuronal dysfunction or injury. We looked for reactive astrocytosis with glial fibrillary acidic protein (GFAP), microgliosis with the macrophage/microglia-specific calcium binding protein iba1, and overt changes in brain organization and structure with cresyl violet. As shown in Figure 3.10, we observed no differences in GFAP or microglial markers between wild-type (ntg), MJD15.4 and MJD84.2 mice at 12 months of age. Additionally, we observed no major change in the number of neurons in pontine nuclei stained with cresyl violet (Fig. 3.10), and no massive change in brain organization or structure (data not shown). Although the original paper describing the MJD84.2 line reported an increase in GFAP-positive cells in several brain regions and a loss of calbindin-positive Purkinje cells in the

cerebellum (Cemal et al., 2002), we could not replicate either finding (Fig. 3.10, data not shown).

Since other reports of MJD84.2 mouse behavior revealed phenotypes at young ages, we decided to expand the phenotypic characterization of this line by performing open field analysis of spontaneous motor activity in aged MJD84.2 mice. Surprisingly, open field testing of old MJD84.2 mice revealed no decrease in large or small movements compared to wild-type animals (Fig. 3.11, ages 13.5-17.5 months, n=7 for ntg, n=9 for MJD84.2). In contrast, preliminary evidence from other researchers in our laboratory suggest that MJD84.2 animals have a behavioral phenotype at 6 weeks of age compared to nontransgenic littermate controls (V.G. Shakkottai, unpublished observation). We conclude that open field testing is not the best measure of the MJD84.2 phenotype.

The Q71-B line develops robust behavioral changes only when animals are homozygous for the transgene (Goti et al., 2004). Therefore we expected to find neuropathology differences between the hemizygous and homozygous Q71-B mice. As shown in Fig. 3.12, GFAP labeling is higher in Q71-B$^{+/+}$ mice in brain regions usually affected in SCA3/MJD than in Q71-B$^{+/-}$ and nontransgenic mice. No increase in GFAP-positive cells is observed in the cerebral cortex, an area that is essentially spared in SCA3/MJD (Fig. 3.12).

Although reactive astrocytosis is observed in Q71-B$^{+/+}$ mice with a severe behavioral phenotype, it is not observed in the MJD84.2 line, which has a milder phenotype. Since signs of reactive astrogliosis and microgliosis are not consistent across both SCA3 mouse models, we conclude that glial proliferation in affected areas, which is

often used as a proxy for neuronal degeneration, is not a shared phenomenon in phenotypically-expressing SCA3 mice.

Absence of disease-correlated ataxin-3 cleavage fragments in SCA3 mice. If proteolytic cleavage of ataxin-3 is important for pathogenesis, we would expect to observe ataxin-3 species smaller than full-length ataxin-3 in SCA3 mouse brain lysates. Previously, the Q71-B mouse was reported to express cleavage products of ataxin-3 of 30-36kD and aggregated forms of ataxin-3 that remained in the stack of standard SDS-PAGE gels (Goti et al., 2004). In contrast, MJD84.2 mouse brain was not reported to contain ataxin-3 fragments (Cemal et al., 2002). In brain lysates from Q71-B mice, we observed an ataxin-3 immunoreactive band that is smaller than endogenous ataxin-3 and present in hemizygous and homozygous mice at the same level (Fig. 3.13). In MJD84.2 mice, ataxin-3 antibody labeled bands smaller than endogenous ataxin-3 which were also noted in MJD15.4 and nontransgenic animals (Fig. 3.13). Though conceivably ataxin-3 fragments could be generated and become irreversibly stuck in aggregates that cannot be resolved by SDS-PAGE, we interpret these results as showing that ataxin-3 fragments are not present to a greater degree in disease mice than in healthy mice and therefore do not correlate with phenotypic severity.

Overexpression of wild type or expanded human ataxin-3 does not alter the size of protein complexes formed by endogenous ataxin-3. Recent data suggest that loss-of-function mechanisms may contribute to polyQ disease pathogenesis (Lim et al., 2008; Friedman et al., 2007). Loss-of-function may occur through alterations in the function of

polyQ protein-containing complexes, as in the references mentioned above, or may occur

through sequestration of the normal protein into aggregates, preventing the

nonpathogenic protein from carrying out its normal functions. Since ataxin-3 can bind

other ataxin-3 molecules (Gales et al., 2005; Jia et al., 2008; Ellisdon et al., 2006), we

wondered whether overexpression of expanded ataxin-3 would bind endogenous ataxin-3

and alter the protein complexes formed by endogenous ataxin-3. We employed SEC to

see whether expanded ataxin-3 expression altered the elution profile of endogenous

ataxin-3. Endogenous ataxin-3 from brain tends to fractionate in two major peaks, one

higher molecular weight peak of ~1000kD, and a second lower molecular weight peak of

~150kD (Fig. 3.14A). This lower molecular weight peak may correspond to monomeric

ataxin-3, because as a non-globular protein ataxin-3 is expected to run at a larger

apparent size on SEC than its actual size (Chow et al., 2006). We confirmed the accuracy

of our sizing by checking the elution profiles of other proteins that should elute

differently than ataxin-3 (Fig. 3.14B). We confirmed that VCP runs at ~600kD, its

expected size as a hexamer, and each of the other proteins of interest we analyzed had a

unique profile as well (Fig. 3.14B). Satisfied that our elution profile for ataxin-3 was

accurate and reproducible, we performed SEC analysis of brain lysates from 6-month-old

mice, followed by quantification of endogenous ataxin-3 western blot signal (Fig. 3.14C).

The only difference we noted was a small increase in the proportion of endogenous (i.e.

murine) ataxin-3 eluting in fraction 7 in MJD84.2 mice compared to nontransgenic mice

(one-way ANOVA, p=0.044). Thus, overexpression of either normal or expanded human

ataxin-3 does not alter the elution pattern of endogenous ataxin-3, suggesting that neither

wild-type nor expanded ataxin-3 drives endogenous ataxin-3 into abnormal

macromolecular complexes in the brain. The elution patterns for the two transproteins differ slightly, with a higher percentage of MJD15.4 ataxin-3 monomer detected in fraction 4 compared to MJD84.2 monomer (p=0.040) (Fig. 3.14D). The reduction of MJD84.2 monomer in fraction 4 may be due to its incorporation into HMW ataxin-3 microaggregates.

Overexpression of wild-type or expanded human ataxin-3 does not alter subcellular localization of known ataxin-3 interacting proteins. Several ataxin-3 interacting proteins have been identified using various techniques (Shen et al., 2005; Ferro et al., 2007; Wang et al., 2000; Wang et al., 2007) (Table 3.2). Of particular interest among these are VCP, CHIP and E4B because of their importance in protein folding and degradation (Dickey et al., 2007b; Qian et al., 2006; Janiesch et al., 2007). In the case of VCP, the protein is normally found in both the cytoplasm and nucleus of nonneuronal cells (Weihl et al., 2006; Greenberg et al., 2007), but has been described as mostly cytoplasmic in human brain (Guyant-Maréchal et al., 2006). VCP is widely expressed throughout the brain, especially in Purkinje cells, hippocampal neurons, and midbrain and vestibular nuclei (Lein et al., 2007). VCP is known to translocate to the nucleus upon stimulation with EGF or other VCP-binding proteins (Zhang et al., 2000; Laser et al., 2006; Greenberg et al., 2007). CHIP is primarily a cytoplasmic protein, although it does have two potential nuclear localizing sequences and may shuttle between the nucleus and the cytoplasm in response to an appropriate stimulus (Ballinger et al., 1999; Miller et al., 2005). Some portion of the cytosolic pool of CHIP localizes to the ER surface, and relocalizes to aggresomes when certain client proteins, like CFTR, are overexpressed (Meacham et al.,

2001). CHIP is expressed throughout the body, and in the brain it is highly expressed in the olfactory bulb, hippocampus, Purkinje cells, vestibular nuclei and deep cerebellar nuclei (Lein et al., 2007). CHIP does not colocalize to inclusions formed by GFP-tagged polyQ protein (Miller et al., 2005). E4B is important for cardiac development and neuronal responses to ER stress (Kaneko-Oshikawa et al., 2005). E4B is primarily cytoplasmic (Kaneko et al., 2003) and is highly expressed in cortical projection neurons, thalamic nuclei, hippocampus, vestibular nuclei, Purkinje cells, deep cerebellar nuclei, and to a lesser extent in most other brain regions (Kaneko et al., 2003; Lein et al., 2007).

To determine whether overexpression of expanded ataxin-3 alters the regional or subcellular localization of its interacting proteins, we used immunohistochemistry to compare the MJD15.4 and MJD84.2 lines with nontransgenic controls. As shown in Figure 3.15, overexpression of wild-type or expanded ataxin-3 does not appreciably change the subcellular localization of VCP, CHIP, or E4B.

Discussion

Aggregation is an important feature of all polyQ diseases. We have attempted to address the question of whether soluble microaggregates of ataxin-3 are the pathogenic species in SCA3. Our results show both that SDS-resistant ataxin-3 microaggregates form *in vivo* only when ataxin-3 contains the polyQ expansion and that these microaggregates are a shared feature of two genetically distinct SCA3 transgenic mouse models expressing full length, expanded ataxin-3. Ataxin-3 microaggregates are found only in the selectively vulnerable tissue in SCA3, the brain. In the Q71-B model, microaggregate levels correlate with phenotypic severity. Since the MJD84.2 phenotype does not

progress as rapidly nor is the phenotype as severe as the Q71-B$^{+/+}$ mouse (Fig. 3.11; Cemal et al., 2002; Chen et al., 2008), we conclude that the presence of microaggregates correlates with the MJD84.2 phenotype but cannot conclude that phenotypic severity correlates with increasing microaggregate levels in this model. Our results do not rule out the possibility that misfolded ataxin-3 monomer also contributes to pathogenesis. Indeed, misfolded monomeric ataxin-3 is likely critical to the formation of higher order, misfolded ataxin-3 complexes, as suggested by *in vitro* studies showing that a single misfolded polyQ protein serves as the nidus for polyQ aggregation (Chen et al., 2002; Ellisdon et al., 2007). The soluble, SDS-resistant ataxin-3 microaggregates we observe meet most of our *a priori* criteria for being a (or the) toxic protein species in SCA3: they occur in two genetically distinct mouse models, occur to a greater degree in symptomatic animals, and are found only in the affected tissue type. Whether they meet the fourth criterion, that their presence should correlate with the onset of disease, will be discussed below.

Although our SEC results do not provide a precise size calculation, they are consistent with pure ataxin-3 homo-oligomers of ~15 monomers in size (assuming MJD84.2 transprotein is 65kD, as it appears on SDS-PAGE, and assuming no other protein comprises a major portion of microaggregates; see Figs. 3.4 and 3.9). To confirm that microaggregates are pure oligomers we would need to analyze them by mass spectrometry. Coomassie staining of SEC fractions on gels demonstrates that many other proteins co-elute with microaggregates (data not shown); these contaminants would need to be removed prior to mass spectrometry analysis. We have attempted to immunopurify ataxin-3 microaggregates from SEC fractions, but have not been able to detect ataxin-3

microaggregates after immunopurification (data not shown). In the future, other methods such as hydrophobic interaction chromatography or ion exchange chromatography may assist us in further purifying these microaggregates. Although we have not been able to detect other candidate proteins in ataxin-3 microaggregates by Western blot, they may be present in levels too low for Western blot detection, or are bound within microaggregates such that they are protected from antibody access.

Many reports have shown that nuclear localization of polyQ disease protein is important for pathogenesis (Saudou et al., 1998; Klement et al., 1998; Kordasiewicz, et al., 2006; Bichelmeier et al., 2007; Cummings et al., 1998). We observed nuclear localization of expanded ataxin-3 in both Q71-B and MJD84.2 mice, while wild-type ataxin-3 was distributed in both the nucleus and cytoplasm in MJD15.4 mice. It is still poorly understood why polyQ proteins tend to localize to the nucleus when expanded. We have several potential hypotheses to explain why ataxin-3, in particular, goes to the nucleus in SCA3. One possibility is that when ataxin-3 enters the nucleus during its normal shuttling, the nuclear environment somehow leads it to aggregate, thus preventing its export back to the cytoplasm. Another possibility, related to the fact that ataxin-3 functions in protein quality control, is that ataxin-3 gets recruited to the nucleus as part of a cellular response to the stress of polyQ protein expression. If this is true, we would expect to find ataxin-3 in the nucleus of cells expressing other expanded polyQ proteins, and perhaps in other neurodegenerative diseases. Ataxin-3 nuclear relocalization in response to heat shock has been reported by another group (Reina, C.P., Zhong, X., Pittman, R.N. Proteotoxic stresses alter ataxin-3 interactions with Rad23b and VCP and heat shock induces nuclear localization of ataxin-3. Program No. 444.4/V20. 2008

Neuroscience Meeting Planner. Washington, DC: Society for Neuroscience, 2008. Online.). Work is underway in our lab to determine if ataxin-3 nuclear localization occurs in other neurodegenerative disease models, including HD and AD mouse models.

We did not detect major neuronal loss in MJD84.2 mice. These results differ from Cemal et al. (2002) and Chen et al. (2008) who both reported neuronal loss in aged MJD84.2 mice, albeit by different methods and in different brain regions. Cemal et al. (2002) reported 30% loss of pontine neurons, 40% loss of dentate neurons, degeneration of Purkinje cells of the cerebellum (no percentage reported) and some demyelination of peripheral nerves by 12 months of age, but they also reported that brain mass was proportional to body weight in MJD84.2 mice. In contrast, unbiased stereological analysis of 13.5-month-old MJD84.2 mice performed by Chen et al. (2008) revealed small but significant reductions in both TH-positive substantia nigra neurons (15%) and pontine neurons (15%), along with a 10% decrease in brain mass (no calculation of body weight was made in this paper). The differences between the Cemal et al. (2002) and Chen et al. (2008) results could be due to methodological differences or to some genetic alteration that occurred when the MJD84.2 line was rederived via *in vitro* fertilization in the C57BL/6 strain by Chen et al. (2008). Since the MJD84.2 line had to be recreated from frozen sperm and donor C57BL/6 eggs, it is possible that the donor egg's DNA contained polymorphisms not present in the original MJD84.2 line which could contribute to differences in the phenotypes of MJD84.2 mice created by the Chamberlain lab and the Bezprozvanny lab. We cannot test this possibility since the Chamberlain lab no longer possesses its original MJD84.2 line. If genetic differences in the rederived mouse background contribute to phenotype, we would expect our results to be more

similar to Chen et al.'s results since we acquired the MJD84.2 line from that lab after its rederivation. It is also possible that we did not observe small but significant differences in neuronal counts because we did not use unbiased stereology or because the MJD84.2 mice used in our studies were slightly younger (12 months). Additionally, Cemal et al. (2002) reported that >50% of pontine neurons and >40% of dentate nucleus neurons contain intranuclear inclusions, but we had difficulty finding more than a few inclusions in an entire 12-month-old MJD84.2 brain. If there are polymorphisms between the two MJD84.2 lines in genes like dynein or HDAC6 which subtly alter their capacity to promote inclusion formation, this might lead to large changes in the number of inclusions we see in mouse brains.

We also did not detect a reduction in spontaneous activity in aged MJD84.2 mice compared to control mice (Fig. 3.11). We did not, however, perform other corroborating behavioral tests nor did we test young mice. Our results in these mice differ from the other two published reports, which in turn differ slightly from each other. Using multiple beam-walking tests and gait analysis, Chen et al. (2008), found mild, quantifiable motor phenotypes as early as 7.5 months. Some tests revealed mild phenotypic progression over time, while others showed no significant progression as the mice aged. Cemal at al (2002) described qualitative motor impairments in MJD84.2 mice as early as 4 weeks, but did not report quantitative test results. In preliminary studies currently underway in our laboratory, we may be observing electrophysiological abnormalities in Purkinje cells by 6 weeks of age (V.G. Shakkottai, unpublished observation). It will be important for our lab to perform further systematic and linked behavioral, biochemical, and

electrophysiological studies on MJD84.2 mice to determine precisely the age of phenotypic onset in these animals.

The fact that we saw no alterations in endogenous ataxin-3 levels or in normal ataxin-3-containing complexes when expanded ataxin-3 is expressed agrees with data from the ataxin-3 knockout mouse (Schmitt et al., 2007). We also did not observe mislocalization of ataxin-3 interacting proteins in MJD84.2 mice compared to control mice. While this does not rule out alterations in ataxin-3 complexes when ataxin-3 is expanded, it suggests that such alterations, if they do occur, do not take place at the level of subcellular localization. It is possible that complexes containing expanded ataxin-3 still form appropriately, but that their function is altered. Although expanded ataxin-3 has similar *in vitro* activity to wild-type ataxin-3 (Tzvetkov and Breuer, 2007; Winborn et al., 2008), expanded ataxin-3 does not deubiquitinate proteins in cells to the same degree that wild-type ataxin-3 does (Winborn et al., 2008). Since the *in vitro* and *in vivo* activity of expanded ataxin-3 differ, ataxin-3 protein-protein interactions within the cell may be important for regulating its activity. Until we know more about how ataxin-3 complexes function in cells or identify endogenous ataxin-3 substrates, it will be difficult to assess fully whether polyQ expansion perturbs ataxin-3 normal function *in vivo.*

The one criterion we did not satisfy in our studies was to show that microaggregates correlated with the onset of phenotype. We were unable to determine the relationship between timing of microaggregate formation and the onset of symptoms because we could not find an age at which Q71-B$^{+/+}$ mice or MJD84.2 mice were completely devoid of pathology. Even in the MJD84.2 line with its mild phenotype, ataxin-3 was localized to the nucleus in all ages examined, and observation of MJD84.2

mice at weaning (3 weeks) suggests that they are distinguishable from their littermate controls (V.G. Shakkottai, unpublished observation). Our data suggest that both Q71-B$^{+/+}$ and MJD84.2 mice have phenotypes at very young ages and it may be difficult or impossible to find a time at which they are completely normal. Of the mouse models we used, the Q71-B$^{+/-}$ mice are closest to "presymptomatic" in the sense that they have mild neuropathological and no behavioral symptoms up to 15 months of age (Goti et al., 2004). Although Q71-B$^{+/-}$ mice were reported to have no behavioral phenotype, observations in our lab of Q71-B$^{+/-}$ mice aged beyond 15 months suggest that they develop clasping behavior and tremor at 20-23 months of age (G. M. Harris, unpublished observations). Therefore, the fact that we observe a small amount of ataxin-3 microaggregates in Q71-B$^{+/-}$ mice suggests that microaggregates develop prior to behavioral symptoms and neuronal loss. To solidify this claim, we would first need to perform detailed behavioral studies of aged Q71-B$^{+/-}$ mice to determine the age of behavioral symptom onset. Then, we would need to perform quantitative measurements of microaggregate levels across the lifespan to determine whether microaggregate levels correlate with behavioral onset. The ideal mouse model of SCA3 would be demonstrably devoid of all neuropathology at young ages, and develop a behavioral phenotype sometime around 6 months of age, so that interventions which hasten or delay symptoms would be easily detectable within a year of study. Some of the SCA3 mouse lines recently generated by Bichelmeier et al. (2007) may meet this criterion, although their standard ataxin-3-Q70 overexpressing mouse reportedly has neuropathological signs at all ages. Our lab is generating a genetically precise knock-in mouse model of SCA3, in which various CAG repeat lengths are placed into the endogenous mouse *Atxn3* gene (G.

M. Harris, unpublished data). Depending on the expansion size, knock-in SCA3 mice could be used for studies of pathogenesis, therapeutic trials or both.

Our neuropathology results from Q71-B mice were similar to those reported by Goti et al. (2004). We observed nuclear localization of ataxin-3 and increased inclusion formation in homozygous versus hemizygous mice, with inclusion density being pronounced in certain brain regions known to be affected in SCA3 (Table 3.1). In addition to this, we found increases in glial markers in certain brain regions, which was not reported by Goti et al. (2004) (Fig. 3.12, Table 3.1). We also assessed polyQ aggregation foci (AF) to see whether they occurred preferentially in affected brain regions and correlated with microaggregate levels (Fig. 3.5, Table 3.1). Although polyQ AF do correlate with phenotypic severity, they can be found throughout the brain, not only in regions we would expect to be affected in SCA3. Since polyQ aggregation foci appear in places traditionally thought to be unaffected in SCA3 (e.g. cerebral cortex), they may not correlate with the presumptive oligomers of interest to us. However, recent neuropathological studies suggest that more areas of the brain are affected in SCA3 than previously recognized (reviewed in Rüb et al., 2008). The field will need to revisit which brain areas are considered "affected" versus "unaffected" regions in studies of mouse models and human disease tissue.

Several conformation-specific antibodies are currently available to study polyQ protein conformation. One of the most widely used is the anti-oligomer antibody, A11, which was raised against beta amyloid oligomers (Kayed et al., 2003). Although the A11 antibody has proved useful in studies of polyQ oligomers *in vitro* (Behrends et al., 2006; Kayed et al., 2007), it has proven difficult to use on brain lysates. This could be due to

the complexity of brain lysate contents and the high levels of chaperones expressed in the brain. Many natively folded cellular proteins bind A11, including many chaperones, and this capacity to bind A11 disappears when the proteins are heat-shocked and unfolded (Yoshiike et al., 2008). While this suggests interesting possibilities for how chaperones function, it may interfere with our ability to use this antibody to detect "toxic" species. Another antibody that may prove useful for studying polyQ protein conformations is 3B5H10 (Brooks et al., 2004). Generated against monomeric expanded huntingtin, 3B5H10 appears to bind specifically to disease-associated polyQ monomers (Peters-Libeu et al., 2005). We would not expect 3B5H10 to bind microaggregates, but if it bound to monomeric expanded ataxin-3 in our SCA3 mice, it would suggest that toxicity in SCA3 mice could reflect monomers as well as microaggregates.

The fact that our antibodies do not reliably detect endogenous, murine ataxin-3 by immunohistochemistry may be due to our methodology. Since our antibodies detect murine ataxin-3 on Western blot, the antigenic epitopes clearly are present in the murine protein. Antigen retrieval methods may help to improve antibody sensitivity on tissue sections. If antigen retrieval does not render the current ataxin-3 antibodies useful for murine ataxin-3 in brain sections, we may need to raise additional antibodies against murine ataxin-3. It is important that we be able to detect endogenous ataxin-3 in tissue sections in order to determine whether endogenous ataxin-3 also localizes to the nucleus in other neurodegenerative diseases, and to follow the disease protein in the knock-in SCA3 mouse we are generating.

A recently published study reports that treating MJD84.2 mice with dantrolene corrects dysregulated calcium signaling and improves their behavioral phenotype (Chen

et al., 2008). Given that we do not know whether dysregulated calcium signaling is a proximal or late event in polyQ disease, it would be interesting to know whether dantrolene-treated MJD84.2 mice show changes in microaggregate levels (Chen et al., 2008). If treated mice have lower levels of microaggregates, this would suggest that microaggregates exist downstream of calcium signaling problems. If microaggregate levels are unchanged in treated mice, then microaggregates may exist upstream of calcium signaling perturbations.

Taken together, our results provide the first animal model evidence for soluble microaggregate formation in the polyQ disease, SCA3. These results agree with data from yeast and mouse models of HD showing that soluble polyQ protein microaggregates correlate with phenotypic severity (Behrends et al., 2006; Weiss et al., 2007). The microaggregates we observe meet most of the criteria we believe are important to establish them as potential toxic species in SCA3. Our results argue against a major role for ataxin-3 proteolysis in SCA3 pathogenesis suggesting instead that the full length protein mediates disease. Improving the ability of neurons to counter ataxin-3 aggregation, either by increasing ataxin-3 solubility or enhancing dissociation and degradation of microaggregates, may prove helpful in treating SCA3. Enhancing the capacity of neurons to reduce microaggregate formation will likely prove useful in neurodegenerative disease therapy in general.

Table 3.1. Neuropathological analysis of the Q71-B mouse line.

Brain Region	Ataxin-3	PolyQ Foci	Ub-positive Inclusions	Gliosis
Neocortex	++ (rare NI) +++ (NI)	++ +++	+ ++	No No
Hippocampus	+ ++ (dots)	++ +++	+ +	No No
Thalamic nuclei	+ ++ (NI)	+ ++	0 0	No Mild
Caudate/putamen	+ +++ (NI)	0 +	0 0	No No
Nucleus accumbens	+ +++ (NI)	0 +	+ +	No No
Substantia nigra, pars compacta	+ +++	+ ++	0 0	No YES
Pontine nuclei	+ +++ (NI)	+ +++	+ +++ (NI)	No YES
Red nucleus	++ ++	+ ++	0 ++ (NI)	No No
Cranial nerve nuclei	+ +++	+ +++	+ (small NI) +++ (NI and periNI)	No YES
Deep cerebellar nuclei	+ +++	+ ++	0 +++ (NI and periNI)	No YES

Note: Brain sections from 4-month-old female mice were stained with the indicated antibodies or probes. Q71-B$^{+/-}$ results are indicated in green, Q71-B$^{+/+}$ results are in blue. The intensity of labeling or number of aggregation foci in each stain is indicated by the number of "+" marks. NI = nuclear inclusions; periNI = perinuclear inclusions.

Table 3.2. Known ataxin-3 interacting proteins.

interacting protein	gene name (human)	proposed function	ID method	reference
Pre1 (20S proteasome subunit)	PSMB2	20S proteasome core beta subunit	co-IP	Doss-Pepe et al, 2003
p45	PSMC5	ATPase subunit of 19S proteasomal cap	GST pull-down (recomb protein), co-IP	Wang et al, 2007
VCP/CDC48/p97	IBMPFD	AAA ATPase, protein degradation	co-IP w/mass spec	Doss-Pepe et al, 2003; Zhong and Pittman, 2006
ataxin-3	ATXN3	deubiquitinating enzyme	GST pull-down (recomb protein), co-IP	Jia et al, 2008
SUMO	SUMO1	ubiquitin-like modifier	yeast two-hybrid	Shen et al, 2005
NEDD-8	NEDD8	ubiquitin-like modifier	yeast two-hybrid, GST pull-down (recomb protein)	Ferro et al, 2007
ubiquilin-1/PLIC-1	PLIC1	ubiquitin-like protein, proteasome shuttling factor	GST pull-down (recomb protein)	Heir et al, 2006
CHIP	STUB1	co-chaperone, ubiquitin ligase	co-IP	Jana et al, 2005
Hsp90	HSP90	chaperone	pull-down w/mass spec	Zhong and Pittman, 2006
Hsc70	HSPA8	chaperone	pull-down w/mass spec	Zhong and Pittman, 2006
E4B	UBE4B	ubiquitin ligase	GST pull-down, co-IP	Matsumoto et al, 2004
parkin	PRKN, PARK2	ubiquitin ligase	co-IP with truncated ataxin-3	Tsai et al, 2003
glycogen synthase kinase 3 beta	GSK3B	phosphorylation of multiple substrates	GST pull-down (recomb protein)	Fei et al, 2007
casein kinase 2	CK2	serine/threonine kinase	GST pull-down (recomb protein), co-IP	Tao et al, 2008
hHR23A	HHR23A, RAD23A	nucleotide excision repair	yeast two-hybrid, GST pull-down (recomb protein)	Wang et al, 2000
hhR23B	HHR23B, RAD23B	nucleotide excision repair	GST pull-down (recomb protein), yeast two-hybrid	Doss-Pepe et al, 2003; Wang et al, 2000
neurofilament light chain	NFL	cytoskeletal protein	pull-down w/mass spec	Zhong and Pittman, 2006
alpha-tubulin	TUBA	cytoskeletal protein	pull-down w/mass spec	Zhong and Pittman, 2006
dynein	DYN	microtubule motor protein	co-IP	Burnett and Pittman, 2005

Table 3.2. Continued.

interacting protein	gene name (human)	proposed function	ID method	reference
histone deacetylase 3	HDAC3	histone deacetylase	GST pull-down (recomb protein), co-IP	Evert et al, 2006
histone deacetylase 6	HDAC6	histone and tubulin deacetylase	co-IP	Burnett and Pittman, 2005
CBP	CREBBP	histone acetyltransferase	in vitro pull-down, co-IP	Li et al, 2002, Chai et al, 2001
p300	EP300	histone acetyltransferase	in vitro pull-down, co-IP	Li et al, 2002
PCAF	GCN5, KAT2A	histone acetyltransferase	in vitro pull-down, co-IP	Li et al, 2002
PML	PML, TRIM19	transcription factor and tumor suppressor	co-IP	Chai et al, 2001
nuclear receptor corepressor	NCOR1	short-term active transcription repression	co-IP	Evert et al, 2006
Ewing sarcoma breakpoint region 1	EWSR1	putative RNA binding protein	yeast two-hybrid	Lim et al, 2006
Rho GTPase activating protein 19	ARHGAP19	negative regulator of Rho GTPase	yeast two-hybrid	Lim et al, 2006
Rho GDP dissociation inhibitor alpha	ARHGDIA	inactivation of Rho proteins	yeast two-hybrid	Shen et al, 2005
neuronal amiloride-sensitive cation channel 2	ACCN2	putative ion channel	yeast two-hybrid	Shen et al, 2005
protein interacting with PRKCA 1	PRKCABP, PICK1	may organize the localization of membrane proteins	yeast two-hybrid	Lim et al, 2006
Lin10	C16orf70	function unknown	yeast two-hybrid	Lim et al, 2006
testis expressed 11	TEX11	expressed only in male germ cells	yeast two-hybrid	Lim et al, 2006

Note: Proteins documented to interact with ataxin-3 via physical interaction are listed here, along with their putative function if known, and the method by which interaction with ataxin-3 was detected.
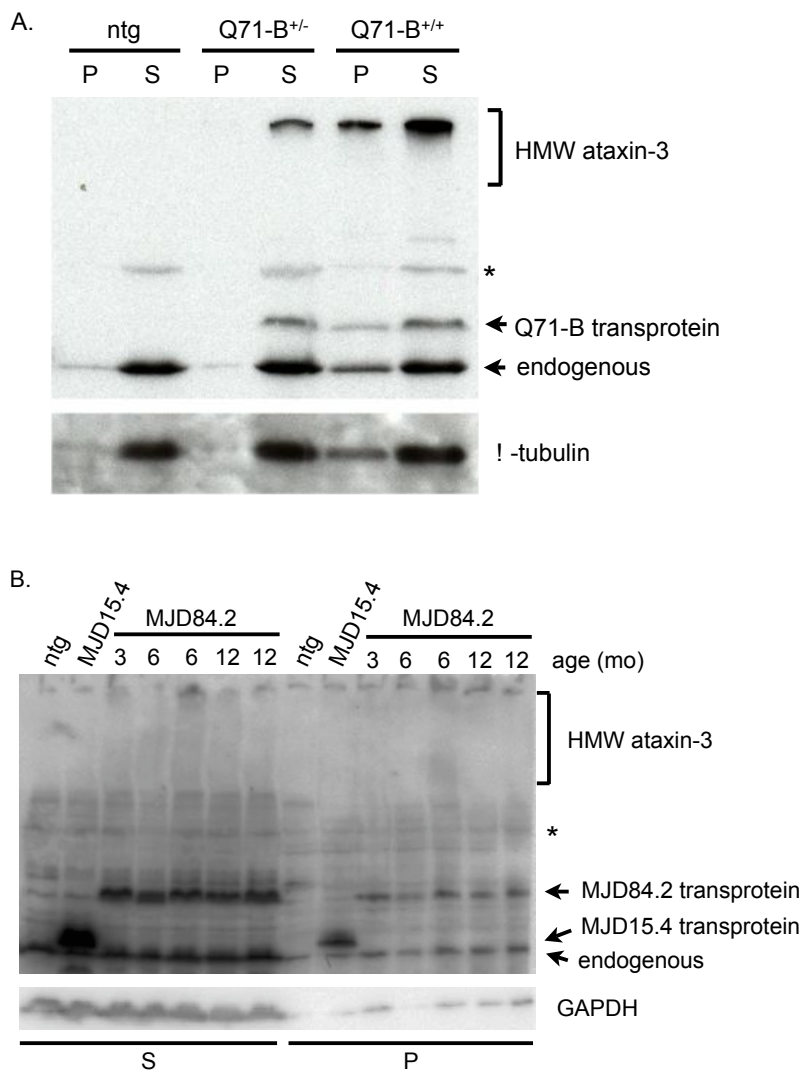
Figure 3.1. Transgenic mice overexpressing expanded ataxin-3 develop soluble SDS-resistant microaggregates. *A.* Brain lysates from 6-month-old Q71-B mice were separated into soluble (S) and pellet (P) fractions at 4000rpm, and separated by SDS-PAGE. Ataxin-3 immunoblotting reveals endogenous ataxin-3, monomeric Q71-B transprotein, and high-molecular-weight (HMW) ataxin-3 that remains at the top of the stacking gel. *B.* Brain lysates from 6-month-old nontransgenic and MJD15.4 mice, or from MJD84.2 mice of 3-12 months of age as indicated, were separated into soluble and pelletable fractions as in *A*. Ataxin-3 immunoblotting reveals the indicated ataxin-3 species. GAPDH is shown as loading control.
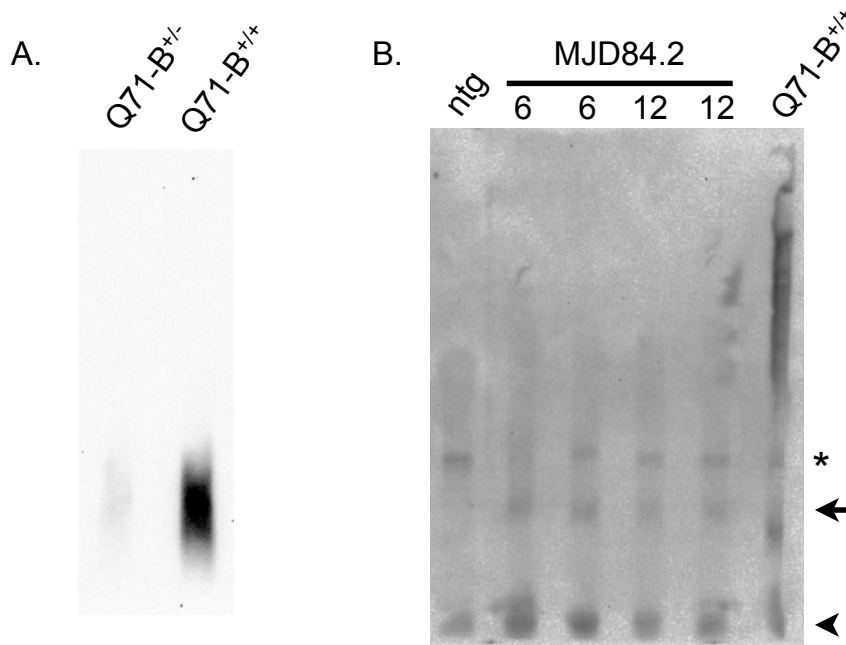
Figure 3.2. SDS-agarose gel electrophoresis confirms the presence of soluble ataxin-3 microaggregates in SCA3 transgenic mouse brain. *A.* Q71-B$^{+/+}$ mice have higher levels of microaggregates than Q71-B$^{+/-}$ mice. Soluble brain lysates from 6-month-old mice were separated by SDS-PAGE then probed for ataxin-3. *B.* MJD84.2 mice have low levels of microaggregates (arrow) detectable by SDS-agarose gel probed for ataxin-3. The arrowhead indicates the dye front, which contains all proteins too small to be separated on the gel. Nontransgenic (ntg) and Q71-B$^{+/+}$ lysate included for comparison. * = nonspecific band.

A.

ntg   Q71-B$^{+/-}$ Q71-B$^{+/+}$

B H L K B H L K B H L K

M$_r$

HMW ata[

250
150
100
75   *
50   ← Q71-B tr[
37   ← endogen[

25
20

15

GAPDH

B.

Q71-B$^{+/-}$ Q71-B$^{+/+}$

B   H   L   K   B   H   L   K

.3. SDS-resistant microaggregates occur only in brain. *A*. Soluble brain
t (H), liver (L), and kidney (K) lysates were separated by SDS-PAGE and
or ataxin-3 with a polyclonal antibody. The brain is the only organ to show
e microaggregate accumulation. GAPDH is shown as loading control. *B*.
prepared as in *A* were separated by SDS-agarose. Even by this more sensitive
microaggregates are only detected in brain.
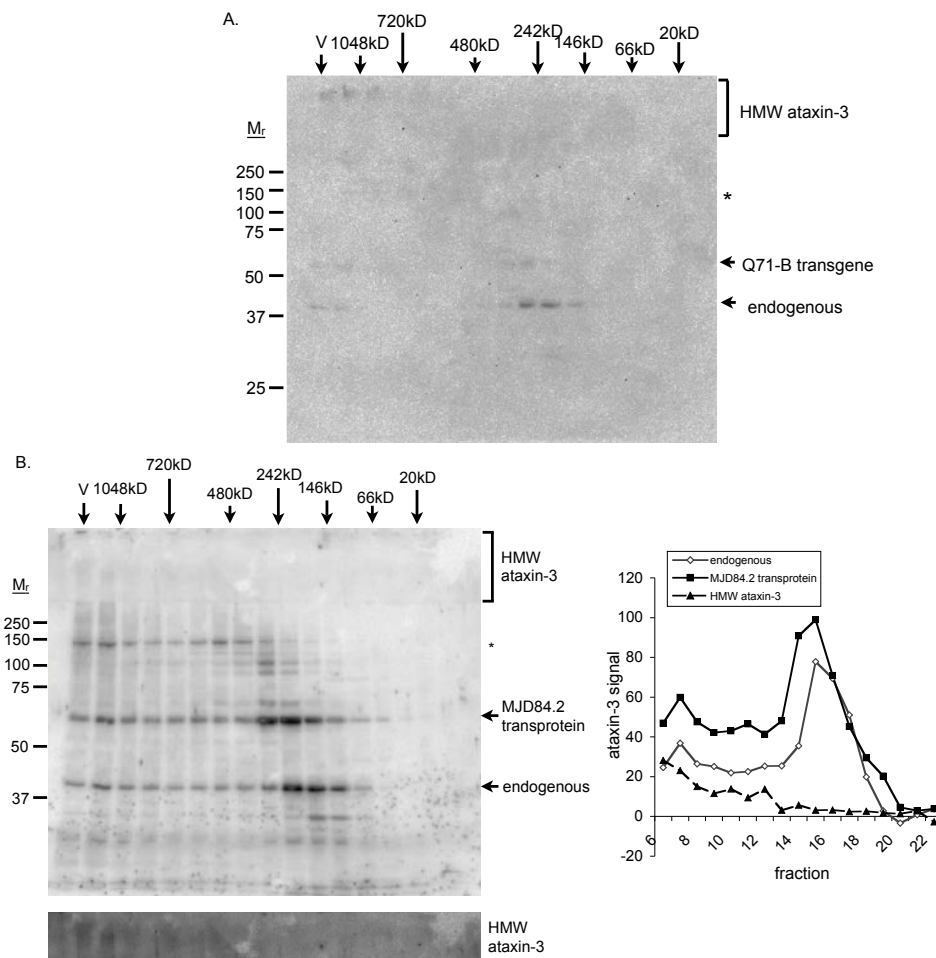
Figure 3.4. SDS-resistant microaggregates in SCA3 transgenic mouse brains are soluble with an elution peak around 1048kD. *A.* Soluble Q71-B$^{+/+}$ brain lysate (5-month-old) was fractionated by SEC into 0.5mL fractions and analyzed by SDS-PAGE. Ataxin-3 blotting reveals endogenous ataxin-3, monomeric Q71-B transprotein, and microaggregates (HMW ataxin-3). The latter runs in the stacking gel in fractions larger than ~720kD. Molecular weight elution markers labeled at top, V=void volume, * = nonspecific band. *B.* S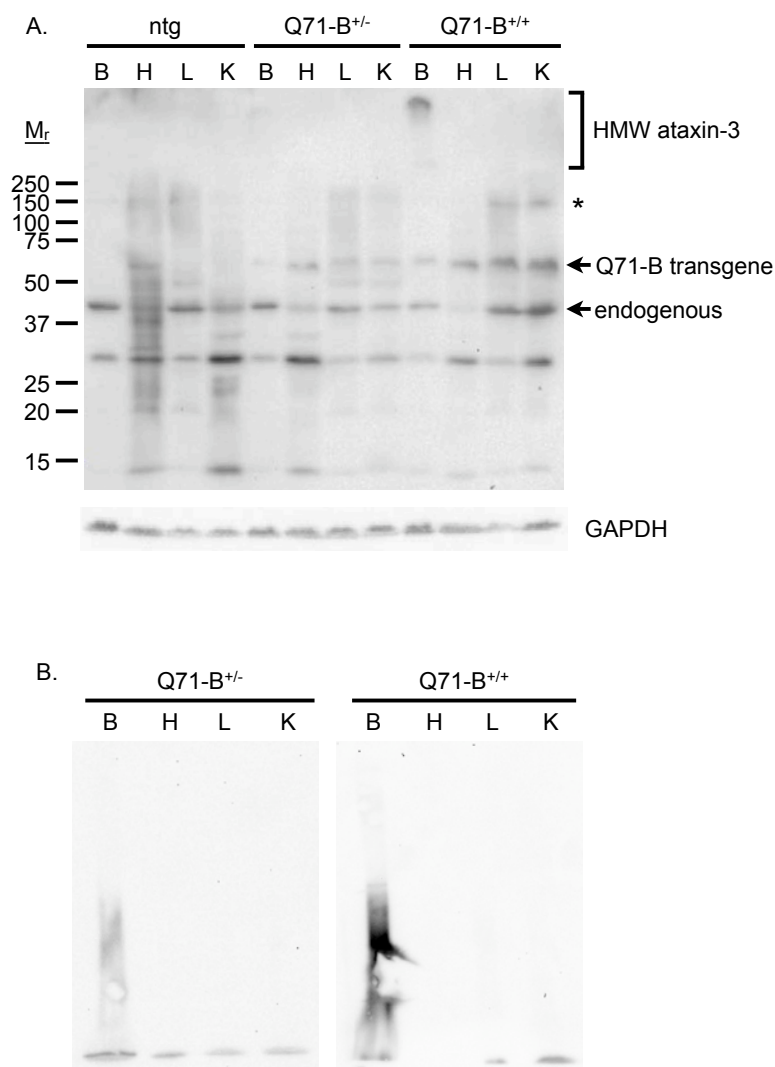oluble brain lysate from a 12-month-old MJD84.2 mouse was analyzed as in *A*, using a special detection reagent for low-abundance proteins. Ataxin-3 blotting shows monomeric endogenous ataxin-3 and transprotein as well as microaggregates in the stacking gel eluting in fractions surrounding the 1048kD marker. A darker exposure of the microaggregates is shown below the full blot. The relative optical density of each ataxin-3 species was calculated for each fraction, corrected for background signal, and graphed to the right. *C.* Soluble brain lysate from an 11.5-month-old MJD15.4 mouse analyzed as in *B*. Ataxin-3 blotting reveals no signal in the stacking gel. *D.* Quantitation of HMW ataxin-3 from 6-month-old MJD84.2 brain lysates analyzed as in *B,* but using larger 1mL fractions to enhance ataxin-3 signal. The amount of HMW ataxin-3 per fraction is expressed as a percentage of the total HMW ataxin-3 on the blot. Most HMW ataxin-3 elutes in the fraction containing the 1048kD marker (fraction 4), with variable amounts in the void fraction (fraction 3). N=3, error bar = 1 S.D.

Figure 3.4. Continued.

	ntg	Q71-B$^{+/-}$	Q71-B$^{+/+}$
pons			
cortex			
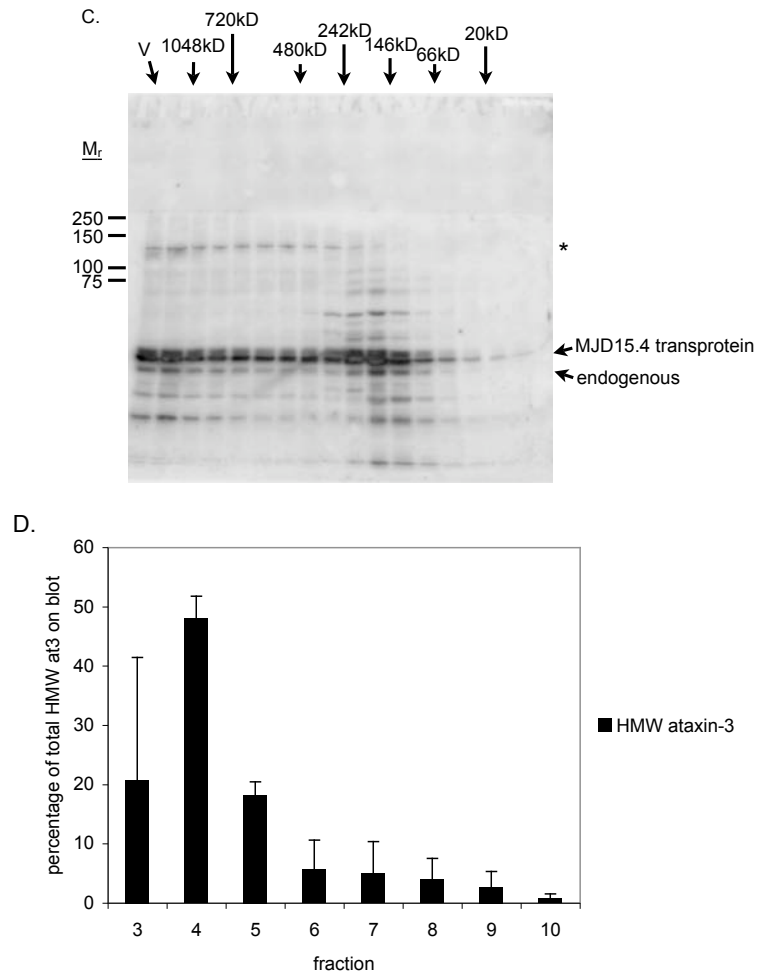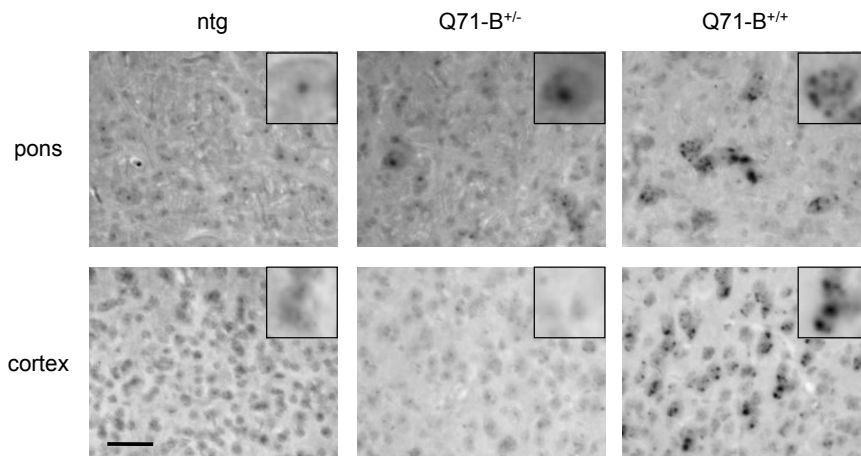
Figure 3.5. PolyQ aggregation foci may correspond to soluble microaggregates in tissue. 4-month-old Q71-B mouse brain sections were labeled with biotinylated Q30 peptides and nickel-DAB to detect areas of active intracellular polyQ recruitment and aggregation. Q71-B$^{+/+}$ mice have polyQ aggregation foci in classically affected (pons) and unaffected (cortex) brain areas. Q71-B$^{+/-}$ mice develop aggregation foci in the pons and other classically affected brain regions (detailed in Table 3.1), but the levels are much lower than the levels observed in Q71-B$^{+/+}$ mice. Nontransgenic animals (ntg) do not have polyQ aggregation foci in any brain region examined. Insets show higher power image of each section.
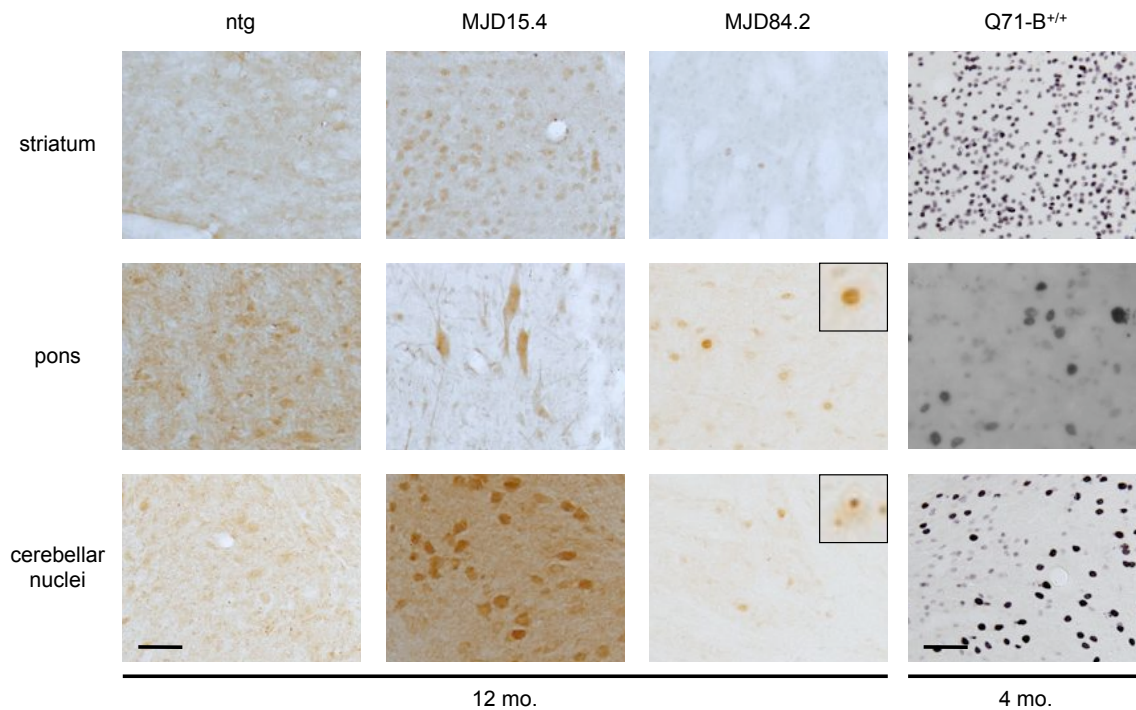
Figure 3.6. Expanded ataxin-3 localizes primarily to the nucleus in SCA3 transgenic mouse brain. Ataxin-3 immunohistochemistry in both MJD84.2 and Q71-B$^{+/+}$ brain reveals that most ataxin-3 is in nuclei. In MJD15.4 mice, ataxin-3 is found in both the cytoplasm and the nucleus. In Q71-B$^{+/+}$ mice, transgene expression is high in all brain regions shown. Nontransgenic, MJD15.4, and MJD84.2 mouse brains were stained with standard DAB immunohistochemistry; Q71-B$^{+/+}$ brain was stained with nickel-DAB. Scalebars = 50 micrometers.

MJD84.2

3 mo.
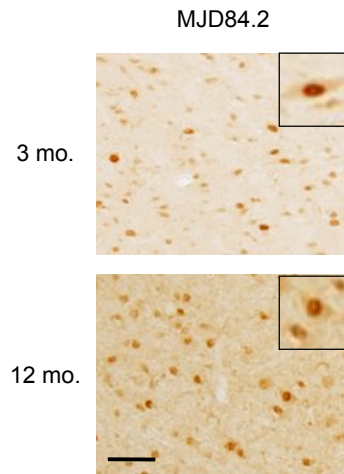
12 mo.

Figure 3.7. Localization of ataxin-3 in adult MJD84.2 mice does not change over time. Serial sections through brains from 3-month-old and 12-month-old MJD84.2 mice were stained for ataxin-3. Brain region shown is pontine reticular nuclei. Higher power insets show that ataxin-3 stains primarily cell nuclei without prominent inclusion formation at both ages. Scalebar = 50 micrometers.
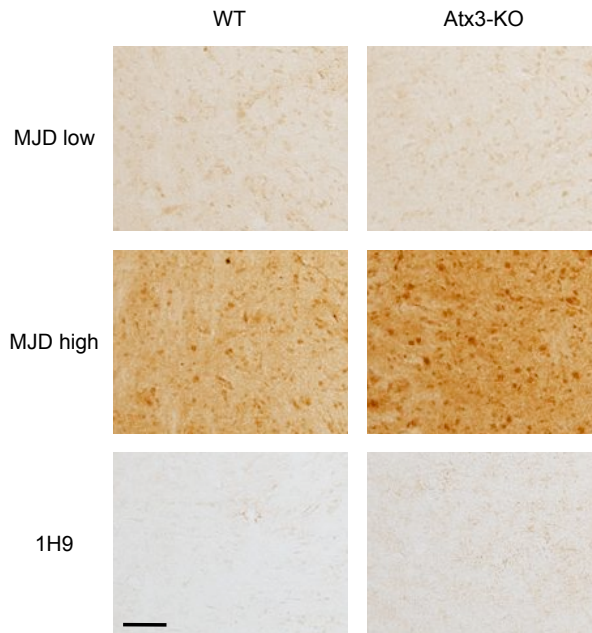
Figure 3.8. Ataxin-3 antibodies do not detect endogenous murine ataxin-3 by immunohistochemistry. Both polyclonal (MJD) and monoclonal (1H9) antibodies were used to stain wild-type (WT) and ataxin-3 knockout (Atx3-KO) brain sections. Shown are sections from the pontine reticular nucleus. Regardless of antibody concentration or origin, ataxin-3 immunostaining was identical in wild-type and knockout mice. Q71-B$^{+/+}$ brain were used as a positive control for each set of antibody conditions (not shown). Scalebar = 50 micrometers.
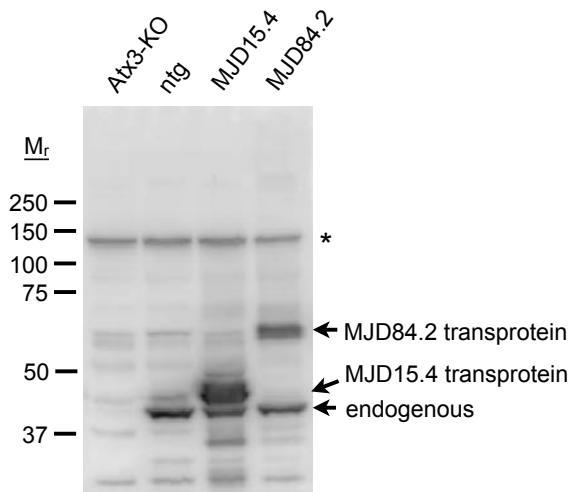
Figure 3.9. Ataxin-3 antibodies detect endogenous murine ataxin-3 by Western blot. Soluble brain lysates from ataxin-3 knockout (Atx3-KO), nontransgenic (from the MJD line), MJD15.4 and MJD84.2 mice were separated by standard SDS-PAGE. Blotting with polyclonal ataxin-3 antibody reveals endogenous murine ataxin-3 as well as monomeric transgenic proteins MJD15.4 and MJD84.2. * = nonspecific band.
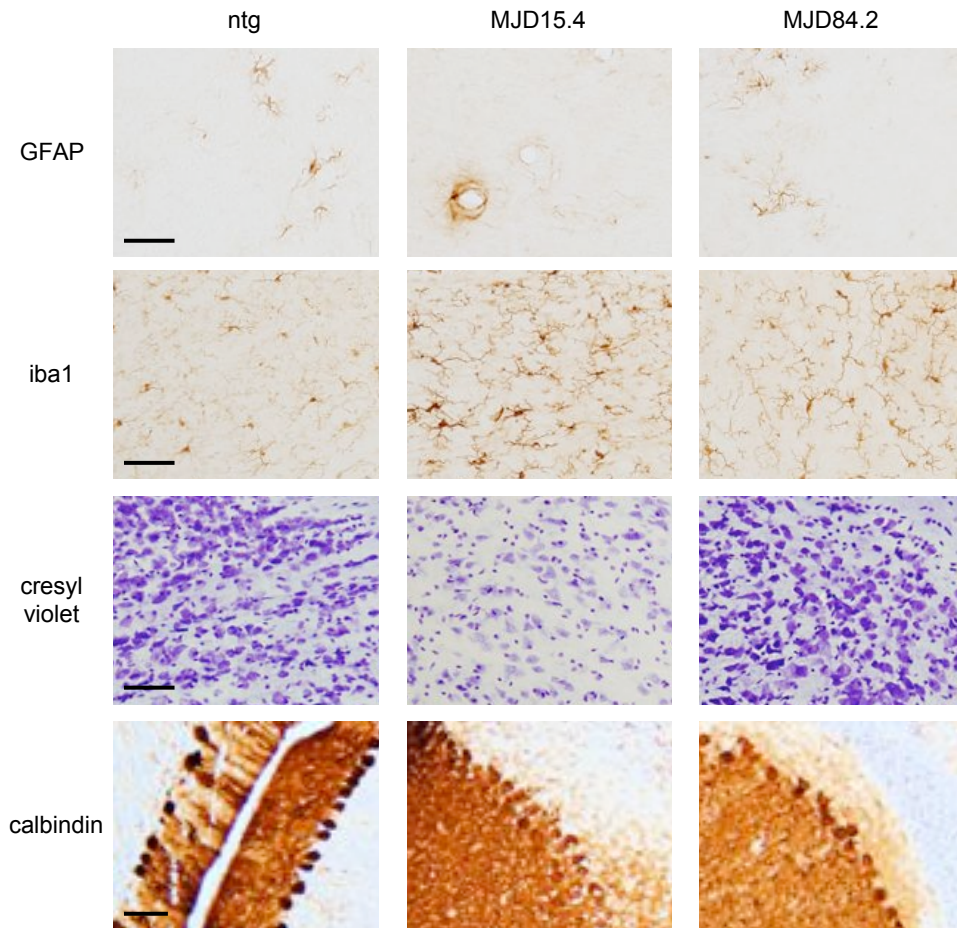
Figure 3.10. Aged MJD84.2 mice do not exhibit reactive astrogliosis or microgliosis. 12-month-old brain sections from nontransgenic (ntg), MJD15.4, and MJD84.2 were stained with antibodies against GFAP to show astrocytes and iba1 to show microglia. There is no difference between genotypes in the number of GFAP-positive or iba1-positive cells in any brain region studied. Cresyl violet staining reveals no major difference in neuron number, despite differences in staining intensity (an artifact of exhausting the dye bath). For GFAP, iba1, and cresyl violet, sections of pontine reticular nuclei are shown. For calbindin, sections of cerebellar cortex are shown, revealing no differences in Purkinje cell number or morphology between genotypes. Scalebars = 50 micrometers.
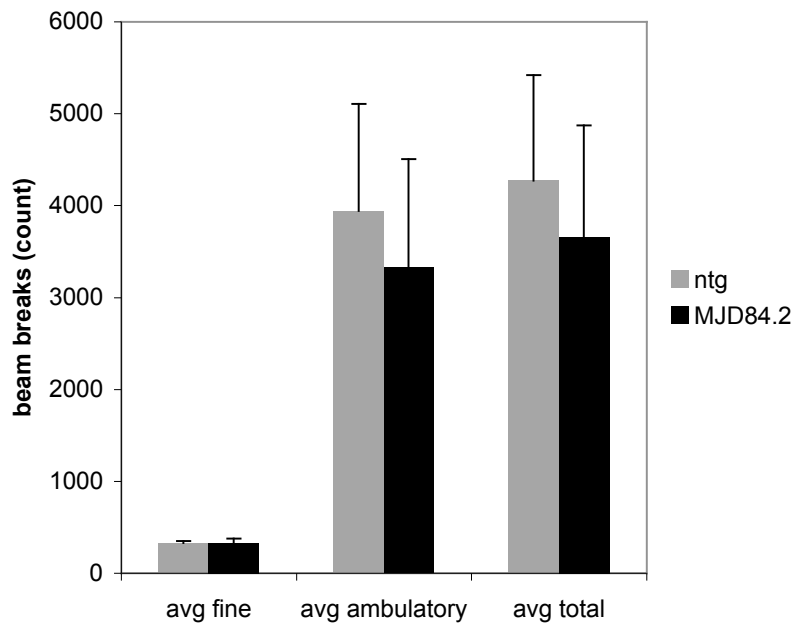
Figure 3.11. Aged MJD84.2 mice do not display decreased spontaneous motor activity compared to nontransgenic mice. Aged MJD84.2 mice and nontransgenic (ntg) controls were tested for levels of spontaneous movement during the dark cycle. Spontaneous movement was quantified as the number of beam breaks over a 30-minute period. Fine movements were defined as breaking the same beam repeatedly, as in cleaning or rearing. Ambulatory movements were defined as breaking adjacent beams sequentially. Analysis of both types of movements individually or combined (total) revealed no decrease in spontaneous motor activity compared to wild-type animals by Students t-test. Ages 13.5-17.5 months, n=7 for ntg, n=9 for MJD84.2. Error bars = 1 S.D.
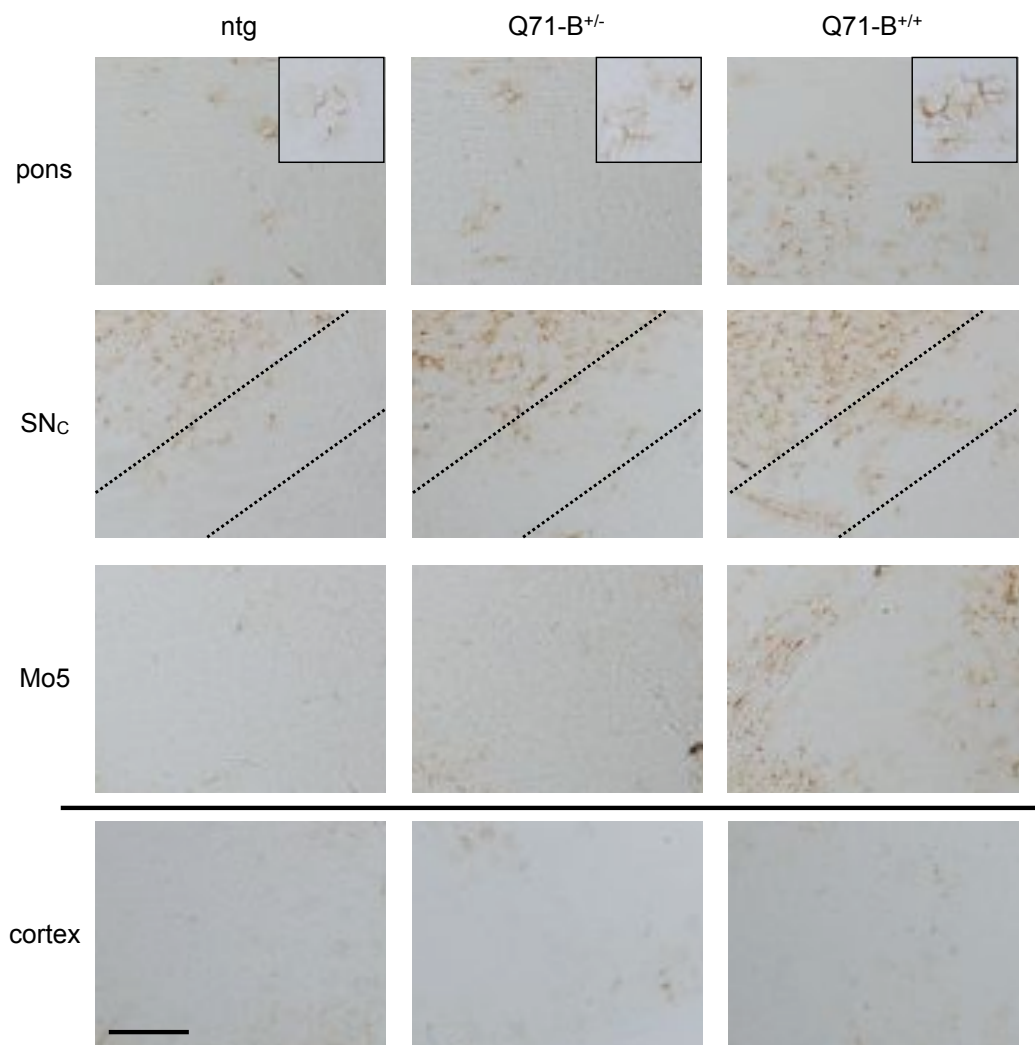
Figure 3.12. Homozygous Q71-B mice exhibit reactive astrogliosis in affected brain areas. 4-month-old brain sections from nontransgenic (ntg), Q71-B$^{+/-}$ and Q71-B$^{+/+}$ mice were stained with antibodies against GFAP to show astrocytes. Q71-B$^{+/+}$ mice have more GFAP-positive cells in brain regions thought to be affected in SCA3, including pontine reticular nuclei (pons), substantia nigra pars compacta (SN$_C$), and the motor trigeminal nucleus in the brainstem (Mo5). Q71-B$^{+/+}$ astrocytes have a more branched morphology and appear more intensely stained than wildtype and Q71-B$^{+/-}$ astrocytes (pons, inset), indicative of a reactive phenotype. Reactive astrogliosis is not observed in any genotype in the cortex, an area thought to be unaffected in SCA3. Dashed lines indicate the borders of the SN$_C$. Scalebar = 200 micrometers.
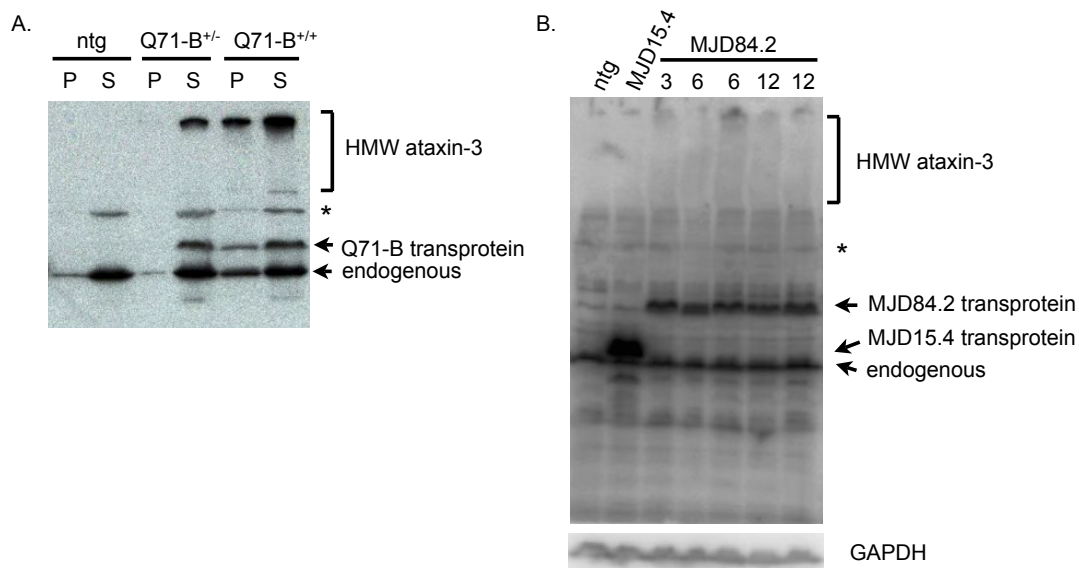
Figure 3.13. Ataxin-3 proteolytic fragments are not associated with phenotype.
Full length blots from Figure 3.1 are shown here. *A*. A smaller, faintly detected
ataxin-3 immmunoreactive band electrophoresing below the endogenous ataxin-3 band
is present in both asymptomatic Q71-B$^{+/-}$ mice and symptomatic Q71-B$^{+/+}$ mice (both 6
months old). *B*. All ataxin-3 immunoreactive bands electrophoresing below the
endogenous ataxin-3 are present in nontransgenic, MJD15.4 and MJD84.2 mice. There
is no detectable ataxin-3 fragment present only in MJD84.2 mice or that changes in
level over time in MJD84.2 mice.
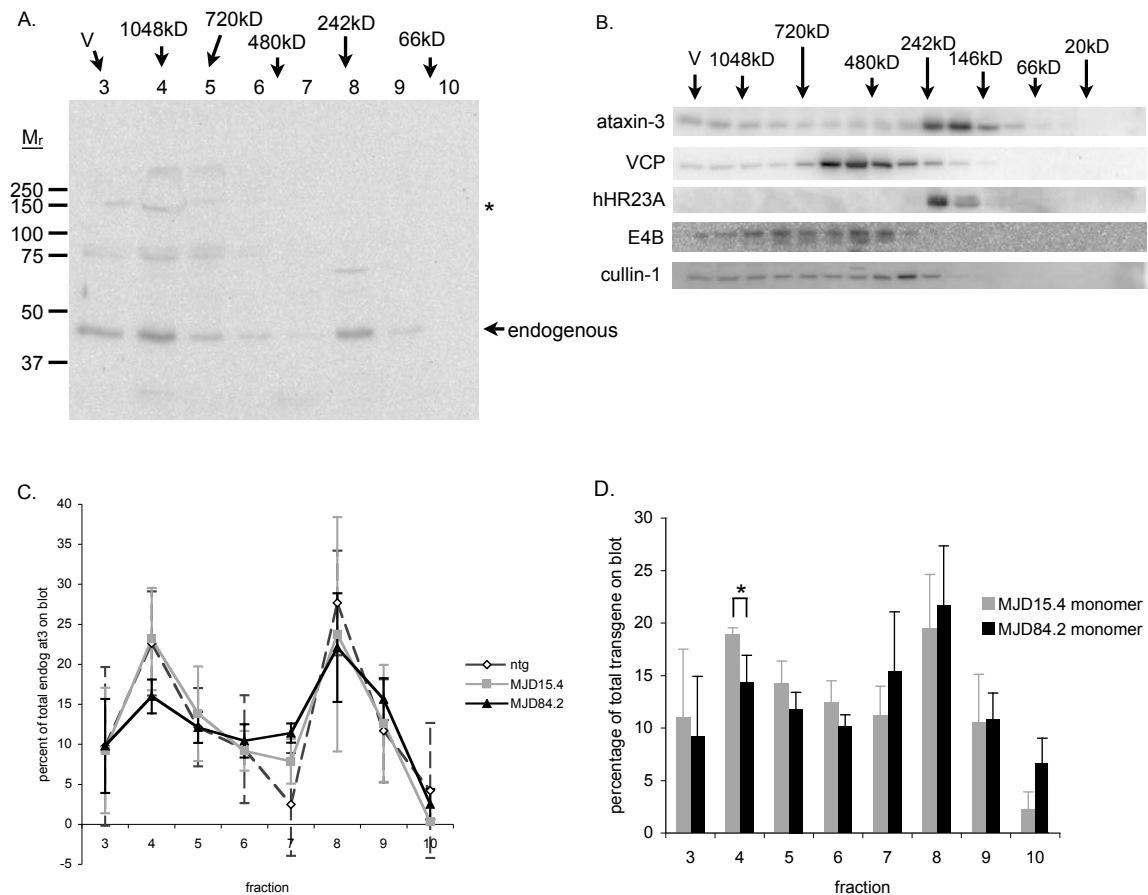
Figure 3.14. Overexpression of expanded ataxin-3 does not alter the elution pattern of endogenous ataxin-3. *A.* Soluble brain lysate from a 6-month-old nontransgenic mouse was fractionated as 1mL fractions by SEC and analyzed by standard SDS-PAGE and immunoblot. Ataxin-3 blotting reveals two major ataxin-3 peaks, one corresponding to presumed monomeric ataxin-3 (fractions 8-9) and one corresponding to ataxin-3 higher molecular weight protein complexes that dissociate into monomeric ataxin-3 on SDS-PAGE (fractions 3-5). B. Soluble brain lysate from a 12-month-old nontransgenic mouse was fractionated into 0.5mL fractions by SEC and analyzed by standard SDS-PAGE and immunoblot. Blotting for the protein indicated reveals a unique pattern for each protein of interest. *C.* Soluble brain lysates from nontransgenic (ntg), MJD15.4, and MJD84.2 mice were analyzed as in *A*. The amount of "monomeric" endogenous ataxin-3 in each fraction was quantified, then expressed as a percentage of the total monomeric endogenous ataxin-3 on the blot. Error bars = 1 S.D. N=3 per genotype. *D.* The same blots analyzed in *B* were analyzed again for the elution pattern of the monomeric transproteins. Monomeric transprotein (either MJD15.4 or MJD84.2) was quantified in each fraction, then expressed as a percentage of the total monomeric transprotein present on the blot. The proportion of MJD84.2 transprotein that elutes in fraction 4 (corresponding to 1048kD) is lower than the proportion of MJD15.4 transgene eluting in that same fraction (two-tailed Students *t*-test, p=0.040).
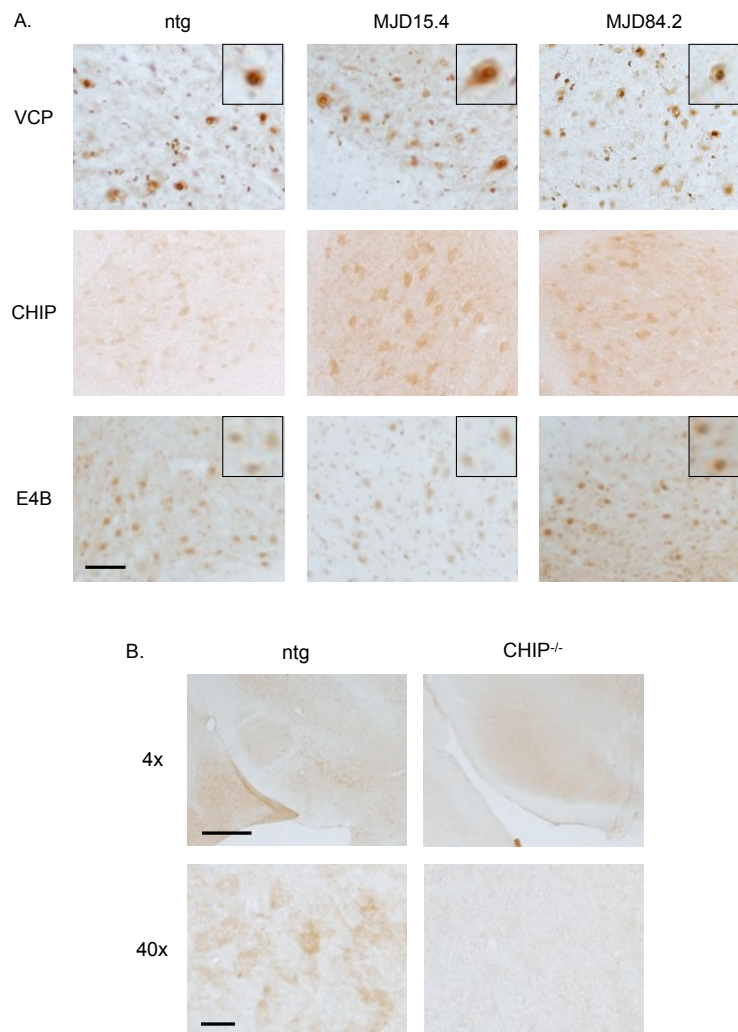
Figure 3.15. Overexpression of expanded ataxin-3 does not alter the localization of certain ataxin-3 interacting proteins. *A.* Brain sections from 12-month-old mice were stained with antibodies against valosin-containing protein (VCP), CHIP and E4B. Neither overexpression of wild-type nor expanded ataxin-3 appears to change the localization of any of these proteins in comparison to nontransgenic animals in any brain region studied. Shown are sections from deep cerebellar nuclei. Scalebar = 50 micrometers. *B.* Brain sections from 12-month-old mice were stained with anti-CHIP antibodies. *CHIP*-knockout (CHIP-/-) mice have no detectable CHIP protein by immunohistochemistry. Shown is the substantia nigra pars compacta. Scalebar = 300 micrometers for 4x pictures, scalebar = 20 micrometers for 40x pictures.

CHAPTER 4

GENERAL DISCUSSION AND FUTURE DIRECTIONS

Abstract

The major goal of my thesis was to define the toxic protein species in SCA3. My results provide important first steps toward establishing that soluble ataxin-3 microaggregates are the pathogenic entity in SCA3. The data point the way to several areas for future research, and suggest potential routes to therapeutic intervention. In this chapter, I will discuss both short-term and long-term future studies aimed at elucidating the structural composition of soluble ataxin-3 microaggregates. Getting a better handle on the biochemical characteristics of soluble microaggregates may help us understand how they form and how they affect other cellular proteins. I will also discuss how my results may guide potential treatment strategies for this fatal protein conformational disease.

Toxic Protein Species in SCA3

A major unanswered question in polyQ disease research is: what is the neurotoxic protein species? As discussed in the introduction to this dissertation, many hypotheses have been proposed to explain the neurotoxicity of polyQ proteins (Fig. 1.2). Our results point to aggregation of the disease protein, ataxin-3, as an early mediator of neuronal dysfunction in mouse models of the polyQ disease, SCA3. In our search for a pathogenic protein species in this disease, we relied on several criteria that a protein species should meet in order to be considered a potential toxic species. These criteria include that the toxic species must: 1) occur in at least two genetically distinct, symptomatic mouse models; 2) vary between sick and healthy animals; 3) occur to a greater degree in disease

tissue; and 4) correlate with the onset of disease signs. In two mouse models of SCA3, we found that ataxin-3 microaggregates best fit these criteria. Our results in one SCA3 mouse model further suggest that CHIP is an important regulator of soluble microaggregate formation in the brain.

A number of experiments could help elucidate the nature of the microaggregates detected in SCA3 mice. To study microaggregate structure and content, one would need to purify microaggregates from SCA3 mouse brain or, ideally, from MJD patient brain. Our attempts to enrich for microaggregates by SEC resulted in fractions that were too contaminated with other proteins to be used for atomic force microscopy, mass spectrometry, or other high-resolution techniques.

A key step, therefore, would be to develop methods for purifying large enough quantities of microaggregates for such analysis. One possible method would be the use of multi-step chromatography to enrich microaggregates by exploiting their unique chemical characteristics. For example, microaggregates likely have different exposed surfaces than soluble monomers; this is strongly suggested by the fact that some conformation-specific antibodies, such as 1C2, A11, and 3B5H10, bind differentially to oligomers and monomers (Behrends et al., 2006; Kayed et al., 2003; Kayed et al., 2007; Brooks et al., 2004). Misfolding and aggregation of polyQ proteins likely exposes different epitopes than those present on properly folded monomers such that hydrophobic interaction chromatography could assist in separating polyQ microaggregates from other proteins. Disease brain lysates first could be subjected to hydrophobic interaction chromatography, then fractionated in a second dimension by SEC. A similar method has already proven efficacious for purifying various protein complexes (Azevedo et al., 2008; Jin et al.,

2008) and to purify proteins from brain lysates, which is a highly complex proteinaceous material (Galadari et al., 1998; Schlaf et al., 1996). Considering the relatively low abundance of microaggregates in disease brain (Chapter 3), we would probably need to start with large amounts of brain lysate for multi-step chromatography.

Following purification, microaggregates could be analyzed by mass spectrometry to determine with certainty whether they are composed primarily or purely of ataxin-3 (and thus represent homo-oligomers) or represent a heterogenous complex of proteins including ataxin-3. Pilot experiments would have to be performed to determine how pure the microaggregate population would need to be for high-resolution structural analysis methods such as atomic force microscopy. Mass spectrometry could help clarify whether ataxin-3 in microaggregates is posttranslationally modified such that it differs from non-aggregated ataxin-3, as may be true for ataxin-1 (Choi et al., 2007). If aggregated ataxin-3 does have a different set of posttranslational modifications than non-aggregated ataxin-3, then the next step would involve studying how these posttranslational modifications might alter aggregation *in vitro* and *in vivo*, and what cellular pathways are important for these modifications. Knowing how and why ataxin-3 gets modified by ubiquitin, phosphorylation, or some other moiety could help direct us toward pathways to target for therapy. If, for example, phosphorylation of ataxin-3 by a certain kinase was linked to enhanced aggregation, we could use specific inhibitors of that kinase in cells to determine whether blocking kinase activity also blocks ataxin-3 aggregation, and ultimately, whether blocking kinase activity prevents the SCA3 phenotype in mice.

Basis of Selective Neurotoxicity

Another important, unanswered question in all polyQ diseases is, why is the nervous system selectively affected? All known polyQ proteins are expressed widely in the body throughout development, so expression of polyQ proteins clearly cannot be equally toxic to all cell types. My results from both chapters 2 and 3 indicate that SDS-resistant soluble ataxin-3 microaggregates are detected only in the brain and in no other organ. As highly specialized postmitotic cells, neurons may handle misfolded proteins differently from other cell types or be particularly sensitive to the consequences of altered protein-protein interactions. Additionally, it has been proposed that as neurons age their ability to cope with proteotoxic stress is reduced (Balch et al., 2008). Perhaps neurons express a different array of chaperones, ubiquitin proteasome system (UPS) components, or protein quality control regulatory proteins than do other unaffected cell types in the liver and kidney, for example. Since some proteins and pathways that control protein folding homeostasis in cells, such as daf-16 and hsf-1 in the insulin growth factor signaling pathway, also have roles in regulating longevity (Hsu et al., 2003; Cohen et al., 2006), it is possible that age-related diseases are in fact caused by decreased proteostatic capacity in the aging brain.

In the case of ataxin-3, we know that it is expressed widely throughout the body and, on a subcellular level, shuttles between the nucleus and cytoplasm. We also know that nuclear localization of expanded ataxin-3 accelerates disease in mice (Bichelmeier et al., 2007), and that certain stressors cause wild-type ataxin-3 to localize to nuclei in cell culture (Reina, C.P., Zhong, X., Pittman, R.N. Proteotoxic stresses alter ataxin-3 interactions with Rad23b and VCP and heat shock induces nuclear localization of ataxin-

3. Program No. 444.4/V20. 2008 Neuroscience Meeting Planner. Washington, DC: Society for Neuroscience, 2008. Online.). The signals that trigger this shuttling are unknown, but nucleocytoplasmic shuttling depends partly upon the catalytic activity of ataxin-3 (Todi et al., 2007). It is possible that posttranslational modifications of ataxin-3 regulate its function and subcellular localization, which may differentially affect its propensity to aggregate and its toxicity to cells. This is certainly true for ataxin-1, an unrelated poyQ disease protein, since phosphorylation of serine 776 is known to enhance ataxin-1 aggregation (Emamian et al., 2003), and mutation of this residue to block phosphorylation virtually eliminates ataxin-1 neurotoxicity (Emamian et al., 2003). Similarly, Fei and colleagues (2007) showed that blocking phosphorylation of ataxin-3 by GSK3beta on serine 256 enhanced ataxin-3 aggregation. The effects of ataxin-3 aggregation on cell health and survival were not assessed. The role of casein kinase 2 phosphorylation of ataxin-3 is an area of active investigation, and some recent reports suggest that ataxin-3 phosphorylation affects both its subcellular localization and inclusion formation (Mueller, T.; Evert, B.O.; Klockgether, T.; Wuellner, U. Phosphorylation of Ataxin-3. Program No. 487.4/X14. 2007 Neuroscience Meeting Planner. San Diego, CA: Society for Neuroscience, 2007. Online.). Although to date no work has been reported regarding neuronal specificity of ataxin-3 posttranslational modifications, this may turn out to be important for SCA3 pathogenesis.

While little is known about why neurons generally are susceptible to polyQ toxicity, several recent studies have examined susceptibility differences among different types of neurons. This has revealed that distinct types of neurons can handle the same mutant protein differently. Brignull and colleagues (2006) showed that a near-threshold

length polyQ protein aggregated in some *C. elegans* neurons but not in others, demonstrating that different types of neurons have different protein quality control mechanisms and capacities. It is possible that in SCA3, expanded ataxin-3 can aggregate in certain neurons, while other neurons have more effective means of inhibiting the formation of soluble aggregates (e.g. higher levels of CHIP, more robust inclusion formation). Further immunohistochemical studies of the expression of ataxin-3 and its interacting proteins in the brain, along with data from the Allen Brain Atlas (Lein et al., 2007), could serve as a foundation from which to ask why certain regions of the brain are more susceptible to degeneration in SCA3.

Recently, Tagawa and colleagues (2007) described a mechanism that might help explain the basis for differential neuronal subtype sensitivity. Tagawa and colleagues transfected different types of primary neurons with wild-type or expanded huntingtin, then used microarray analysis of gene expression to determine which genes might be important for determining neuron subtype-specific susceptibility to expanded huntingtin. They showed that mutant huntingtin expression caused a more robust induction of Hsp70 in cerebellar granule neurons (which are resistant to huntingtin toxicity) than in cortical neurons (which are sensitive to huntingtin toxicity). A similar type of assay may be helpful in SCA3, since cerebellar granule cells are thought to be sensitive to ataxin-3 toxicity while cortical neurons are thought to be resistant (the exact opposite of huntingtin). It would be relatively straightforward to transfect both types of primary neurons with wild-type and expanded ataxin-3, and perform microarray analysis to assess changes in gene expression or assay changes in individual candidate genes. We would first eliminate from further analysis genes that change expression levels to a similar

degree in response to both wild-type and expanded ataxin-3 in each neuronal subtype. We would then look for genes whose expression levels differ by at least 2-fold between the "sensitive" (cerebellar granule neuron) and the "resistant" (cortical neuron) subtypes. The genes thus identified could be analyzed further to determine whether they can confer resistance to a sensitive neuronal subtype. For example, if we found that E4B was more upregulated in cortical neurons than cerebellar granule neurons in response to expanded ataxin-3, then we could transfect E4B into cerebellar granule neurons and see if this protected them from expanded ataxin-3 toxicity. This type of experiment would not only help describe the basis of neuronal selectivity in SCA3, but could also help identify promising therapeutic targets for modulation by gene therapy or small molecules.

The Role of Protein Quality Control Systems in PolyQ
Disease

It is well established that protein quality control systems play a major role in polyQ disease pathogenesis (Balch et al., 2008; Bennett et al., 2007; Bilen and Bonini, 2007; Branco et al., 2008; Chan et al., 2002; Gatchel and Zoghbi, 2005; Muchowski and Wacker, 2005; Nollen et al., 2004). The question now becomes: in what ways are these systems involved in disease pathogenesis, and are they amenable to change as therapeutic targets?

Chaperones. Members of the HSP family of chaperones are often found in inclusions. Overexpression of some Hsp70 and Hsp40 proteins has been shown to reduce polyQ toxicity in *Drosophila* models of disease (Chan et al., 2002; Chan et al., 2000; Warrick et

al., 1999), although these findings have not yet been replicated in mouse models.

Overexpression of Hsp27 alone did not ameliorate the phenotype of a mouse model of

HD (Zourlidou et al., 2007), but overexpression of HSF-1, a transcription factor which

induces expression of multiple heat shock proteins, improved lifespan in the same HD

mouse model (Fujimoto et al., 2005). Hsp27 overexpression did suppress polyQ toxicity

in a mouse model of SCA17 (Friedman et al., 2007), suggesting some variability in how

chaperones function in different polyQ diseases. My results in chapter 2 show that

CHIP's role in enhancing expanded ataxin-3 solubility is crucial for neuronal defense

against polyQ toxicity in mouse models (Chapter 2). Overexpression of CHIP can reduce

the toxicity of the expanded androgen receptor in an SBMA mouse model by enhancing

androgen receptor degradation (Adachi et al., 2007). The mechanism by which CHIP

reduces polyQ toxicity appears to depend on the particular disease protein, because in

different polyQ disease models it has been shown to function as a co-chaperone (Miller et

al., 2005; Choi et al., 2007) and as a ubiquitin ligase (Al-Ramahi et al., 2006; Jana et al.,

2005). It is currently unknown why CHIP uses different mechanisms to alter the toxicity

of different polyQ proteins. It is possible that the sequence of the polyQ protein itself

determines how CHIP will act, or it may be that other proteins complexed with the polyQ

protein determine CHIP's mode of action. Even if CHIP does not interact directly with a

specific disease protein, it may still influence disease as a master regulator of cellular

responses to misfolded protein stress (Dai et al., 2003; Qian et al., 2006).

Ubiquitin proteasome system. Ubiquitin and other UPS components are frequently found

in polyQ inclusions. There is some debate about whether polyQ proteins can be degraded

effectively by the proteasome, and whether expression of polyQ proteins in cells impairs overall proteasome function. It is clear that wild-type ataxin-3 is degraded by the proteasome, and it appears that expanded ataxin-3 can be degraded with similar efficiency (Berke et al., 2005; Todi et al., 2007). Inhibiting the proteasome enhances polyQ toxicity in *Drosophila* (Chan et al., 2002), but to date no studies have shown that enhancement of proteasomal activity *in vivo* reduces polyQ toxicity. Interestingly, inhibition of the proteasome can enhance autophagy (discussed next), which may be more capable of degrading aggregated proteins than the proteasome (Ravikumar et al., 2002), and may prove to be a therapeutic strategy in polyQ disease (Ravikumar and Rubinsztein, 2004).

Autophagy. Loss of autophagy in neurons, even in the absence of pathogenic mutations or stressors, leads to neurodegeneration and a motor phenotype in mice (Komatsu et al., 2006; Hara et al., 2006), suggesting that impairments in autophagy are relevant to age-related neurodegeneration. Indeed, autophagic capacity appears to decrease with age (Cuervo, 2008), and increasing one type of autophagy (chaperone-mediated autophagy) in the aging liver enhances organ function (Zhang and Cuervo, 2008). Some data suggest that autophagy is generally responsible for degradation of aggregated proteins (Ravikumar et al., 2002), although some recent findings suggest that this activity may not be universal (Wong et al., 2008). Additionally, one of the drugs often used to induce autophagy, rapamycin, also decreases protein synthesis (King et al., 2008), suggesting that results from studies where rapamycin was used to induce autophagy may need to be reevaluated with this new drug action in mind. It is possible that some of the observed

benefits of rapamycin treatment in neurodegenerative disease models may be attributable to decreases in the synthesis of disease-related proteins as well as autophagic clearance of toxic protein species.

Among the polyQ disease proteins, ataxin-3 may have a particularly interesting link to autophagy. Overexpression of expanded ataxin-3 in *Drosophila* induces autophagy on its own (Bilen and Bonini, 2007). Subsequent genome-wide screening for modifiers of ataxin-3 toxicity revealed that some modifiers act through autophagic pathways, even though autophagic proteins themselves were not represented in the list of genetic modifiers (Bilen and Bonini, 2007). Overexpression of Atg6/Beclin-1 in a rat model of MJD reduced signs of neuronal degeneration and apoptotic cell death (Nascimento-Ferreira, I.; Pereira de Almeida, L.; Sousa-Ferreira, L.; Santos-Ferreira, T.; Alves, S.; Dufour, N.; Déglon, N. Lentiviral delivery of beclin-1 in the rat brain reduces neuronal dysfunction and neurodegeneration associated with Machado-Joseph Disease. Program No. 444.3/V19 2008 Neuroscience Meeting Planner. Washington, DC: Society for Neuroscience, 2008. Online.). Interestingly, the ataxin-3 interacting protein, HDAC6, has been identified as a link between the UPS and autophagy systems, whereby HDAC6 mediates a switch to autophagy when the UPS is impaired (Pandey et al., 2007). Expanded ataxin-3 might play some role in altering this communication, especially if aggregated ataxin-3 interacts differently with HDAC6 than does nonaggregated ataxin-3. The possibility of an altered ataxin-3:HDAC6 interaction will be important to investigate in the future, as it may a) explain how ataxin-3 can suppress the toxicity of other polyQ proteins (Warrick et al., 2005) and b) inform our view of how ataxin-3 microaggregates cause neurotoxicity.

Routes to Therapy

The findings described in this thesis favor a revised model of polyQ disease pathogenesis (Fig. 1.3). In this model, expanded polyQ protein is prone to adopt a conformation that provides an accessible, reactive polypeptide surface favoring aberrant protein interactions. The resultant protein complexes, whether they are subtly altered "normal" (i.e. native) complexes, novel heteroprotein complexes, or detergent-resistant microaggregates (including homo-oligomers), could contribute to neuronal dysfunction culminating in cell death. Our results confirm that microaggregates are good candidates to be toxic species in SCA3, but the situation may differ for other polyQ diseases. Our results do not rule out the possibility that aberrant complexes downstream of microaggregates have their own inherent toxicity. Although A-beta oligomers appear to be the most important neurotoxic species in AD, recent evidence in the polyQ disease field suggests that the "neurotoxic" complexes formed by any given polyQ protein will prove to be more heterogenous and complex. Our results concerning the size of ataxin-3 microaggregates in SCA3 transgenic mice (Fig. 3.4) are consistent with the idea that polyQ aggregates may not be homogenous. Accordingly, therapeutic initiatives should not only attempt to prevent the formation of disease-specific heteroprotein or oligomeric complexes, (which may be relevant for only one or a few polyQ diseases), but should also include efforts to enhance neuronal protein quality control pathways and reduce intracellular levels of the mutant polyQ disease proteins through RNA interference or protein clearance pathways (Friedman et al., 2007; Adachi et al., 2007; Balch et al., 2008; Waza et al., 2005).

One highly specific way to reduce levels of a target protein is through RNA interference (RNAi). Several studies have shown that RNAi can be targeted toward a mutant allele while not affecting the expression of the normal allele (Miller et al., 2003; Alves et al., 2008; van Bilsen et al., 2008; Xia et al., 2006). Such an allele-specific approach is ideal for polyQ disease treatment since the functions of most polyQ disease proteins are unknown, and silencing of the normal allele may be detrimental. Unfortunately, the mutation in polyQ diseases is not an easily targeted point mutation or deletion, but rather an extension of a sequence that occurs in the normal allele, which may make allele-specific silencing difficult if no other unique DNA features like SNPs segregate 100% with the CAG expansions. However, with respect to ataxin-3 specifically, ataxin-3 knockout animals do not have apparent motor or neuropathological phenotypes (Schmitt et al., 2007; Rodrigues et al., 2007), suggesting that other proteins may be functionally redundant with ataxin-3 (e.g. other members of the josephin family). If this is true, then RNAi knockdown of ataxin-3 in a non-allele selective manner might prove to be a successful therapeutic strategy. Since ataxin-3 knockout mice have subtle behavioral phenotypes suggestive of increased anxiety (Schmitt et al., 2007), anxiety symptoms would need to be assessed in any therapeutic trial.

Because protein misfolding appears central to polyQ disease pathogenesis, increasing the expression or activity of neuronal protein refolding machinery holds therapeutic potential (Balch et al., 2008). For example, Hsp90 inhibitors, which increase substrate degradation by the proteasome, are one class of drugs that modulate protein homeostasis. Certain Hsp90 inhibitors have already demonstrated efficacy in animal models of polyQ disease (Waza et al., 2005). Further medicinal chemistry endeavors

may discover compounds that act in diverse ways to alter the activity of specific components of the neuronal protein quality control apparatus. For example, small molecules have been identified that bind both chaperones and A-beta (Gestwicki et al., 2004), thereby enhancing the interaction between a disease protein and a protein quality control component that can suppress its aggregation. Such bifunctional small molecules are an area of active research in the polyQ field.

Enhancing certain types of aggregation may be beneficial in polyQ disease as well. Both Arrasate et al. (2004) and Schiffer et al. (2008) showed that the toxicity of polyQ protein fragments was decreased when they accumulated as visible inclusions in cells. Behrends et al. (2006) showed in a yeast model of polyQ disease that overexpressing the eukaryotic chaperonin TRiC suppressed polyQ toxicity at the same time that it promoted the formation of larger nontoxic aggregates from smaller toxic aggregates. In an unrelated neurodegenerative disease, AD, it was recently shown that mutations causing an increased rate of fibrillization decreased the neurotoxicity of A-beta peptides in neuronal cultures and in AD mice (Cheng et al., 2007; Hung et al., 2008). Thus, it is possible that breaking up aggregates may be detrimental to cells if it turns less toxic aggregates into more toxic soluble species. Our data from Q71-B/*CHIP* mice suggest that higher levels of soluble aggregates correspond to higher toxicity; therefore dissociating microaggregates into monomers via enhanced chaperone or chaperonin activity would, we predict, reduce toxicity. But in AD, small soluble oligomers of A-beta (dimers, trimers and tetramers) correlate with toxicity (Shankar et al., 2008; Walsh and Selkoe, 2007; Walsh and Selkoe, 2004). Since some aggregates appear to be toxic while others are not, the experiments proposed at the beginning of this chapter to structurally

define soluble microaggregates in SCA3 become very important. If we know how to define and detect toxic aggregates biochemically, we may be able to use them as biomarkers of efficacy in treatment trials in mice.

Conclusions

The results described in this thesis provide strong animal model support for the role of soluble microaggregates in polyQ disease. The field now must move forward with research aimed at describing the physical structure and contents of these microaggregates to understand how they form and what cellular processes contribute to this process. Armed with this knowledge, scientists can use mouse models and human tissue to find small molecules or proteins that can modify polyQ microaggregates into less toxic structures. Hopefully, such research will result in novel treatments for these fatal proteinopathies.

REFERENCES

Adachi H, Waza M, Tokui K, Katsuno M, Minamiyama M, Tanaka F, Doyu M, Sobue G (2007) CHIP overexpression reduces mutant androgen receptor protein and ameliorates phenotypes of the spinal and bulbar muscular atrophy transgenic mouse model. J Neurosci 27:5115-5126.

Al-Ramahi I, Lam YC, Chen HK, de Gouyon B, Zhang M, Perez AM, Branco J, de Haro M, Patterson C, Zoghbi HY, Botas J (2006) CHIP protects from the neurotoxicity of expanded and wild-type ataxin-1 and promotes their ubiquitination and degradation. J Biol Chem 281:26714-26724.

Alves S, Nascimento-Ferreira I, Auregan G, Hassig R, Dufour N, Brouillet E, Pedroso de Lima MC, Hantraye P, Pereira de Almeida L, Deglon N (2008) Allele-specific RNA silencing of mutant ataxin-3 mediates neuroprotection in a rat model of Machado-Joseph disease. PLoS ONE 3:e3341.

Arrasate M, Mitra S, Schweitzer ES, Segal MR, Finkbeiner S (2004) Inclusion body formation reduces levels of mutant huntingtin and the risk of neuronal death. Nature 431:805-810.

Azevedo AM, Rosa PA, Ferreira IF, Aires-Barros MR (2008) Integrated process for the purification of antibodies combining aqueous two-phase extraction, hydrophobic interaction chromatography and size-exclusion chromatography. J Chromatogr A.

Bagriantsev SN, Kushnirov VV, Liebman SW (2006) Analysis of amyloid aggregates using agarose gel electrophoresis. Methods Enzymol 412:33-48.

Balch WE, Morimoto RI, Dillin A, Kelly JW (2008) Adapting proteostasis for disease intervention. Science 319:916-919.

Ballinger CA, Connell P, Wu Y, Hu Z, Thompson LJ, Yin LY, Patterson C (1999) Identification of CHIP, a novel tetratricopeptide repeat-containing protein that interacts with heat shock proteins and negatively regulates chaperone functions. Mol Cell Biol 19:4535-4545.

Behrends C, Langer CA, Boteva R, Bottcher UM, Stemp MJ, Schaffar G, Rao BV, Giese A, Kretzschmar H, Siegers K, Hartl FU (2006) Chaperonin TRiC promotes the assembly of polyQ expansion proteins into nontoxic oligomers. Mol Cell 23:887-897.

Bence NF, Sampat RM, Kopito RR (2001) Impairment of the ubiquitin-proteasome system by protein aggregation. Science 292:1552-1555.

Bennett EJ, Bence NF, Jayakumar R, Kopito RR (2005) Global impairment of the ubiquitin-proteasome system by nuclear or cytoplasmic protein aggregates precedes inclusion body formation. Mol Cell 17:351-365.

Bennett EJ, Shaler TA, Woodman B, Ryu KY, Zaitseva TS, Becker CH, Bates GP, Schulman H, Kopito RR (2007) Global changes to the ubiquitin system in Huntington's disease. Nature 448:704-708.

Berke SJ, Chai Y, Marrs GL, Wen H, Paulson HL (2005) Defining the role of ubiquitin-interacting motifs in the polyglutamine disease protein, ataxin-3. J Biol Chem 280:32026-32034.

Berke SJ, Schmied FA, Brunt ER, Ellerby LM, Paulson HL (2004) Caspase-mediated proteolysis of the polyglutamine disease protein ataxin-3. J Neurochem 89:908-918.

Bevivino AE, Loll PJ (2001) An expanded glutamine repeat destabilizes native ataxin-3 structure and mediates formation of parallel beta -fibrils. Proc Natl Acad Sci U S A 98:11955-11960.

Bhattacharyya AM, Thakur AK, Wetzel R (2005) polyglutamine aggregation nucleation: thermodynamics of a highly unfavorable protein folding reaction. Proc Natl Acad Sci U S A 102:15400-15405.

Bichelmeier U, Schmidt T, Hubener J, Boy J, Ruttiger L, Habig K, Poths S, Bonin M, Knipper M, Schmidt WJ, Wilbertz J, Wolburg H, Laccone F, Riess O (2007) Nuclear localization of ataxin-3 is required for the manifestation of symptoms in SCA3: in vivo evidence. J Neurosci 27:7418-7428.

Bilen J, Bonini NM (2007) Genome-wide screen for modifiers of ataxin-3 neurodegeneration in Drosophila. PLoS Genet 3:1950-1964.

Boeddrich A, Gaumer S, Haacke A, Tzvetkov N, Albrecht M, Evert BO, Muller EC, Lurz R, Breuer P, Schugardt N, Plassmann S, Xu K, Warrick JM, Suopanki J, Wullner U, Frank R, Hartl UF, Bonini NM, Wanker EE (2006) An arginine/lysine-rich motif is crucial for VCP/p97-mediated modulation of ataxin-3 fibrillogenesis. Embo J 25:1547-1558.

Bowman AB, Yoo SY, Dantuma NP, Zoghbi HY (2005) Neuronal dysfunction in a polyglutamine disease model occurs in the absence of ubiquitin-proteasome system impairment and inversely correlates with the degree of nuclear inclusion formation. Hum Mol Genet 14:679-691.

Branco J, Al-Ramahi I, Ukani L, Perez AM, Fernandez-Funez P, Rincon-Limas D, Botas J (2008) Comparative analysis of genetic modifiers in Drosophila points to common and distinct mechanisms of pathogenesis among polyglutamine diseases. Hum Mol Genet 17:376-390.

Brignull HR, Moore FE, Tang SJ, Morimoto RI (2006) Polyglutamine proteins at the pathogenic threshold display neuron-specific aggregation in a pan-neuronal Caenorhabditis elegans model. J Neurosci 26:7597-7606.

Brooks E, Arrasate M, Cheung K, Finkbeiner SM (2004) Using antibodies to analyze polyglutamine stretches. Methods Mol Biol 277:103-128.

Bucciantini M, Giannoni E, Chiti F, Baroni F, Formigli L, Zurdo J, Taddei N, Ramponi G, Dobson CM, Stefani M (2002) Inherent toxicity of aggregates implies a common mechanism for protein misfolding diseases. Nature 416:507-511.

Bulone D, Masino L, Thomas DJ, San Biagio PL, Pastore A (2006) The interplay between PolyQ and protein context delays aggregation by forming a reservoir of protofibrils. PLoS ONE 1:e111.

Burnett B, Li F, Pittman RN (2003) The polyglutamine neurodegenerative protein ataxin-3 binds polyubiquitylated proteins and has ubiquitin protease activity. Hum Mol Genet 12:3195-3205.

Burnett BG, Pittman RN (2005) The polyglutamine neurodegenerative protein ataxin 3 regulates aggresome formation. Proc Natl Acad Sci U S A 102:4330-4335.

Butland SL, Devon RS, Huang Y, Mead CL, Meynert AM, Neal SJ, Lee SS, Wilkinson A, Yang GS, Yuen MM, Hayden MR, Holt RA, Leavitt BR, Ouellette BF (2007) CAG-encoded polyglutamine length polymorphism in the human genome. BMC Genomics 8:126.

Cemal CK, Carroll CJ, Lawrence L, Lowrie MB, Ruddle P, Al-Mahdawi S, King RH, Pook MA, Huxley C, Chamberlain S (2002) YAC transgenic mice carrying pathological alleles of the MJD1 locus exhibit a mild and slowly progressive cerebellar deficit. Hum Mol Genet 11:1075-1094.

Chai Y, Wu L, Griffin JD, Paulson HL (2001) The role of protein composition in specifying nuclear inclusion formation in polyglutamine disease. J Biol Chem 276:44889-44897.

Chan HY, Warrick JM, Andriola I, Merry D, Bonini NM (2002) Genetic modulation of polyglutamine toxicity by protein conjugation pathways in Drosophila. Hum Mol Genet 11:2895-2904.

Chan HY, Warrick JM, Gray-Board GL, Paulson HL, Bonini NM (2000) Mechanisms of chaperone suppression of polyglutamine disease: selectivity, synergy and modulation of protein solubility in Drosophila. Hum Mol Genet 9:2811-2820.

Chen HK, Fernandez-Funez P, Acevedo SF, Lam YC, Kaytor MD, Fernandez MH, Aitken A, Skoulakis EM, Orr HT, Botas J, Zoghbi HY (2003) Interaction of Akt-phosphorylated ataxin-1 with 14-3-3 mediates neurodegeneration in spinocerebellar ataxia type 1. Cell 113:457-468.

Chen S, Berthelier V, Hamilton JB, O'Nuallain B, Wetzel R (2002) Amyloid-like features of polyglutamine aggregates and their assembly kinetics. Biochemistry 41:7391-7399.

Chen S, Ferrone FA, Wetzel R (2002) Huntington's disease age-of-onset linked to polyglutamine aggregation nucleation. Proc Natl Acad Sci U S A 99:11884-11889.

Chen X, Tang TS, Tu H, Nelson O, Pook M, Hammer R, Nukina N, Bezprozvanny I (2008) Deranged Calcium Signaling and Neurodegeneration in Spinocerebellar Ataxia Type 3. J Neurosci 28:12713-12724.

Cheng IH, Scearce-Levie K, Legleiter J, Palop JJ, Gerstein H, Bien-Ly N, Puolivali J, Lesne S, Ashe KH, Muchowski PJ, Mucke L (2007) Accelerating amyloid-beta fibrillization reduces oligomer levels and functional deficits in Alzheimer disease mouse models. J Biol Chem 282:23818-23828.

Choi JY, Ryu JH, Kim HS, Park SG, Bae KH, Kang S, Myung PK, Cho S, Park BC, Lee do H (2007) Co-chaperone CHIP promotes aggregation of ataxin-1. Mol Cell Neurosci 34:69-79.

Chow MK, Ellisdon AM, Cabrita LD, Bottomley SP (2004) Polyglutamine expansion in ataxin-3 does not affect protein stability: implications for misfolding and disease. J Biol Chem 279:47643-47651.

Chow MK, Ellisdon AM, Cabrita LD, Bottomley SP (2006) Purification of polyglutamine proteins. Methods Enzymol 413:1-19.

Cohen E, Bieschke J, Perciavalle RM, Kelly JW, Dillin A (2006) Opposing activities protect against age-onset proteotoxicity. Science 313:1604-1610.

Colby DW, Cassady JP, Lin GC, Ingram VM, Wittrup KD (2006) Stochastic kinetics of intracellular huntingtin aggregate formation. Nat Chem Biol 2:319-323.

Connell P, Ballinger CA, Jiang J, Wu Y, Thompson LJ, Hohfeld J, Patterson C (2001) The co-chaperone CHIP regulates protein triage decisions mediated by heat-shock proteins. Nat Cell Biol 3:93-96.

Cowan KJ, Diamond MI, Welch WJ (2003) Polyglutamine protein aggregation and toxicity are linked to the cellular stress response. Hum Mol Genet 12:1377-1391.

Cuervo AM (2008) Autophagy and aging: keeping that old broom working. Trends Genet.

Cummings CJ, Mancini MA, Antalffy B, DeFranco DB, Orr HT, Zoghbi HY (1998) Chaperone suppression of aggregation and altered subcellular proteasome localization imply protein misfolding in SCA1. Nat Genet 19:148-154.

Cummings CJ, Reinstein E, Sun Y, Antalffy B, Jiang Y, Ciechanover A, Orr HT, Beaudet AL, Zoghbi HY (1999) Mutation of the E6-AP ubiquitin ligase reduces nuclear inclusion frequency while accelerating polyglutamine-induced pathology in SCA1 mice. Neuron 24:879-892.

Dai Q, Zhang C, Wu Y, McDonough H, Whaley RA, Godfrey V, Li HH, Madamanchi N, Xu W, Neckers L, Cyr D, Patterson C (2003) CHIP activates HSF1 and confers protection against apoptosis and cellular stress. Embo J 22:5446-5458.

Danzer KM, Haasen D, Karow AR, Moussaud S, Habeck M, Giese A, Kretzschmar H, Hengerer B, Kostka M (2007) Different species of alpha-synuclein oligomers induce calcium influx and seeding. J Neurosci 27:9220-9232.

Diaz-Hernandez M, Torres-Peraza J, Salvatori-Abarca A, Moran MA, Gomez-Ramos P, Alberch J, Lucas JJ (2005) Full motor recovery despite striatal neuron loss and formation of irreversible amyloid-like inclusions in a conditional mouse model of Huntington's disease. J Neurosci 25:9773-9781.

Dickey CA, Kamal A, Lundgren K, Klosak N, Bailey RM, Dunmore J, Ash P, Shoraka S, Zlatkovic J, Eckman CB, Patterson C, Dickson DW, Nahman NS, Jr., Hutton M, Burrows F, Petrucelli L (2007) The high-affinity HSP90-CHIP complex recognizes and selectively degrades phosphorylated tau client proteins. J Clin Invest 117:648-658.

Dickey CA, Patterson C, Dickson D, Petrucelli L (2007) Brain CHIP: removing the culprits in neurodegenerative disease. Trends Mol Med 13:32-38.

Dickey CA, Yue M, Lin WL, Dickson DW, Dunmore JH, Lee WC, Zehr C, West G, Cao S, Clark AM, Caldwell GA, Caldwell KA, Eckman C, Patterson C, Hutton M, Petrucelli L (2006) Deletion of the ubiquitin ligase CHIP leads to the accumulation, but not the aggregation, of both endogenous phospho- and caspase-3-cleaved tau species. J Neurosci 26:6985-6996.

Doss-Pepe EW, Stenroos ES, Johnson WG, Madura K (2003) Ataxin-3 interactions with rad23 and valosin-containing protein and its associations with ubiquitin chains and the proteasome are consistent with a role in ubiquitin-mediated proteolysis. Mol Cell Biol 23:6469-6483.

Ellisdon AM, Pearce MC, Bottomley SP (2007) Mechanisms of ataxin-3 misfolding and fibril formation: kinetic analysis of a disease-associated polyglutamine protein. J Mol Biol 368:595-605.

Ellisdon AM, Thomas B, Bottomley SP (2006) The two-stage pathway of ataxin-3 fibrillogenesis involves a polyglutamine-independent step. J Biol Chem 281:16888-16896.

Emamian ES, Kaytor MD, Duvick LA, Zu T, Tousey SK, Zoghbi HY, Clark HB, Orr HT (2003) Serine 776 of ataxin-1 is critical for polyglutamine-induced disease in SCA1 transgenic mice. Neuron 38:375-387.

Evert BO, Araujo J, Vieira-Saecker AM, de Vos RA, Harendza S, Klockgether T, Wullner U (2006) Ataxin-3 represses transcription via chromatin binding, interaction with histone deacetylase 3, and histone deacetylation. J Neurosci 26:11474-11486.

Fei E, Jia N, Zhang T, Ma X, Wang H, Liu C, Zhang W, Ding L, Nukina N, Wang G (2007) Phosphorylation of ataxin-3 by glycogen synthase kinase 3beta at serine 256 regulates the aggregation of ataxin-3. Biochem Biophys Res Commun 357:487-492.

Ferro A, Carvalho AL, Teixeira-Castro A, Almeida C, Tome RJ, Cortes L, Rodrigues AJ, Logarinho E, Sequeiros J, Macedo-Ribeiro S, Maciel P (2007) NEDD8: a new ataxin-3 interactor. Biochim Biophys Acta 1773:1619-1627.

Friedman MJ, Shah AG, Fang ZH, Ward EG, Warren ST, Li S, Li XJ (2007) Polyglutamine domain modulates the TBP-TFIIB interaction: implications for its normal function and neurodegeneration. Nat Neurosci 10:1519-1528.

Fujigasaki H, Uchihara T, Takahashi J, Matsushita H, Nakamura A, Koyano S, Iwabuchi K, Hirai S, Mizusawa H (2001) Preferential recruitment of ataxin-3 independent of expanded polyglutamine: an immunohistochemical study on Marinesco bodies. J Neurol Neurosurg Psychiatry 71:518-520.

Fujimoto M, Takaki E, Hayashi T, Kitaura Y, Tanaka Y, Inouye S, Nakai A (2005) Active HSF1 significantly suppresses polyglutamine aggregate formation in cellular and mouse models. J Biol Chem 280:34908-34916.

Galadari S, Kishikawa K, Kamibayashi C, Mumby MC, Hannun YA (1998) Purification and characterization of ceramide-activated protein phosphatases. Biochemistry 37:11232-11238.

Gales L, Cortes L, Almeida C, Melo CV, do Carmo Costa M, Maciel P, Clarke DT, Damas AM, Macedo-Ribeiro S (2005) Towards a structural understanding of the fibrillization pathway in Machado-Joseph's disease: trapping early oligomers of non-expanded ataxin-3. J Mol Biol 353:642-654.

Gatchel JR, Zoghbi HY (2005) Diseases of unstable repeat expansion: mechanisms and common principles. Nat Rev Genet 6:743-755.

Gestwicki JE, Crabtree GR, Graef IA (2004) Harnessing chaperones to generate small-molecule inhibitors of amyloid beta aggregation. Science 306:865-869.

Gidalevitz T, Ben-Zvi A, Ho KH, Brignull HR, Morimoto RI (2006) Progressive disruption of cellular protein folding in models of polyglutamine diseases. Science 311:1471-1474.

Goldberg YP, Nicholson DW, Rasper DM, Kalchman MA, Koide HB, Graham RK, Bromm M, Kazemi-Esfarjani P, Thornberry NA, Vaillancourt JP, Hayden MR (1996) Cleavage of huntingtin by apopain, a proapoptotic cysteine protease, is modulated by the polyglutamine tract. Nat Genet 13:442-449.

Goti D, Katzen SM, Mez J, Kurtis N, Kiluk J, Ben-Haiem L, Jenkins NA, Copeland NG, Kakizuka A, Sharp AH, Ross CA, Mouton PR, Colomer V (2004) A mutant ataxin-3 putative-cleavage fragment in brains of Machado-Joseph disease patients and transgenic mice is cytotoxic above a critical concentration. J Neurosci 24:10266-10279.

Graham RK, Deng Y, Slow EJ, Haigh B, Bissada N, Lu G, Pearson J, Shehadeh J, Bertram L, Murphy Z, Warby SC, Doty CN, Roy S, Wellington CL, Leavitt BR, Raymond LA, Nicholson DW, Hayden MR (2006) Cleavage at the caspase-6 site is required for neuronal dysfunction and degeneration due to mutant huntingtin. Cell 125:1179-1191.

Greenberg SA, Watts GD, Kimonis VE, Amato AA, Pinkus JL (2007) Nuclear localization of valosin-containing protein in normal muscle and muscle affected by inclusion-body myositis. Muscle Nerve 36:447-454.

Guyant-Marechal L, Laquerriere A, Duyckaerts C, Dumanchin C, Bou J, Dugny F, Le Ber I, Frebourg T, Hannequin D, Campion D (2006) Valosin-containing protein gene mutations: clinical and neuropathologic features. Neurology 67:644-651.

Haacke A, Broadley SA, Boteva R, Tzvetkov N, Hartl FU, Breuer P (2006) Proteolytic cleavage of polyglutamine-expanded ataxin-3 is critical for aggregation and sequestration of non-expanded ataxin-3. Hum Mol Genet 15:555-568.

Hara T, Nakamura K, Matsui M, Yamamoto A, Nakahara Y, Suzuki-Migishima R, Yokoyama M, Mishima K, Saito I, Okano H, Mizushima N (2006) Suppression of basal autophagy in neural cells causes neurodegenerative disease in mice. Nature 441:885-889.

Hay DG, Sathasivam K, Tobaben S, Stahl B, Marber M, Mestril R, Mahal A, Smith DL, Woodman B, Bates GP (2004) Progressive decrease in chaperone protein levels in a mouse model of Huntington's disease and induction of stress proteins as a therapeutic approach. Hum Mol Genet 13:1389-1405.

He B, Bai S, Hnat AT, Kalman RI, Minges JT, Patterson C, Wilson EM (2004) An androgen receptor NH2-terminal conserved motif interacts with the COOH terminus of the Hsp70-interacting protein (CHIP). J Biol Chem 279:30643-30653.

Heir R, Ablasou C, Dumontier E, Elliott M, Fagotto-Kaufmann C, Bedford FK (2006) The UBL domain of PLIC-1 regulates aggresome formation. EMBO Rep 7:1252-1258.

Helmlinger D, Hardy S, Abou-Sleymane G, Eberlin A, Bowman AB, Gansmuller A, Picaud S, Zoghbi HY, Trottier Y, Tora L, Devys D (2006) Glutamine-expanded ataxin-7 alters TFTC/STAGA recruitment and chromatin structure leading to photoreceptor dysfunction. PLoS Biol 4:e67.

Hill JA, Karimi M, Kutschke W, Davisson RL, Zimmerman K, Wang Z, Kerber RE, Weiss RM (2000) Cardiac hypertrophy is not a required compensatory response to short-term pressure overload. Circulation 101:2863-2869.

Hoppe T, Cassata G, Barral JM, Springer W, Hutagalung AH, Epstein HF, Baumeister R (2004) Regulation of the myosin-directed chaperone UNC-45 by a novel E3/E4-multiubiquitylation complex in C. elegans. Cell 118:337-349.

Hsu AL, Murphy CT, Kenyon C (2003) Regulation of aging and age-related disease by DAF-16 and heat-shock factor. Science 300:1142-1145.

Humbert S, Bryson EA, Cordelieres FP, Connors NC, Datta SR, Finkbeiner S, Greenberg ME, Saudou F (2002) The IGF-1/Akt pathway is neuroprotective in Huntington's disease and involves Huntingtin phosphorylation by Akt. Dev Cell 2:831-837.

Hung LW, Ciccotosto GD, Giannakis E, Tew DJ, Perez K, Masters CL, Cappai R, Wade JD, Barnham KJ (2008) Amyloid-{beta} Peptide (A{beta}) Neurotoxicity Is Modulated by the Rate of Peptide Aggregation: A{beta} Dimers and Trimers Correlate with Neurotoxicity. J Neurosci 28:11950-11958.

Ignatova Z, Gierasch LM (2006) Extended polyglutamine tracts cause aggregation and structural perturbation of an adjacent beta barrel protein. J Biol Chem 281:12959-12967.

Imai Y, Soda M, Hatakeyama S, Akagi T, Hashikawa T, Nakayama KI, Takahashi R (2002) CHIP is associated with Parkin, a gene responsible for familial Parkinson's disease, and enhances its ubiquitin ligase activity. Mol Cell 10:55-67.

Ishikawa K, Watanabe M, Yoshizawa K, Fujita T, Iwamoto H, Yoshizawa T, Harada K, Nakamagoe K, Komatsuzaki Y, Satoh A, Doi M, Ogata T, Kanazawa I, Shoji S, Mizusawa H (1999) Clinical, neuropathological, and molecular study in two families with spinocerebellar ataxia type 6 (SCA6). J Neurol Neurosurg Psychiatry 67:86-89.

Jana NR, Dikshit P, Goswami A, Kotliarova S, Murata S, Tanaka K, Nukina N (2005) Co-chaperone CHIP associates with expanded polyglutamine protein and promotes their degradation by proteasomes. J Biol Chem 280:11635-11640.

Janiesch PC, Kim J, Mouysset J, Barikbin R, Lochmuller H, Cassata G, Krause S, Hoppe T (2007) The ubiquitin-selective chaperone CDC-48/p97 links myosin assembly to human myopathy. Nat Cell Biol 9:379-390.

Jarosch E, Taxis C, Volkwein C, Bordallo J, Finley D, Wolf DH, Sommer T (2002) Protein dislocation from the ER requires polyubiquitination and the AAA-ATPase Cdc48. Nat Cell Biol 4:134-139.

Jia K, Hart AC, Levine B (2007) Autophagy genes protect against disease caused by polyglutamine expansion proteins in Caenorhabditis elegans. Autophagy 3:21-25.

Jia NL, Fei EK, Ying Z, Wang HF, Wang GH (2008) PolyQ-expanded ataxin-3 interacts with full-length ataxin-3 in a polyQ length-dependent manner. Neurosci Bull 24:201-208.

Jin T, Albillos SM, Chen YW, Kothary MH, Fu TJ, Zhang YZ (2008) Purification and characterization of the 7S vicilin from Korean pine (Pinus koraiensis). J Agric Food Chem 56:8159-8165.

Kaltenbach LS, Romero E, Becklin RR, Chettier R, Bell R, Phansalkar A, Strand A, Torcassi C, Savage J, Hurlburt A, Cha GH, Ukani L, Chepanoske CL, Zhen Y, Sahasrabudhe S, Olson J, Kurschner C, Ellerby LM, Peltier JM, Botas J, Hughes RE (2007) Huntingtin interacting proteins are genetic modifiers of neurodegeneration. PLoS Genet 3:e82.

Kampinga HH, Kanon B, Salomons FA, Kabakov AE, Patterson C (2003) Overexpression of the cochaperone CHIP enhances Hsp70-dependent folding activity in mammalian cells. Mol Cell Biol 23:4948-4958.

Kaneko C, Hatakeyama S, Matsumoto M, Yada M, Nakayama K, Nakayama KI (2003) Characterization of the mouse gene for the U-box-type ubiquitin ligase UFD2a. Biochem Biophys Res Commun 300:297-304.

Kaneko-Oshikawa C, Nakagawa T, Yamada M, Yoshikawa H, Matsumoto M, Yada M, Hatakeyama S, Nakayama K, Nakayama KI (2005) Mammalian E4 is required for cardiac development and maintenance of the nervous system. Mol Cell Biol 25:10953-10964.

Katsuno M, Adachi H, Kume A, Li M, Nakagomi Y, Niwa H, Sang C, Kobayashi Y, Doyu M, Sobue G (2002) Testosterone reduction prevents phenotypic expression in a transgenic mouse model of spinal and bulbar muscular atrophy. Neuron 35:843-854.

Katsuno M, Adachi H, Waza M, Banno H, Suzuki K, Tanaka F, Doyu M, Sobue G (2006) Pathogenesis, animal models and therapeutics in spinal and bulbar muscular atrophy (SBMA). Exp Neurol 200:8-18.

Kawaguchi Y, Okamoto T, Taniwaki M, Aizawa M, Inoue M, Katayama S, Kawakami H, Nakamura S, Nishimura M, Akiguchi I, et al. (1994) CAG expansions in a novel gene for Machado-Joseph disease at chromosome 14q32.1. Nat Genet 8:221-228.

Kayed R, Head E, Sarsoza F, Saing T, Cotman CW, Necula M, Margol L, Wu J, Breydo L, Thompson JL, Rasool S, Gurlo T, Butler P, Glabe CG (2007) Fibril specific, conformation dependent antibodies recognize a generic epitope common to amyloid fibrils and fibrillar oligomers that is absent in prefibrillar oligomers. Mol Neurodegener 2:18.

Kayed R, Head E, Thompson JL, McIntire TM, Milton SC, Cotman CW, Glabe CG (2003) Common structure of soluble amyloid oligomers implies common mechanism of pathogenesis. Science 300:486-489.

King MA, Hands S, Hafiz F, Mizushima N, Tolkovsky AM, Wyttenbach A (2008) Rapamycin inhibits polyglutamine aggregation independently of autophagy by reducing protein synthesis. Mol Pharmacol 73:1052-1063.

Kitamura A, Kubota H, Pack CG, Matsumoto G, Hirayama S, Takahashi Y, Kimura H, Kinjo M, Morimoto RI, Nagata K (2006) Cytosolic chaperonin prevents polyglutamine toxicity with altering the aggregation state. Nat Cell Biol 8:1163-1170.

Klein FA, Pastore A, Masino L, Zeder-Lutz G, Nierengarten H, Oulad-Abdelghani M, Altschuh D, Mandel JL, Trottier Y (2007) Pathogenic and non-pathogenic polyglutamine tracts have similar structural properties: towards a length-dependent toxicity gradient. J Mol Biol 371:235-244.

Klement IA, Skinner PJ, Kaytor MD, Yi H, Hersch SM, Clark HB, Zoghbi HY, Orr HT (1998) Ataxin-1 nuclear localization and aggregation: role in polyglutamine-induced disease in SCA1 transgenic mice. Cell 95:41-53.

Komatsu M, Waguri S, Chiba T, Murata S, Iwata J, Tanida I, Ueno T, Koike M, Uchiyama Y, Kominami E, Tanaka K (2006) Loss of autophagy in the central nervous system causes neurodegeneration in mice. Nature 441:880-884.

Kordasiewicz HB, Thompson RM, Clark HB, Gomez CM (2006) C-termini of P/Q-type Ca2+ channel alpha1A subunits translocate to nuclei and promote polyglutamine-mediated toxicity. Hum Mol Genet 15:1587-1599.

Kostka M, Hogen T, Danzer KM, Levin J, Habeck M, Wirth A, Wagner R, Glabe CG, Finger S, Heinzelmann U, Garidel P, Duan W, Ross CA, Kretzschmar H, Giese A (2008) Single particle characterization of iron-induced pore-forming alpha-synuclein oligomers. J Biol Chem 283:10992-11003.

Kouroku Y, Fujita E, Jimbo A, Kikuchi T, Yamagata T, Momoi MY, Kominami E, Kuida K, Sakamaki K, Yonehara S, Momoi T (2002) Polyglutamine aggregates stimulate ER stress signals and caspase-12 activation. Hum Mol Genet 11:1505-1515.

Kouroku Y, Fujita E, Tanida I, Ueno T, Isoai A, Kumagai H, Ogawa S, Kaufman RJ, Kominami E, Momoi T (2007) ER stress (PERK/eIF2alpha phosphorylation) mediates the polyglutamine-induced LC3 conversion, an essential step for autophagy formation. Cell Death Differ 14:230-239.

Kumada S, Uchihara T, Hayashi M, Nakamura A, Kikuchi E, Mizutani T, Oda M (2002) Promyelocytic leukemia protein is redistributed during the formation of intranuclear inclusions independent of polyglutamine expansion: an immunohistochemical study on Marinesco bodies. J Neuropathol Exp Neurol 61:984-991.

Kumar P, Ambasta RK, Veereshwarayya V, Rosen KM, Kosik KS, Band H, Mestril R, Patterson C, Querfurth HW (2007) CHIP and HSPs interact with {beta}-APP in a proteasome-dependent manner and influence A{beta} metabolism. Hum Mol Genet 16:848-864.

Lam YC, Bowman AB, Jafar-Nejad P, Lim J, Richman R, Fryer JD, Hyun ED, Duvick LA, Orr HT, Botas J, Zoghbi HY (2006) ATAXIN-1 interacts with the repressor Capicua in its native complex to cause SCA1 neuropathology. Cell 127:1335-1347.

Laser H, Conforti L, Morreale G, Mack TG, Heyer M, Haley JE, Wishart TM, Beirowski B, Walker SA, Haase G, Celik A, Adalbert R, Wagner D, Grumme D, Ribchester RR, Plomann M, Coleman MP (2006) The slow Wallerian degeneration protein, WldS, binds directly to VCP/p97 and partially redistributes it within the nucleus. Mol Biol Cell 17:1075-1084.

Lein ES, Hawrylycz MJ, Ao N, Ayres M, Bensinger A, Bernard A, Boe AF, Boguski MS, Brockway KS, Byrnes EJ, Chen L, Chen L, Chen TM, Chin MC, Chong J, Crook BE, Czaplinska A, Dang CN, Datta S, Dee NR, Desaki AL, Desta T, Diep E, Dolbeare TA, Donelan MJ, Dong HW, Dougherty JG, Duncan BJ, Ebbert AJ, Eichele G, Estin LK, Faber C, Facer BA, Fields R, Fischer SR, Fliss TP, Frensley C, Gates SN, Glattfelder KJ, Halverson KR, Hart MR, Hohmann JG, Howell MP, Jeung DP, Johnson RA, Karr PT, Kawal R, Kidney JM, Knapik RH, Kuan CL, Lake JH, Laramee AR, Larsen KD, Lau C, Lemon TA, Liang AJ, Liu Y, Luong LT, Michaels J, Morgan JJ, Morgan RJ, Mortrud MT, Mosqueda NF, Ng LL, Ng R, Orta GJ, Overly CC, Pak TH, Parry SE, Pathak SD, Pearson OC, Puchalski RB, Riley ZL, Rockett HR, Rowland SA, Royall JJ, Ruiz MJ, Sarno NR, Schaffnit K, Shapovalova NV, Sivisay T, Slaughterbeck CR, Smith SC, Smith KA, Smith BI, Sodt AJ, Stewart NN, Stumpf KR, Sunkin SM, Sutram M, Tam A, Teemer CD, Thaller C, Thompson CL, Varnam LR, Visel A, Whitlock RM, Wohnoutka PE, Wolkey CK, Wong VY, et al. (2007) Genome-wide atlas of gene expression in the adult mouse brain. Nature 445:168-176.

Lesne S, Koh MT, Kotilinek L, Kayed R, Glabe CG, Yang A, Gallagher M, Ashe KH (2006) A specific amyloid-beta protein assembly in the brain impairs memory. Nature 440:352-357.

Li F, Macfarlan T, Pittman RN, Chakravarti D (2002) Ataxin-3 is a histone-binding protein with two independent transcriptional corepressor activities. J Biol Chem 277:45004-45012.

Li LB, Yu Z, Teng X, Bonini NM (2008) RNA toxicity is a component of ataxin-3 degeneration in Drosophila. Nature 453:1107-1111.

Li M, Chevalier-Larsen ES, Merry DE, Diamond MI (2007) Soluble androgen receptor oligomers underlie pathology in a mouse model of spinobulbar muscular atrophy. J Biol Chem 282:3157-3164.

Li M, Miwa S, Kobayashi Y, Merry DE, Yamamoto M, Tanaka F, Doyu M, Hashizume Y, Fischbeck KH, Sobue G (1998) Nuclear inclusions of the androgen receptor protein in spinal and bulbar muscular atrophy. Ann Neurol 44:249-254.

Li P, Huey-Tubman KE, Gao T, Li X, West AP, Jr., Bennett MJ, Bjorkman PJ (2007) The structure of a polyQ-anti-polyQ complex reveals binding according to a linear lattice model. Nat Struct Mol Biol 14:381-387.

Lim J, Crespo-Barreto J, Jafar-Nejad P, Bowman AB, Richman R, Hill DE, Orr HT, Zoghbi HY (2008) Opposing effects of polyglutamine expansion on native protein complexes contribute to SCA1. Nature 452:713-718.

Lim J, Hao T, Shaw C, Patel AJ, Szabo G, Rual JF, Fisk CJ, Li N, Smolyar A, Hill DE, Barabasi AL, Vidal M, Zoghbi HY (2006) A protein-protein interaction network for human inherited ataxias and disorders of Purkinje cell degeneration. Cell 125:801-814.

Macario AJ (1995) Heat-shock proteins and molecular chaperones: implications for pathogenesis, diagnostics, and therapeutics. Int J Clin Lab Res 25:59-70.

Marchut AJ, Hall CK (2006) Side-chain interactions determine amyloid formation by model polyglutamine peptides in molecular dynamics simulations. Biophys J 90:4574-4584.

Marques C, Guo W, Pereira P, Taylor A, Patterson C, Evans PC, Shang F (2006) The triage of damaged proteins: degradation by the ubiquitin-proteasome pathway or repair by molecular chaperones. Faseb J 20:741-743.

Matsumoto M, Yada M, Hatakeyama S, Ishimoto H, Tanimura T, Tsuji S, Kakizuka A, Kitagawa M, Nakayama KI (2004) Molecular clearance of ataxin-3 is regulated by a mammalian E4. Embo J 23:659-669.

Mauri PL, Riva M, Ambu D, De Palma A, Secundo F, Benazzi L, Valtorta M, Tortora P, Fusi P (2006) Ataxin-3 is subject to autolytic cleavage. Febs J 273:4277-4286.

Meacham GC, Patterson C, Zhang W, Younger JM, Cyr DM (2001) The Hsc70 co-chaperone CHIP targets immature CFTR for proteasomal degradation. Nat Cell Biol 3:100-105.

Melville MW, McClellan AJ, Meyer AS, Darveau A, Frydman J (2003) The Hsp70 and TRiC/CCT chaperone systems cooperate in vivo to assemble the von Hippel-Lindau tumor suppressor complex. Mol Cell Biol 23:3141-3151.

Merry DE, Kobayashi Y, Bailey CK, Taye AA, Fischbeck KH (1998) Cleavage, aggregation and toxicity of the expanded androgen receptor in spinal and bulbar muscular atrophy. Hum Mol Genet 7:693-701.

Miller VM, Nelson RF, Gouvion CM, Williams A, Rodriguez-Lebron E, Harper SQ, Davidson BL, Rebagliati MR, Paulson HL (2005) CHIP suppresses polyglutamine aggregation and toxicity in vitro and in vivo. J Neurosci 25:9152-9161.

Miller VM, Xia H, Marrs GL, Gouvion CM, Lee G, Davidson BL, Paulson HL (2003) Allele-specific silencing of dominant disease genes. Proc Natl Acad Sci U S A 100:7195-7200.

Min JN, Whaley RA, Sharpless NE, Lockyer P, Portbury AL, Patterson C (2008) CHIP deficiency decreases longevity with accelerated aging phenotypes accompanied by altered protein quality control. Mol Cell Biol.

Mishra A, Dikshit P, Purkayastha S, Sharma J, Nukina N, Jana NR (2008) E6-AP Promotes Misfolded Polyglutamine Proteins for Proteasomal Degradation and Suppresses Polyglutamine Protein Aggregation and Toxicity. J Biol Chem 283:7648-7656.

Morimoto RI (1998) Regulation of the heat shock transcriptional response: cross talk between a family of heat shock factors, molecular chaperones, and negative regulators. Genes Dev 12:3788-3796.

Morley JF, Brignull HR, Weyers JJ, Morimoto RI (2002) The threshold for polyglutamine-expansion protein aggregation and cellular toxicity is dynamic and influenced by aging in Caenorhabditis elegans. Proc Natl Acad Sci U S A 99:10417-10422.

Muchowski PJ, Wacker JL (2005) Modulation of neurodegeneration by molecular chaperones. Nat Rev Neurosci 6:11-22.

Nagai Y, Inui T, Popiel HA, Fujikake N, Hasegawa K, Urade Y, Goto Y, Naiki H, Toda T (2007) A toxic monomeric conformer of the polyglutamine protein. Nat Struct Mol Biol 14:332-340.

Nagaoka U, Uchihara T, Iwabuchi K, Konno H, Tobita M, Funata N, Yagishita S, Kato T (2003) Attenuated nuclear shrinkage in neurones with nuclear inclusions of SCA1 brains. J Neurol Neurosurg Psychiatry 74:597-601.

Nguyen HP, Kobbe P, Rahne H, Worpel T, Jager B, Stephan M, Pabst R, Holzmann C, Riess O, Korr H, Kantor O, Petrasch-Parwez E, Wetzel R, Osmand A, von Horsten S (2006) Behavioral abnormalities precede neuropathological markers in rats transgenic for Huntington's disease. Hum Mol Genet 15:3177-3194.

Nishitoh H, Matsuzawa A, Tobiume K, Saegusa K, Takeda K, Inoue K, Hori S, Kakizuka A, Ichijo H (2002) ASK1 is essential for endoplasmic reticulum stress-induced neuronal cell death triggered by expanded polyglutamine repeats. Genes Dev 16:1345-1355.

Nollen EA, Garcia SM, van Haaften G, Kim S, Chavez A, Morimoto RI, Plasterk RH (2004) Genome-wide RNA interference screen identifies previously undescribed regulators of polyglutamine aggregation. Proc Natl Acad Sci U S A 101:6403-6408.

Ona VO, Li M, Vonsattel JP, Andrews LJ, Khan SQ, Chung WM, Frey AS, Menon AS, Li XJ, Stieg PE, Yuan J, Penney JB, Young AB, Cha JH, Friedlander RM (1999) Inhibition of caspase-1 slows disease progression in a mouse model of Huntington's disease. Nature 399:263-267.

Osmand AP, Berthelier V, Wetzel R (2006) Imaging polyglutamine deposits in brain tissue. Methods Enzymol 412:106-122.

Palhan VB, Chen S, Peng GH, Tjernberg A, Gamper AM, Fan Y, Chait BT, La Spada AR, Roeder RG (2005) Polyglutamine-expanded ataxin-7 inhibits STAGA histone acetyltransferase activity to produce retinal degeneration. Proc Natl Acad Sci U S A 102:8472-8477.

Pandey UB, Nie Z, Batlevi Y, McCray BA, Ritson GP, Nedelsky NB, Schwartz SL, DiProspero NA, Knight MA, Schuldiner O, Padmanabhan R, Hild M, Berry DL, Garza D, Hubbert CC, Yao TP, Baehrecke EH, Taylor JP (2007) HDAC6 rescues neurodegeneration and provides an essential link between autophagy and the UPS. Nature 447:859-863.

Paulson HL, Das SS, Crino PB, Perez MK, Patel SC, Gotsdiner D, Fischbeck KH, Pittman RN (1997) Machado-Joseph disease gene product is a cytoplasmic protein widely expressed in brain. Ann Neurol 41:453-462.

Paulson HL, Perez MK, Trottier Y, Trojanowski JQ, Subramony SH, Das SS, Vig P, Mandel JL, Fischbeck KH, Pittman RN (1997) Intranuclear inclusions of expanded polyglutamine protein in spinocerebellar ataxia type 3. Neuron 19:333-344.

Peters-Libeu C, Newhouse Y, Krishnan P, Cheung K, Brooks E, Weisgraber K, Finkbeiner S (2005) Crystallization and diffraction properties of the Fab fragment of 3B5H10, an antibody specific for disease-causing polyglutamine stretches. Acta Crystallogr Sect F Struct Biol Cryst Commun 61:1065-1068.

Poirier MA, Li H, Macosko J, Cai S, Amzel M, Ross CA (2002) Huntingtin spheroids and protofibrils as precursors in polyglutamine fibrilization. J Biol Chem 277:41032-41037.

Pozzi C, Valtorta M, Tedeschi G, Galbusera E, Pastori V, Bigi A, Nonnis S, Grassi E, Fusi P (2008) Study of subcellular localization and proteolysis of ataxin-3. Neurobiol Dis 30:190-200.

Qian SB, McDonough H, Boellmann F, Cyr DM, Patterson C (2006) CHIP-mediated stress recovery by sequential ubiquitination of substrates and Hsp70. Nature 440:551-555.

Rabinovich E, Kerem A, Frohlich KU, Diamant N, Bar-Nun S (2002) AAA-ATPase p97/Cdc48p, a cytosolic chaperone required for endoplasmic reticulum-associated protein degradation. Mol Cell Biol 22:626-634.

Ravikumar B, Duden R, Rubinsztein DC (2002) Aggregate-prone proteins with polyglutamine and polyalanine expansions are degraded by autophagy. Hum Mol Genet 11:1107-1117.

Ravikumar B, Rubinsztein DC (2004) Can autophagy protect against neurodegeneration caused by aggregate-prone proteins? Neuroreport 15:2443-2445.

Reijonen S, Putkonen N, Norremolle A, Lindholm D, Korhonen L (2008) Inhibition of endoplasmic reticulum stress counteracts neuronal cell death and protein aggregation caused by N-terminal mutant huntingtin proteins. Exp Cell Res 314:950-960.

Richly H, Rape M, Braun S, Rumpf S, Hoege C, Jentsch S (2005) A series of ubiquitin binding factors connects CDC48/p97 to substrate multiubiquitylation and proteasomal targeting. Cell 120:73-84.

Rodrigues AJ, Coppola G, Santos C, Costa Mdo C, Ailion M, Sequeiros J, Geschwind DH, Maciel P (2007) Functional genomics and biochemical characterization of the C. elegans orthologue of the Machado-Joseph disease protein ataxin-3. Faseb J 21:1126-1136.

Ross CA, Poirier MA (2004) Protein aggregation and neurodegenerative disease. Nat Med 10 Suppl:S10-17.

Rosser MF, Washburn E, Muchowski PJ, Patterson C, Cyr DM (2007) Chaperone functions of the E3 ubiquitin ligase CHIP. J Biol Chem 282:22267-22277.

Rub U, Brunt ER, Deller T (2008) New insights into the pathoanatomy of spinocerebellar ataxia type 3 (Machado-Joseph disease). Curr Opin Neurol 21:111-116.

Rub U, de Vos RA, Brunt ER, Sebesteny T, Schols L, Auburger G, Bohl J, Ghebremedhin E, Gierga K, Seidel K, den Dunnen W, Heinsen H, Paulson H, Deller T (2006) Spinocerebellar ataxia type 3 (SCA3): thalamic neurodegeneration occurs independently from thalamic ataxin-3 immunopositive neuronal intranuclear inclusions. Brain Pathol 16:218-227.

Sanchez I, Mahlke C, Yuan J (2003) Pivotal role of oligomerization in expanded polyglutamine neurodegenerative disorders. Nature 421:373-379.

Sanchez I, Xu CJ, Juo P, Kakizaka A, Blenis J, Yuan J (1999) Caspase-8 is required for cell death induced by expanded polyglutamine repeats. Neuron 22:623-633.

Saudou F, Finkbeiner S, Devys D, Greenberg ME (1998) Huntingtin acts in the nucleus to induce apoptosis but death does not correlate with the formation of intranuclear inclusions. Cell 95:55-66.

Schaffar G, Breuer P, Boteva R, Behrends C, Tzvetkov N, Strippel N, Sakahira H, Siegers K, Hayer-Hartl M, Hartl FU (2004) Cellular toxicity of polyglutamine expansion proteins: mechanism of transcription factor deactivation. Mol Cell 15:95-105.

Schiffer NW, Ceraline J, Hartl FU, Broadley SA (2008) N-terminal polyglutamine-containing fragments inhibit androgen receptor transactivation function. Biol Chem.

Schlaf G, Goddecke M, Wolff JR, Felgenhauer K, Mader M (1996) Large-scale purification of synaptophysin and quantification with a newly established enzyme-linked immunosorbent assay. Biol Chem 377:591-597.

Schmidt BJ, Greenberg CR, Allingham-Hawkins DJ, Spriggs EL (2002) Expression of X-linked bulbospinal muscular atrophy (Kennedy disease) in two homozygous women. Neurology 59:770-772.

Schmitt I, Linden M, Khazneh H, Evert BO, Breuer P, Klockgether T, Wuellner U (2007) Inactivation of the mouse Atxn3 (ataxin-3) gene increases protein ubiquitination. Biochem Biophys Res Commun 362:734-739.

Seilhean D, Takahashi J, El Hachimi KH, Fujigasaki H, Lebre AS, Biancalana V, Durr A, Salachas F, Hogenhuis J, de The H, Hauw JJ, Meininger V, Brice A, Duyckaerts C (2004) Amyotrophic lateral sclerosis with neuronal intranuclear protein inclusions. Acta Neuropathol 108:81-87.

Selkoe DJ (2004) Cell biology of protein misfolding: the examples of Alzheimer's and Parkinson's diseases. Nat Cell Biol 6:1054-1061.

Shankar GM, Li S, Mehta TH, Garcia-Munoz A, Shepardson NE, Smith I, Brett FM, Farrell MA, Rowan MJ, Lemere CA, Regan CM, Walsh DM, Sabatini BL, Selkoe DJ (2008) Amyloid-beta protein dimers isolated directly from Alzheimer's brains impair synaptic plasticity and memory. Nat Med.

Shen L, Tang JG, Tang BS, Jiang H, Zhao GH, Xia K, Zhang YH, Cai F, Tan LM, Pan Q (2005) Research on screening and identification of proteins interacting with ataxin-3. Zhonghua Yi Xue Yi Chuan Xue Za Zhi 22:242-247.

Shin Y, Klucken J, Patterson C, Hyman BT, McLean PJ (2005) The co-chaperone carboxyl terminus of Hsp70-interacting protein (CHIP) mediates alpha-synuclein degradation decisions between proteasomal and lysosomal pathways. J Biol Chem 280:23727-23734.

Slow EJ, Graham RK, Osmand AP, Devon RS, Lu G, Deng Y, Pearson J, Vaid K, Bissada N, Wetzel R, Leavitt BR, Hayden MR (2005) Absence of behavioral abnormalities and neurodegeneration in vivo despite widespread neuronal huntingtin inclusions. Proc Natl Acad Sci U S A 102:11402-11407.

Steffan JS, Agrawal N, Pallos J, Rockabrand E, Trotman LC, Slepko N, Illes K, Lukacsovich T, Zhu YZ, Cattaneo E, Pandolfi PP, Thompson LM, Marsh JL (2004) SUMO modification of Huntingtin and Huntington's disease pathology. Science 304:100-104.

Tagawa K, Marubuchi S, Qi ML, Enokido Y, Tamura T, Inagaki R, Murata M, Kanazawa I, Wanker EE, Okazawa H (2007) The induction levels of heat shock protein 70 differentiate the vulnerabilities to mutant huntingtin among neuronal subtypes. J Neurosci 27:868-880.

Takahashi J, Tanaka J, Arai K, Funata N, Hattori T, Fukuda T, Fujigasaki H, Uchihara T (2001) Recruitment of nonexpanded polyglutamine proteins to intranuclear aggregates in neuronal intranuclear hyaline inclusion disease. J Neuropathol Exp Neurol 60:369-376.

Takahashi T, Kikuchi S, Katada S, Nagai Y, Nishizawa M, Onodera O (2008) Soluble polyglutamine oligomers formed prior to inclusion body formation are cytotoxic. Hum Mol Genet 17:345-356.

Takahashi Y, Okamoto Y, Popiel HA, Fujikake N, Toda T, Kinjo M, Nagai Y (2007) Detection of polyglutamine protein oligomers in cells by fluorescence correlation spectroscopy. J Biol Chem 282:24039-24048.

Tam S, Geller R, Spiess C, Frydman J (2006) The chaperonin TRiC controls polyglutamine aggregation and toxicity through subunit-specific interactions. Nat Cell Biol 8:1155-1162.

Tao RS, Fei EK, Ying Z, Wang HF, Wang GH (2008) Casein kinase 2 interacts with and phosphorylates ataxin-3. Neurosci Bull 24:271-277.

Taylor JP, Hardy J, Fischbeck KH (2002) Toxic proteins in neurodegenerative disease. Science 296:1991-1995.

Tetzlaff JE, Putcha P, Outeiro TF, Ivanov A, Berezovska O, Hyman BT, McLean PJ (2008) CHIP targets toxic alpha-Synuclein oligomers for degradation. J Biol Chem 283:17962-17968.

Thomas M, Harrell JM, Morishima Y, Peng HM, Pratt WB, Lieberman AP (2006) Pharmacologic and genetic inhibition of hsp90-dependent trafficking reduces aggregation and promotes degradation of the expanded glutamine androgen receptor without stress protein induction. Hum Mol Genet 15:1876-1883.

Thomas M, Yu Z, Dadgar N, Varambally S, Yu J, Chinnaiyan AM, Lieberman AP (2005) The unfolded protein response modulates toxicity of the expanded glutamine androgen receptor. J Biol Chem 280:21264-21271.

Todi SV, Laco MN, Winborn BJ, Travis SM, Wen HM, Paulson HL (2007) Cellular turnover of the polyglutamine disease protein ataxin-3 is regulated by its catalytic activity. J Biol Chem 282:29348-29358.

Tsai YC, Fishman PS, Thakor NV, Oyler GA (2003) Parkin facilitates the elimination of expanded polyglutamine proteins and leads to preservation of proteasome function. J Biol Chem 278:22044-22055.

Tsuda H, Jafar-Nejad H, Patel AJ, Sun Y, Chen HK, Rose MF, Venken KJ, Botas J, Orr HT, Bellen HJ, Zoghbi HY (2005) The AXH domain of Ataxin-1 mediates neurodegeneration through its interaction with Gfi-1/Senseless proteins. Cell 122:633-644.

Tzvetkov N, Breuer P (2007) Josephin domain-containing proteins from a variety of species are active de-ubiquitination enzymes. Biol Chem 388:973-978.

Uchihara T, Fujigasaki H, Koyano S, Nakamura A, Yagishita S, Iwabuchi K (2001) Non-expanded polyglutamine proteins in intranuclear inclusions of hereditary ataxias--triple-labeling immunofluorescence study. Acta Neuropathol 102:149-152.

van Bilsen PH, Jaspers L, Lombardi MS, Odekerken JC, Burright EN, Kaemmerer WF (2008) Identification and allele-specific silencing of the mutant huntingtin allele in Huntington's disease patient-derived fibroblasts. Hum Gene Ther 19:710-719.

Verhoef LG, Lindsten K, Masucci MG, Dantuma NP (2002) Aggregate formation inhibits proteasomal degradation of polyglutamine proteins. Hum Mol Genet 11:2689-2700.

Walsh DM, Selkoe DJ (2004) Oligomers on the brain: the emerging role of soluble protein aggregates in neurodegeneration. Protein Pept Lett 11:213-228.

Walsh DM, Selkoe DJ (2007) Abeta Oligomers - a decade of discovery. J Neurochem 101:1172-1184.

Wang G, Sawai N, Kotliarova S, Kanazawa I, Nukina N (2000) Ataxin-3, the MJD1 gene product, interacts with the two human homologs of yeast DNA repair protein RAD23, HHR23A and HHR23B. Hum Mol Genet 9:1795-1803.

Wang H, Jia N, Fei E, Wang Z, Liu C, Zhang T, Fan J, Wu M, Chen L, Nukina N, Zhou J, Wang G (2007) p45, an ATPase subunit of the 19S proteasome, targets the polyglutamine disease protein ataxin-3 to the proteasome. J Neurochem 101:1651-1661.

Wang Q, Li L, Ye Y (2008) Inhibition of p97-dependent protein degradation by Eeyarestatin I. J Biol Chem 283:7445-7454.

Warrick JM, Chan HY, Gray-Board GL, Chai Y, Paulson HL, Bonini NM (1999) Suppression of polyglutamine-mediated neurodegeneration in Drosophila by the molecular chaperone HSP70. Nat Genet 23:425-428.

Warrick JM, Morabito LM, Bilen J, Gordesky-Gold B, Faust LZ, Paulson HL, Bonini NM (2005) Ataxin-3 suppresses polyglutamine neurodegeneration in Drosophila by a ubiquitin-associated mechanism. Mol Cell 18:37-48.

Watase K, Weeber EJ, Xu B, Antalffy B, Yuva-Paylor L, Hashimoto K, Kano M, Atkinson R, Sun Y, Armstrong DL, Sweatt JD, Orr HT, Paylor R, Zoghbi HY (2002) A long CAG repeat in the mouse Sca1 locus replicates SCA1 features and reveals the impact of protein solubility on selective neurodegeneration. Neuron 34:905-919.

Waza M, Adachi H, Katsuno M, Minamiyama M, Sang C, Tanaka F, Inukai A, Doyu M, Sobue G (2005) 17-AAG, an Hsp90 inhibitor, ameliorates polyglutamine-mediated motor neuron degeneration. Nat Med 11:1088-1095.

Weihl CC, Dalal S, Pestronk A, Hanson PI (2006) Inclusion body myopathy-associated mutations in p97/VCP impair endoplasmic reticulum-associated degradation. Hum Mol Genet 15:189-199.

Weiss A, Klein C, Woodman B, Sathasivam K, Bibel M, Regulier E, Bates GP, Paganetti P (2008) Sensitive biochemical aggregate detection reveals aggregation onset before symptom development in cellular and murine models of Huntington's disease. J Neurochem 104:846-858.

Weiss RM, Ohashi M, Miller JD, Young SG, Heistad DD (2006) Calcific aortic valve stenosis in old hypercholesterolemic mice. Circulation 114:2065-2069.

Wellington CL, Ellerby LM, Hackam AS, Margolis RL, Trifiro MA, Singaraja R, McCutcheon K, Salvesen GS, Propp SS, Bromm M, Rowland KJ, Zhang T, Rasper D, Roy S, Thornberry N, Pinsky L, Kakizuka A, Ross CA, Nicholson DW, Bredesen DE, Hayden MR (1998) Caspase cleavage of gene products associated with triplet expansion disorders generates truncated fragments containing the polyglutamine tract. J Biol Chem 273:9158-9167.

Wellington CL, Hayden MR (2000) Caspases and neurodegeneration: on the cutting edge of new therapeutic approaches. Clin Genet 57:1-10.

Wellington CL, Singaraja R, Ellerby L, Savill J, Roy S, Leavitt B, Cattaneo E, Hackam A, Sharp A, Thornberry N, Nicholson DW, Bredesen DE, Hayden MR (2000) Inhibiting caspase cleavage of huntingtin reduces toxicity and aggregate formation in neuronal and nonneuronal cells. J Biol Chem 275:19831-19838.

Winborn BJ, Travis SM, Todi SV, Scaglione KM, Xu P, Williams AJ, Cohen RE, Peng J, Paulson HL (2008) The deubiquitinating enzyme ataxin-3, a polyglutamine disease protein, edits Lys63 linkages in mixed linkage ubiquitin chains. J Biol Chem 283:26436-26443.

Wong ES, Tan JM, Soong WE, Hussein K, Nukina N, Dawson VL, Dawson TM, Cuervo AM, Lim KL (2008) Autophagy-mediated clearance of aggresomes is not a universal phenomenon. Hum Mol Genet 17:2570-2582.

Xia X, Zhou H, Huang Y, Xu Z (2006) Allele-specific RNAi selectively silences mutant SOD1 and achieves significant therapeutic benefit in vivo. Neurobiol Dis 23:578-586.

Xiong JY, Narayanan J, Liu XY, Chong TK, Chen SB, Chung TS (2005) Topology evolution and gelation mechanism of agarose gel. J Phys Chem B Condens Matter Mater Surf Interfaces Biophys 109:5638-5643.

Ye Y, Meyer HH, Rapoport TA (2001) The AAA ATPase Cdc48/p97 and its partners transport proteins from the ER into the cytosol. Nature 414:652-656.

Yoshida H (2007) ER stress and diseases. Febs J 274:630-658.

Yoshiike Y, Minai R, Matsuo Y, Chen YR, Kimura T, Takashima A (2008) Amyloid oligomer conformation in a group of natively folded proteins. PLoS ONE 3:e3235.

Zhang C, Cuervo AM (2008) Restoration of chaperone-mediated autophagy in aging liver improves cellular maintenance and hepatic function. Nat Med 14:959-965.

Zhang C, Xu Z, He XR, Michael LH, Patterson C (2005) CHIP, a cochaperone/ubiquitin ligase that regulates protein quality control, is required for maximal cardioprotection after myocardial infarction in mice. Am J Physiol Heart Circ Physiol 288:H2836-2842.

Zhang H, Wang Q, Kajino K, Greene MI (2000) VCP, a weak ATPase involved in multiple cellular events, interacts physically with BRCA1 in the nucleus of living cells. DNA Cell Biol 19:253-263.

Zhang S, Xu L, Lee J, Xu T (2002) Drosophila atrophin homolog functions as a transcriptional corepressor in multiple developmental processes. Cell 108:45-56.

Zhong X, Pittman RN (2006) Ataxin-3 binds VCP/p97 and regulates retrotranslocation of ERAD substrates. Hum Mol Genet 15:2409-2420.

Zoghbi HY, Orr HT (2000) Glutamine repeats and neurodegeneration. Annu Rev Neurosci 23:217-247.

Zourlidou A, Gidalevitz T, Kristiansen M, Landles C, Woodman B, Wells DJ, Latchman DS, de Belleroche J, Tabrizi SJ, Morimoto RI, Bates GP (2007) Hsp27 overexpression in the R6/2 mouse model of Huntington's disease: chronic neurodegeneration does not induce Hsp27 activation. Hum Mol Genet 16:1078-1090.